The computational neuroethology of weakly electric fish

body modeling, motion analysis, and sensory signal estimation

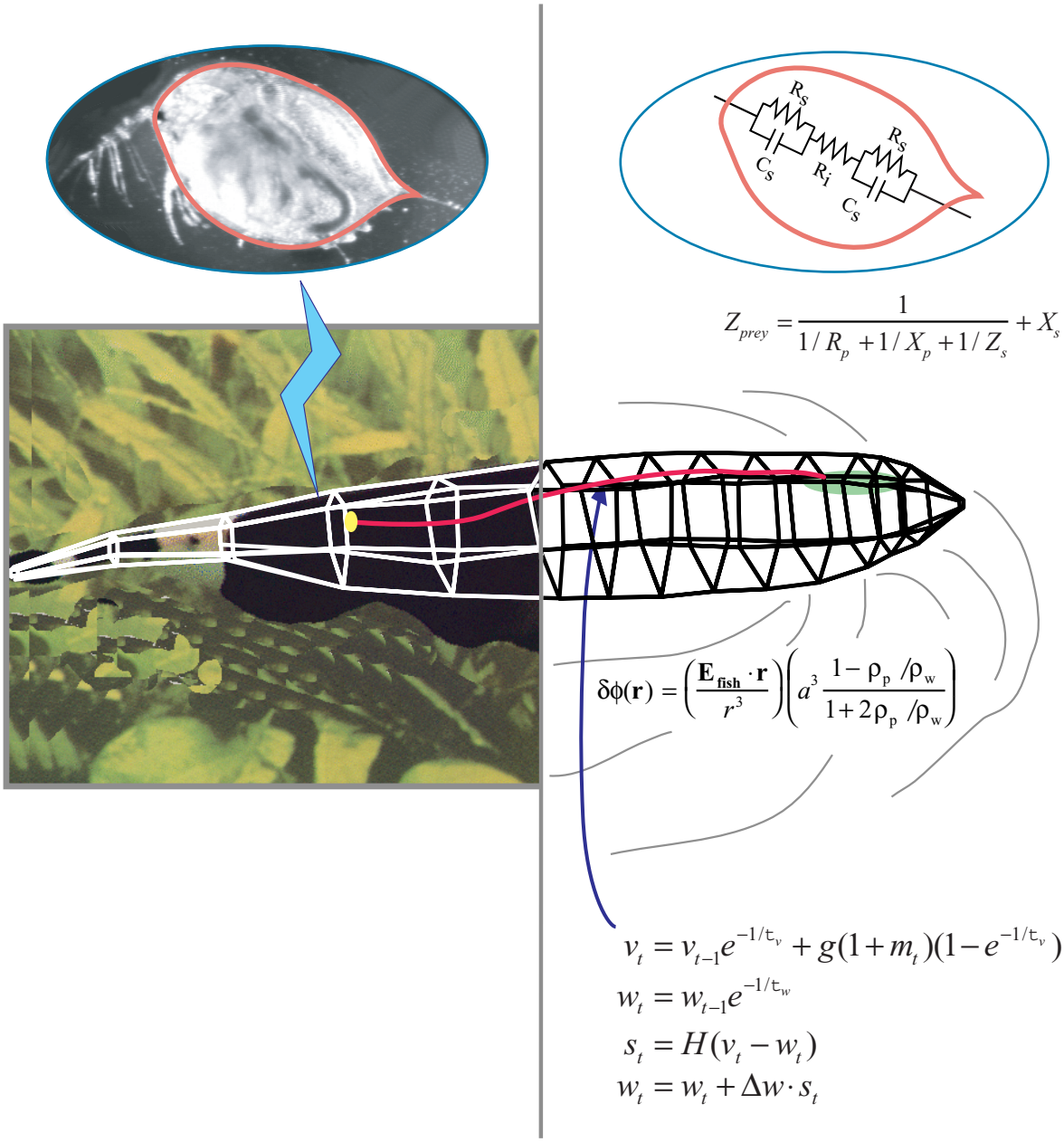

Malcolm Angus MacIver

THE COMPUTATIONAL NEUROETHOLOGY OF WEAKLY ELECTRIC FISH: BODY MODELING, MOTION ANALYSIS, AND SENSORY SIGNAL ESTIMATION

BY

MALCOLM ANGUS MACIVER

B.Sc., University of Toronto, 1991
M.A., University of Toronto, 1992

THESIS

Submitted in partial fulfillment of the requirements
for the degree of Doctor of Philosophy in Neuroscience
in the Graduate College of the
University of Illinois at Urbana-Champaign, 2001

Urbana, Illinois

UNIVERSITY OF ILLINOIS AT URBANA-CHAMPAIGN

THE GRADUATE COLLEGE

MARCH 2001
(date)

WE HEREBY RECOMMEND THAT THE THESIS BY

MALCOLM ANGUS MACIVER

ENTITLED THE COMPUTATIONAL NEUROETHOLOGY OF WEAKLY ELECTRIC FISH: BODY MODELING, MOTION ANALYSIS, AND SENSORY SIGNAL ESTIMATION

BE ACCEPTED IN PARTIAL FULFILLMENT OF THE REQUIREMENTS FOR THE DEGREE OF DOCTOR OF PHILOSOPHY

Mark E. Nelson — Dr. Mark E. Nelson
Director of Thesis Research

Gene E. Robinson — Dr. Gene E. Robinson
Head of Department

Committee on Final Examination†

Mark E. Nelson — Dr. Mark E. Nelson
Chairperson

Thomas J. Anastasio — Dr. Thomas J. Anastasio

Neal J. Cohen — Dr. Neal J. Cohen

Albert S. Feng — Dr. Albert Feng

Joseph G. Malpeli — Dr. Joseph G. Malpeli

† Required for doctor's degree but not for master's.

O-517

ABSTRACT

Animals actively influence the content and quality of sensory information they acquire through the positioning of peripheral sensory surfaces. Investigation of how the body and brain work together for sensory acquisition is hindered by 1) the limited number of techniques for tracking sensory surfaces, few of which provide data on the position of the entire body surface, and by 2) our inability to measure the thousands of sensory afferents stimulated during behavior. I present research on sensory acquisition in weakly electric fish of the genus *Apteronotus*, where I overcame the first barrier by developing a markerless tracking system and have deployed a computational approach toward overcoming the second barrier. This approach allows estimation of the full sense data stream ($\approx$14,000 afferents) over the course of prey capture trials. Analysis of the tracking data showed how *Apteronotus* modified the position of its electrosensory array during predatory behavior and demonstrated that the fish use a closed-loop adaptive tracking strategy to intercept prey. In addition, nonvisual detection distance was dependent on water conductivity, implying that detection is dominated by the electrosense and providing the first evidence for the involvement of this sense in prey capture behavior of gymnotids. An analysis of the spatiotemporal profile of the estimated sensory signal and its neural correlates shows that the signal was $\approx$0.1% of the steady-state level at the time of detection, corresponding to a change in the total spikecount across all afferents of $\approx$0.05%. Due to the regularization of the spikecount over behaviorally relevant time windows, this change may be detectable. Using a simple threshold on the total spikecount, I estimated a neural detection time and found it to be indistinguishable from the behavioral detection time within statistical uncertainty. These results will be useful for understanding the neural and behavioral principles underlying sensory acquisition (http://soma.npa.uiuc.edu/labs/nelson/public_resources.html).

Dedicated with love to my parents, Les and the memory of Diana, who allowed me to avoid letting school get in the way of my education

I owe much gratitude to my advisor Mark Nelson for his tremendous vision and intellect in guiding my thesis work. In addition, Mark has been very supportive during a number of personal trials I went through over the course of working in his lab, for which I am very grateful. Mark gave me the freedom to pursue a large variety of things—from behavior, easily the hardest part of my thesis work, to electrophysiology, fish mold making and casting, large scale *in computo* experiments, and data visualization with virtual reality. I've had an immense amount of fun doing it all. I would like to thank Noura Sharabash for her dedication and excellence in collecting much of the behavioral data. Thanks to Len Maler, Brian Rasnow, and Chris Assad for many useful conversations and inspiration over the years. Also thanks to Brian and Chris for providing the electric field data on *Apteronotus*. I am grateful to Stuart Levy of the National Center for Supercomputing Applications for his role in bringing the 3D fish tracking data into the virtual reality CAVE at the Beckman Institute. A special thanks to Ben Grosser and the staff of the Visualization, Media, and Imaging Laboratory at the Beckman Institute of Advanced Science and Technology for their assistance with numerous aspects of this project, from video digitizing to 3D digitizing and 3D printing. Their cutting-edge facility enabled the development of some key techniques that otherwise may have taken a few more years to come along. I would also like to extend my gratitude to the Beckman Institute. In addition to providing me with a generous one-year research assistantship to begin research into neuromechanical approaches to sensory acquisition in electric fish, the Beckman Institute has proven an ideal interdisciplinary environment for me. I developed close working relationships with a number of groups in the Beckman, relationships which likely would not have developed were it not for the opportunities for cross-disciplinary interaction afforded by the Institute.

TABLE OF CONTENTS

LIST OF TABLES

LIST OF FIGURES

Figure **Page**

CHAPTER 1

The philosophy and the approach

Infinite space is the sensorium of the Deity

–Sir Isaac Newton, *Opticks*, 1704

1.1 Summary

The sparsity of consumable resources within a mobile animal's domain compels a certain logic, one that all such energy-consuming autonomous agents must follow. In particular, an animal must devise a system for detecting food, and this system must be linked to behavioral programs that will result in its successful acquisition. There are a variety of high-level approaches to understanding this primary condition on adaptive behavior. This chapter discusses the basic logic of autonomous agents and the relationships among the active sense, sensory ecology, computational neuroethology, neuromechanical simulation, and biomorphic robotics approaches. I use this discussion to situate the approach used in

this thesis within computational neuroethology; following that I outline the goals of the research presented in the subsequent chapters.

Key words: computational neuroethology, active sensing, sensory ecology, sensory acquisition, neuromechanical simulations, biomorphic robotics

1.2 The logic of autonomous agents

The sparsity of consumable resources within a mobile animal's domain compels a certain logic that all such energy-consuming autonomous agents must follow. In particular, an animal must devise a system for detecting consumable resources, and this system must be linked to behavioral programs that will result in successful acquisition of those resources.

After a far-field object registers on the sensory apparatus (or "sensorium") of an animal, one of the first things the animal does is align this apparatus to the stimulus by modifying the shape, position, or orientation of its body. If the animal decides to approach the object, this tailoring of behavior to sensory signal needs is continued, but now that it has detected the prey, it must feed its neural algorithms the appropriate temporal sequence of sensory data to achieve adaptive motor output.

To put this approach in context, consider two contrasting general views of animal behavior. The first is the approach just presented, that in behavior there is a close coupling of the shape or movement of sensor arrays to the signal requirements of the nervous system; the nervous system uses these signals to direct additional sensing of and behavior toward the object of interest. This emphasis on sensory acquisition behavior is sometimes referred to as the active

sensing approach. The focus on sensory systems and their signal environment has antecedents in ecological psychology (Gibson, 1979), and it also distinguishes a newer methodology called computational neuroethology, as will be discussed below.

The second general model of animal behavior assumes that sensory systems take the world in passively, the information flows to the brain to form rich internal representations of that world, and the animal subsequently acts on the basis of that rich internal model. For example, David Marr (1982) begins his book on vision with the statement that "vision is the process of discovering from images what is present in the world, and where it is"; this is what Andrew Blake calls "a prescription for the seeing couch potato" (Blake, 1995). In contrast, in the active sensing view, behavior is tightly coupled to sensing, and behavioral programs operate on minimalist representations of the world that are computed from changes in the sensory information reaching the animal as it manipulates its body, and thus its biological sensor arrays, through space. Thus, behavior is no less dependent on sensing than sensing is on behavior.

Some of the differences between the active sensing view and the rich internal model approach are made especially clear when considering what animals need, at a minimum, in order to acquire food. In resource acquisition behavior, neither *what* the object is nor *where* it is in space necessarily figures in the initial process. Rather, an indistinguished blip emerges out of the noisy hash of background stimulation, and behavioral processes are engaged to give the sensorium better purchase on the weak and diffuse signals caused by the object's presence. Eventually a behavioral program for acquiring the resource may be engaged. The needs of that behavioral program may be as limited as knowing that it is better to be closer than further away, and that moving the body in such-and-such a way will accomplish this. By zeroing the

azimuth of the stimulus (often accomplished by simply balancing a stimulus being received by bilaterally symmetric sensor arrays; see Hinde, 1970 and MacIver et al., 2001) and elevation of the target relative to the axis of forward motion, an animal can turn a three-dimensional localization problem into one of gradient ascent on the intensity of the sensory signal, something close to a one-dimensional localization problem (for a model of how this may work in the bat, see Kuc, 1994). The need for a more precise fix on the target increases near the end of a capture trajectory. Accurate localization in this phase is in part driven by the need for a prediction that will be robust to sensory occlusion (for example, the acoustic blind spot at the end stage of bat capture sequences, when the inter-echo interval is shorter than the system can process). In the end phase, the sensory signal strength increases due to reduced distance, and for some active sense systems, also due to modifications in signal output (increased pulse rate in bats and pulse-type electric fish). In addition, regional specializations of receptor layout for increased spatial resolution near to the mouth greatly aid capture. For example, in the head region of the black ghost weakly electric fish, receptor density is increased by an order of magnitude from the trunk region where the prey is detected (Fig. 5.3). There is a good reason for our eyes being positioned on our heads near our mouth instead of on our knee caps (besides the problems this arrangement would bring to activities like gardening and washing floors).

While the combination of sense energy physics with behavioral and receptor distribution factors improves resolution in the terminal phase, various capture strategies also allow for the inaccuracy bound to occur in obtaining the intersection of two moving objects in space: the large surface areas of the tail membrane and sometimes wings of echolocating insectivorous

bats are used for catching and scooping small prey into the mouth, and in many species of fish, negative pressure in the buccal cavity is used to suction prey into the mouth.

1.3 The different senses of active sensing

Two quite distinct senses of the word “active” are easily confused. The first has already been discussed: active sensing as a motor strategy for sensory acquisition. The second has a variety of synonymous labels, most confusingly “active sensing,” but also “active sensory system,” “sensing in the active mode,” and in engineering, “active sensor.” What distinguishes this sense of active from the motor strategy sense outlined above is that it is meant to indicate that the animal provides the source of energy for sensing (in engineering, the source would be the sensor or nearby transmitter). In biology, this energy is created in a variety of ways, such as electric fields in electric fish, sound pulses in echolocating bats, mechanical stimulation caused by purposeful manipulation of a tactile sensor around an object (as when rats rhythmically sweep their whiskers over something of interest), and the purposive creation of water flows around objects by body movement that are then sensed by the mechanoreceptors of the superficial and canal neuromast systems (as in the hydrodynamic imaging system of the blind cave fish). Animal’s can also emit signals which result in the creation of extrinsic sense energy in a different sensory modality. For example, this may occur with certain low-frequency discharges of the nocturnal strongly electric Nile catfish—discharging at a low rate saves energy, and causes a startle response in sleeping prey, leading to the creation of mechanosensory cues that the fish can use to locate the prey in the dark (Moller, 1995, p. 63). While the energy is extrinsic, it would not occur were it not for the signal emissions of the catfish, and thus is simi-

lar to the catfish being the direct source of the sense energy. I have not seen cross-modal active sensing discussed in the literature, but it is worth considering how often the strategy of manipulating the behavior of other animals so that they will provide useful sensory cues is utilized. In engineering, there are a variety of active sensing systems, such as radar and laser range-finding scanners. When a sensory system is operating in the passive mode, the source of energy for sensing is not created or caused by the animal. For example, mammalian visual systems, most auditory systems, and chemosensory systems most often function passively, absorbing ambient energy and transducing it into neural activity.

In biology, animals that are able to sense in the active mode can be particularly rich model systems for studying the neural and behavioral basis of sensory acquisition, perhaps because movement of the body modifies the position of the sensors relative to the target as well as the manner in which the target interacts with the signal being created by the animal. However, the human visual system, operating in the passive mode in all but unusual circumstances such as when wearing a headlamp in the dark (or in old paintings depicting the ancient theory of visual perception that we see by way of light coming out of the eye), has been a key domain for understanding the computational role of motor strategies for sensing in higher vertebrates (Blake and Yuille, 1992, review: Blake, 1995).

Because sensors are indiscriminate as to whether a given signal is extrinsic or intrinsic to the animal, as long as the energy falls within their transduction pass band, it is preferable to refer to sensory systems as working in a passive or active “mode” (Montgomery, 1991), rather than as being passive or active sensory systems—this allows us to refer to active and passive modes of the same sensory system without seeming to confuse their “true” function. For ex-

ample, one and the same receptor on weakly electric fish, part of what is usually referred to as the animal's active electrosensory system, is sensitive to the fish's own discharge for sensing distortions caused by objects (active mode), but it is also utilized to sense the discharges of nearby conspecifics for communication or predation (passive mode). By way of contrast, in the engineering of systems that operate with active sensors, the designer can have the equipment emit a signal that is unlike any naturally occurring source, and the sensors can be narrowly tuned to this unique signal to reduce interference. In this case, the sensors would be unable to operate in a passive mode under natural conditions, because by design there are no naturally occurring signals in the sensor's passband. In biology, this solution to the problem of emitted signal interference is not as easy to obtain. For animals sensing in the active mode, interference from conspecifics is reduced by rapid attenuation of the signals, spacing between conspecifics, individual differences in the emitted signal, and in the case of electric fish, frequency shifting to avoid electrolocation interference when in close proximity (the jamming avoidance response, see Heiligenberg, 1991 for a review).

1.4 Sensory ecology from an alien perspective

An animal's mechanics and sensor arrangement typically dictate a preferred axis of motion through space. As the animal moves through space along this axis, in search of resources or in avoidance of threats, the sensors on the periphery of the animal are continually stimulated by the forms of energy to which they are attuned. Waves of compression and rarefaction stimulate mechanoreceptors in the ear; water flow stimulates mechanoreceptors on the surface or in the lateral line canals; air flow stimulates the sense organs at the base of hairs; magnetic fields

stimulate magnetoreceptors or induce small currents that stimulate electroreceptors; electrical fields stimulate electroreceptors; gravitational fields stimulate the mechanoreceptors in orientation sensors; electromagnetic energy in the visible and UV bands stimulates photoreceptors; heat or cold stimulates thermoreceptors; molecules in gas or liquid phases stimulate chemoreceptors in olfactory and gustatory systems; and physical contact stimulates a variety of haptic receptors on the body surface.

For each of these common modes of animal stimulation, the attuned population of sensors is generally quite restrictive about the signals they will transduce into a form usable by the nervous system. Insight into the basis of this selectivity can be found by consideration of the animal's sensory ecology. Our region of photosensitivity matches the peak of the Sun's power spectral density distribution. Ampullary electroreceptors are tuned to respond to fields of 0-50 Hz, which is the frequency range of the bioelectric fields of prey. Tuberous electroreceptors, found on animals that generate electric fields, only respond to fields with spectral properties similar to those of the animal.

The utility of taking sensory ecology seriously goes far beyond insights into the basis of sensor selectivity. To illustrate this point, imagine the following scenario: An alien arrives on Earth and discovers a Pentium III chip lying on the ground. Initially, it is unclear if this is something dangerous, possibly alive, or simply a chunk of useless plastic and metal. The alien goes about systematically trying to discover what it is. It may try chewing on the chip, throwing the chip against a tree in an attempt to obtain a response from this multipedal entity, or other such perturbations. After considerable investigation, the alien discovers that the pins (of which there are just under 300 in a Pentium III) are for sensing applied voltages, and that voltage

levels within certain bands have special significance (in this case, CMOS voltage levels for zero and one). After many more years of investigation, the alien discovers that by strobing the pins with these voltages, with a particular sequence of patterns applied at the rate of a billion voltage changes per second, some very interesting behavior emerges from the chip. Clearly, if the alien had discovered the chip within a computer that was performing data processing, this understanding would have been obtained in much less time.

In neuroscience research dealing with sensory processing and allied structures of the nervous system, we are in a position similar to that of the alien, except here the "chip" has two to four orders of magnitude more pins (sensory input channels) per sensory modality. Thus, traditional neuroscience, which is historically a laboratory science and thus dedicated to the isolation and analysis of natural phenomena under strictly controlled conditions, has problems similar to those of our alien trying to reverse engineer a disembodied Pentium III. An animal is brought into the laboratory, and artificial signals that are easy to generate and analyze, and usually several orders of magnitude stronger than those typically encountered by the animal, are applied to the sensory system under study. These signals are delivered in some convenient fashion, which can entail flooding the entire sensory array. The animal's response to such signals, whose spatiotemporal pattern has little in common with what the system evolved to process, is not likely to elucidate what its nervous system might be doing in its natural context. Concerns of this kind led to the development of neuroethology, which is historically a combination of two very different traditions: the field science of ethology and the laboratory science of physiology. Neuroethology attempts to be sensitive to the conditions under which a nervous system best operates by attending to issues of evolution, ecology, and ethology. Information about these

conditions is used to devise laboratory experiments that are a compromise between field observation of natural behavior and the isolationist experimentation of traditional neuroscience, with its emphasis on simplicity of analysis over ethological and ecological appropriateness.

One goal of this thesis is to follow the lessons of the parable of the chip and neuroethology by going beyond a qualitative appreciation of sensory ecology to the synthesis of measurements with computational models for a quantitative estimation of what every sensor on an animal's body receives during a natural behavior. This work, which could be called quantitative sensory ecology, can be equated to providing the alien of our example with time series data for all the inputs to a Pentium III chip while it is running a commonly executed program within a computer. We can use the estimate of sensor input, along with a computational model of how this is transformed into neural activity for input to the brain, to estimate the full spatiotemporal pattern of the neural data stream during natural behavior. In this thesis I couple tracking data from the prey capture behavior of electric fish to detailed models of the sensor input, and a model of the sensor-to-neural activity transformation, in order to estimate the full contribution of one sensory modality ($\approx$14,000 channels) to the brain during natural behavior. To my knowledge, this level of reconstruction of input to the brain during natural behavior has not been previously achieved.

1.5 Computational neuroethology

Computational neuroethology has certain things in common with the active sense approach, but it has a different set of priorities. Like the active sense approach, computational neuroethology emphasizes the coupling of behavior to sensory signal needs. However, the active sense

approach is driven more by engineering goals than by the goal of understanding how animals generate adaptive behavior. Computational neuroethology is an integrative approach to animal behavior which views it as arising out of a tight interaction among the biomechanics of animal bodies, the mechanical properties of the animal's environment, the animal's sensory ecology, and the nervous system. Because of the coevolution and codevelopment of the nervous system and the periphery, there is often matching and complementarity between them. Further, there is matching and complementarity between the nervous system and periphery and the behaviors that the animal undertakes for survival. Computational neuroethology adds to classical neuroethology an emphasis on closing the loop from sensation to behavior by use of integrative computer simulations that are faithful to biology (review: Cliff, 1995; Beer et al., 1998; Webb, 2001).

1.6 Neuromechanical simulations, biomorphic robotics

A natural extension of computational neuroethology is to build physical models. In part, this is to avoid the difficulties (both computational and epistemic) associated with accurate simulations of the mechanical and sensory milieus in which animals are embedded. The idea, in part expressed by "the world is its own best model" (Simon, 1969), is that embodiment has effects that our simulations have difficulty capturing. The topic of whether robots make good models of biological behavior is large: see Webb, 2001 for a good summary of the issues.

One problem with the physical model approach is the host of technical problems associated with building robots, many due to the inadequacy of currently available actuator and sensor technology. Thus, the research may expend more energy on solving these technical problems

than with more fundamental issues. We can begin to reach the ideal of building physical models by incorporating mechanics into our simulations. In motivating their departure from traditional simulations of isolated nervous systems, Örjan Ekeberg et al. remarked

> Simulation techniques have been used primarily when analyzing either isolated neuronal systems or sensory systems . . . we will instead focus on simulations of a neural system in which an interaction with the environment is crucial . . . To capture the natural behavior of such a system in a simulation, it is necessary to incorporate a model of the mechanical environment, as well as muscles and the sensory feedback acting through mechanoreceptors (Ekeberg et al., 1995).

One interesting result of neuromechanical simulations of the lamprey is the discovery that locomotion through changing hydrodynamic environments appears to depend on the modulation of the feedforward locomotion signals by feedback from stretch receptors embedded in the trunk muscles. The lamprey's neural central pattern generators can provide the necessary locomotory signals in an open-loop, feed-forward manner for unchanging hydrodynamic conditions (Ekeberg et al., 1995).

It is unsurprising that the role of mechanical feedback from the environment would only come to light in simulations that go beyond the isolated nervous system. It is, however, also clear that simulations are in some cases not enough to arrive at an understanding of phenomena both difficult to measure and observe (and thus, to permit the derivation of a computational model), and difficult to simulate in principle (fluid dynamics, for example). In these cases, biomorphic robotics can provide a powerful tool for advancing our understanding. For ex-

ample, when we consider the difficulty of studying and simulating the vortices that some fish use to increase their swimming efficiency, it is unsurprising that the understanding of this phenomenon became clearer with the building of robotic fish (Triantafyllou and Triantafyllou, 1995). The activity of building biomimetic or bio-inspired robots, usually now referred to as biomorphic robotics, has an obvious role to play in these cases. Motivated by these considerations, near the end of my thesis research I began a biomorphic robotics approach to understanding electrosensory signal acquisition in electric fish (MacIver and Nelson, 2001, Appendix B in this work). Biomorphic robotics is part of the more general field of biomorphic engineering, and it shares biomorphic engineering's dual allegiances to developing better technology and advancing scientific understanding (MacIver et al., 1999, Appendix C in this work).

1.7 The research goals of this thesis

A crucial component of adaptive behavior is sensory acquisition. Investigation of how the body and brain work in tandem to acquire sensory information is hindered by the limited number of sensory surface tracking techniques, few of which provide data on the position of the entire body surface. This research has also been rendered more difficult by our inability to measure the thousands of afferents stimulated during behavior. In this thesis, I present research on sensory acquisition in weakly electric fish of the genus *Apteronotus*, where I have overcome the first barrier by developing an accurate markerless animal tracking system and have deployed a computational approach toward overcoming the second barrier. I have developed an integrative computer simulation that utilizes animal tracking data to estimate the full

sense data stream (≈14,000 channels) during a natural behavior, placing this work firmly in the realm of computational neuroethology. Utilizing the tracking system, behavioral experiments, and the integrative computer simulation, I undertook to answer several key issues of sensory acquisition in *Apteronotus*, including:

- how the animal manipulates its sensory surfaces prior to and following prey detection (Chapters 3, "Body modeling and model-based tracking for neuroethology," and 4, "Motion analysis and effects of water conductivity")
- what type of sensory energy the animal utilizes for sensing prey (Chapter 4, "Motion analysis and effects of water conductivity," and Appendix A, "Receptor blockade with Co^{++}: physiology and behavior")
- what the typical sensory signal magnitudes are at the time of prey detection (Chapter 5, "Sensory signal estimation")
- during prey capture behavior, what the spatiotemporal profiles are of a) the signals going to the sensory receptors; and b) following transduction, the firing rate changes occurring on the afferents to the brain (Chapter 5, "Sensory signal estimation")

In the following chapter, I will provide the background on weakly electric fish necessary to elucidate the meaning of the results. [1]

[1]This chapter benefitted from comments from Tony Lewis, Mark Nelson, Scott Robinson, Giulia Bencini, and Timothy Horiuchi on earlier drafts.

CHAPTER 2

An overview of weakly electric fish

2.1 Summary

The ability to sense electric fields is one of the most recently discovered sensory modalities. One organism that is especially dependent on this sense is the weakly electric fish. This animal has become a leading model system for understanding the behavioral and neural basis of sensory acquisition in vertebrates. This chapter briefly reviews some of the history of electrosense and provides some of the background helpful to an appreciation of the unique abilities of weakly electric fish.

Key words: bioelectricity, electrogenic organisms, strongly electric fish, weakly electric fish, electroreception, electrolocation

2.2 History

The history of our interaction with organisms that generate electric fields (hereafter referred to as electrogenic) is a fascinating story of an ancient "pre-ontological" (Heidegger, 1977, p.27) encounter with a strange sensation, which over many centuries slowly became understood to be due to the phenomena of electricity. Electrogenic organisms, along with the occasional static discharge and lightening strike, provided experiences with electrical phenomena long before the nature of electricity was understood. The sensations caused by animals such as the strongly electric marine *Torpedo* and Nile electric catfish were variously ascribed to coldness (because of the numbing of sensation, similar to the effect of cold), or poison (Wu, 1984).[1]

After the invention of the Leyden jar in 1745, and the discovery that the jolts provided by that device had much the same feel as those from certain aquatic animals, there ensued a rapid increase in our understanding of bioelectricity. By 1775, the electrical nature of the discharges of the marine *Torpedo* and the fresh water electric eel had been established, and Joseph Priestly suggested that presence of electricity was not confined to these animals. Shortly afterwards, in 1781 Felice Fontana, a professor of natural philosophy in Pisa and Rome, suggested that muscles are activated through electrical means. Ten years later, Galvani made his discovery that the muscles of frogs could be made to contract by connecting the nerves of the muscles simultaneously in series with two different metals and the animal's spinal cord. Galvani believed, in analogy to the Leyden jar, that living cells in the animal's brain could generate electricity, and that the electricity was transmitted by nerves to muscles and stored there. Upon contact

[1] Much of the remainder of this section is summarized from Wu (1984) and Moller (1995).

with metal, the stored electricity was released and caused a muscle contraction. Volta later created an extended battle with Galvani by arguing that the contraction was not due to intrinsic electricity, but due to extrinsic electricity caused by the dissimilar metals. We now know that Volta was correct in that the contraction was elicited by the extrinsic electricity, but Galvani was also correct in that the contraction could not occur were it not for the intrinsic electrical phenomena involved in nerve conduction and muscle contraction. In 1800 Volta, in one of the first successes of biomorphic engineering (Appendix C), designed what he called an "artificial electric organ," very similar in appearance and structure to the electric organ of the *Torpedo*. It was the first battery.

This history shows the important role of strongly electric fish in the development of our understanding of electricity. The maverick Russian physiologist Babuchin reversed the historical flow of understanding from fish to electricity when he used the electrical properties of nerve and muscle to show that the term "pseudo-electric organ" for a structure in an African fish was a misnomer. In 1877 Babuchin conducted what is in a sense the inverse of Galvani's experiment, using the twitch of a freshly dissected frog's sciatic muscle as a voltmeter to show that a pet *Mormyrus* generated weak electrical discharges (Moller, 1995, p. 27).

The first indication that some animals had the ability to sense electric fields came from John Walsh's experiments with the *Torpedo* and electric eel (*Electrophorus electricus*) in the 1770s and 1780s. In these experiments, two wires were placed into a vessel containing an electric eel. The wires were led out of the vessel and brought to a place out of sight from the eel. At this point, shorting the wires together had a dramatic effect on the eel, resulting in it orienting to the wires and emitting a strong discharge. The ability of some fish to sense changes

in their electrical environment was not explored again until almost 200 years later, when Hans Lissmann became interested in a weakly electric fish, the African *Gymnarchus niloticus*. This interest was due to a visit to the London Zoo (Moller, 1995). At the zoo, Lissmann saw a *Gymnarchus* swimming backwards, easily avoiding obstacles while doing so. Just a few tanks down from there, he observed an electric eel similarly swimming backwards and avoiding obstacles. This brought him to recall 1) von Buddenbrock's suggestion in 1950 that electric eels have to swim by means of a long anal fin because their trunk muscles have been used up to form the massive electric organ; and 2) a mention, by Erdl in 1847, of a small presumed electric organ in *Gymnarchus*.

In that context, Lissmann decided to investigate *G. niloticus*, and discovered in 1958 that these animal's are able to sense and discriminate objects differing only in their electrical properties (Lissmann, 1958; Lissmann and Machin, 1958). Additional work by Bullock, Szabo, Hagiwara, Enger, and Lissmann in the 1960s established the new modality of electroreception, and in 1971 the term "electroreceptor" was adopted for the sense organs mediating the detection of electric fields (Kalmijn, 1988).

2.3 Electroreceptors

The ability to sense electric fields is due to two morphologically distinct classes of electroreceptor. In this section, "electroreceptor" will be used synonymously with the more accurate "electroreceptor organ" (the transduction cells form buds within the receptor organ, similar to the transduction cells within taste buds). The first class, called "ampullary recep-

tors," are sensitive to electric fields with frequency components from 0 Hz (DC) to ≈50 Hz, the approximate range of bioelectric fields from aquatic organisms that are often eaten by electrosensitive animals, and mediating low frequency electrosense. These receptors are sensitive in the 0.001 $\mu V \cdot cm^{-1}$ range in marine organisms, and in the 0.1 $\mu V \cdot cm^{-1}$ range in fresh water organisms. The fresh water and marine forms of these receptors have interestingly different morphologies to account for different water-skin impedance properties (Bullock, 1973). In weakly electric gymnotid fish of the kind considered in this thesis, there are on the order of a few hundred of these receptors scattered over the body surface. In the non-electrogenic (but electrosensitive) paddlefish, there is a very high density on the flattened rostrum, containing many thousands of these receptors.

The second class of receptors, called "tuberous receptors," are sensitive to electric fields with higher frequency components, from ≈100-2,000 Hz, mediating high frequency electrosense and tuned to be most sensitive to the spectral properties of the field generated by the animal (these receptors primarily occur on weakly electrogenic animals) (review: Zakon, 1986; Bennett and Obara, 1986). They are sensitive to changes in the edogenous field in the range of 0.1 $\mu V \cdot cm^{-1}$ (Rasnow, 1996). On *Apteronotus*, there are on the order of ten thousand of these receptors on the surface. In *A. albifrons*, the highest density is on the head, 10-20 receptor·cm^{-2}, with a steep decline around the operculum to 2-4 receptor·cm^{-2} on the ventral and dorsal edges, and 1-2 receptor·cm^{-2} on the lateral surface of the trunk. A scanning environmental electron micrograph of the outer surface of a tuberous receptor is shown in Fig. 5.2, and the variation in receptor density for *A. albifrons* is shown in Fig. 5.3.

There are several varieties of tuberous afferents with distinct response properties. The one that is the focus of this work is called a probability (P-type) coder. This neuron responds to input by varying its firing rate up and down from a certain probability of firing on each EOD cycle. In *Apteronotus*, the probability is 1/3: thus, with typical EOD rates of 1 kHz, the baseline firing rate is 333 spike $\cdot$ s^{-1}. When the voltage across the skin increases, the probability of firing increases. P-type afferents therefore convey information about the strength of a stimulus. Almost all the tuberous receptors on the trunk of *Apteronotus*, where prey detection typically occurs (Fig. 4.6) are of this type (Hagiwara et al., 1965; Szabo and Yvette, 1974). Another type of tuberous afferent is for conveying timing or phase information (T-type). These fire one spike at a fixed phase of each EOD. The information is conveyed along a pathway that has special adaptations for preserving this precise temporal information. This phase information is believed to underlie the animal's ability to detect the capacitance of objects, which may provide cues for detecting the high capacitance of live food (von der Emde, 1998).

Ampullary receptors are found on a large number of different organisms, including lamprey, coelecanths, sturgeon, paddlefish, catfish, electric eels, all weakly electric fish including the African mormyrids and South American gymnotids, rays, skates, and sharks. The ability to generate weak electric fields is largely limited to two families of fish, the mormyrids and gymnotids; thus, tuberous receptors are present on members of these two groups. The strongly electric eel is one of the few strongly electric fish known to have tuberous receptors. These mediate the sensing of a weaker discharge whose function is not fully understood, but may be for sensing objects or perhaps for electrocommunication.

2.4 The electric field source

In electrogenic organisms, there is a structure that is typically located in the tail, extending rostral to the operculum in some species, which generates the electric discharge. This is called the electric organ. It consists of modified muscle cells in most species. In *Apteronotus*, the fish studied for the research presented here, the organ consists of modified neurons. In both cases, a special structure in the brain synchronously depolarizes the innervated surface of the electric organ cells. The other side remains inactive, with the result that a each cell represents a $\approx$60 mV battery. Sufficient numbers of these, depolarized in a synchronous manner, can generate up to a maximum of $\approx$700 V in the electric eel. In weakly electric fish, the organ produces a field with a maximal strength of 10-100 mV $\cdot$ cm^{-1} (review: Bennett, 1971; Bass, 1986). The form of the discharge varies from quasi-sinusoidal and continuous (in "wave-type" electric fish, such as *Apteronotus*), with a duration of $\approx$1 ms, to pulse-like and discontinuous (in "pulse-type" electric fish, such as *Brienomyrus*), with a duration of $\approx$0.1 ms. The spatial structure of the RMS of the field norm for *A. albifrons* is shown in Fig. 5.4.

The role of the electric organ discharge (EOD) is diverse and varies with species. In strongly electric fish, it typically has in part a predatory role, if not to immobilize the prey possibly to startle them so that they can be sensed with the mechanosensory lateral line (hypothesized for the low frequency volley of the strongly electric catfish *Malapterurus*, Moller, 1995, p. 63). However, in all electrogenic fish, social and other non-predatory roles for the EOD have been found (review: Moller, 1995). In weakly electric fish, the use of the EOD

appears primarily limited to communication (review: Kramer, 1990) and the sensing of objects that differ in impedance from the water (electrolocation, discussed below).

2.5 Locomotion and body plan

This section will focus on gymnotids, the South American weakly electric fish. Gymnotids are nocturnal animals that inhabit turbid waters. They have evolved a unique, bi-directional propulsion system that is well suited to sensing prey nonvisually. As discussed further in Chapter 4, this system allows them to swim backward to capture a prey that was dectected during forward motion. We and others have also observed the fish hunting while swimming backwards. The ability to swim forwards and backwards is due to a ventral ribbon fin that runs most of the length of the body. They send traveling waves down this fin according to the direction of desired movement: they can also hover by sending traveling waves from tail to head and from head to tail simultaneously.

The knifelike body plan of these fish has caused considerable speculation. It allows the fish to hold their trunk rigid while swimming. This decoupling of trunk movements from locomotion may aid in utilizing trunk bends for sensory acquisition; alternatively, by allowing the fish to maintain a rigid signal source, it may ease the difficulty of deconvolving reafferent (sensory input due to the movement of the fish) from exafferent sensation (sensory input due to external changes). In this regard, it is interesting to note that Notopterids, which inhabit densely vegetated river banks similar to many gymnotids, have the same body plan but do not

generate an electric field (they also have ampullary receptors to passively detect live prey). This issue is considered further in Section 4.5.5.

2.6 Electrolocation

There are at least three different types of electrolocation, corresponding to active and passive modes of tuberous-mediated electric field sensing, and to the passive mode of ampullary-mediated electric field sensing (reviews of active mode electrolocation: Bastian, 1986, 1994, 1995a; von der Emde, 1999). In the active mode of tuberous, or high frequency, electrosense, objects that differ in impedance from the surrounding water disturb the field created by the EOD. Objects that have higher impedance than the water cause current lines to go around the object. This reduces the current density near the proximal patch of skin of the fish. By Ohm's law, the reduction in current through the skin causes a decrease in the voltage between the approximately isopotential interior of the body and the exterior, which is separated by a skin with unusually high resistance compared to non-electric fish. Tuberous receptors are arranged on the skin so that one face is open to the exterior, and the other face is adjacent to the isopotential interior. Thus, a reduction in the transdermal voltage causes a reduction in the receptor bias voltage, and a corresponding decrease in firing rate for a P-type afferent. Correspondingly, a conductor near to the body causes an increase in the current density across the skin, This situation is depicted in Fig. 2.1.

As mentioned in Chapter 1, tuberous receptors are indiscriminate about whether the field is intrinsic or extrinsic to the animal. Thus, they can also use their high frequency electrosense

in the passive mode by sensing the electric fields of nearby conspecifics, allowing electrocommunication through modulations of the high frequency discharge such as chirps (rapid changes in the frequency and amplitude of the EOD). In addition, electric fish can use their tuberous sensory system to follow the current lines of an external field back to the originating fish, for predation or aggression (Hopkins et al., 1997).

Current evidence suggests that the ampullary system operates exclusively in the passive mode in weakly electric fish. By sensing the weak bioelectric fields that are present around every prey, the fish can find the prey without visual cues. It is also a common mode of detecting prey in non-electric fish, such as the paddlefish (Wilkens et al., 1997).

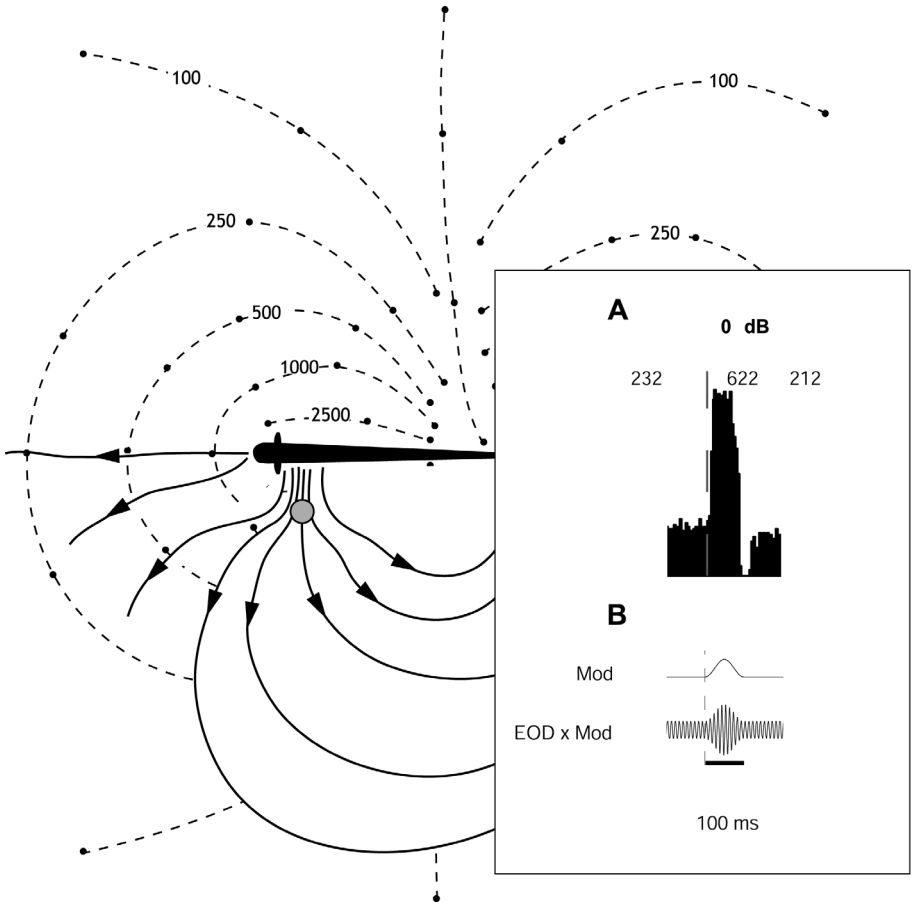

Figure 2.1 Electrolocation of a conductor with afferent response. Field map redrawn from Knudsen, 1975, with isopotentials indicated in μV. The current lines, orthogonal to the field potentials, are shown with arrows indicating current direction during one phase of the EOD. The presence of the conductor causes an increase in the density of current through the proximal patch of skin on the body. Inset (A) illustrates a P-type afferent response to a very large stimulus similar to what would be created by a large conductor brought close (within a millimeter) of the skin. The firing rates of the afferent are indicated during prestimulus, stimulus, and post-stimulus. Inset (B) illustrates the form of the stimulus. The EOD sets up a baseline of oscillating transdermal voltage, and a conductive object induces an increase in the transdermal voltage (Mod) that is superimposed on the EOD (EOD x Mod).

CHAPTER 3

Body modeling and model-based tracking for neuroethology

3.1 Summary

The accurate tracking of an animal's movements and postures through time has broad applicability to questions in neuroethology and animal behavior. In this chapter we describe methods for precision body modeling and model-based tracking of non-rigid animal movements without the use of external markers. We describe the process of obtaining high-fidelity urethane casts of a model organism, the weakly electric knifefish *Apteronotus albifrons*, and the use of a stylus-type 3-D digitizer to create a polygonal model of the animal from the cast. We describe the principles behind markerless model-based tracking software that allows the user to translate, rotate, and deform the polygon model to fit it to digitized video images of the animal. As an illustration of these methods, we discuss how we have used model-based tracking in the study of prey capture in nocturnal weakly electric fish to estimate sensory input during behavior. These methods may be useful for

bridging between the analytical approaches of quantitative neurobiology and the synthetic approaches of integrative computer simulations and the building of biomimetic robots.[1]

Key words: animal tracking; motion capture; casting; moldmaking; infrared; camera calibration; video digitizing; MicroScribe; electroreception; computational neuroethology.

3.2 Introduction

Accurate tracking of a 3-D object from a sequence of time-varying images or sensor readings is an active topic of research in a variety of application areas. The applications are diverse, spanning animal behavior, biomechanics, real-time character animation, gesture-driven user interfaces, sign language translation, surveillance systems, and 3-D interfaces for virtual reality systems. Many of these applications employ marker-based approaches to object tracking. Marker-based approaches rely on the sensing of discrete, spatially localized points or markers on the surface of the object, such as natural body landmarks, attached reflectors, or light-emitting diodes (Kruk, 1997; Spruijt et al., 1992; Winberg et al., 1993; Hughes and Kelly, 1996; Vatine et al., 1998). In contrast, model-based approaches rely on globally fitting a surface model of the object to image or sensor data (Mochimaru and Yamazaki, 1994; Jung, 1997; Gavrila and Davis, 1996; Tillett et al., 1997).

The model-based approach to animal tracking has not received wide application in animal behavior and neuroethological studies. However, it can provide high-resolution data on the time-varying conformation of the entire animal, and may be the best choices in situations

[1]Published as: MacIver, M.A., Nelson, M.E. (2000) Body modeling and model-based tracking for neuroethology. *Journal of Neuroscience Methods*, 95(2): 133-143.

where marker-based systems are impractical or inadequate. In our research on the electrosensory system of weakly electric fish, we use model-based tracking to accurately determine the conformation of the fish's body during prey capture behavior. Model-based tracking allows us to reconstruct electrosensory activation across the receptor array, which provides valuable insights into the neural control of sensory acquisition.

In this chapter, we detail the methodology used for model-based tracking of black ghost knifefish, and discuss general considerations that may be relevant to other applications. First, we describe high-precision casting techniques and methods for the creation of a polygonal surface model based on the cast. Then, we describe how this model is used for tracking fish using a two-camera infrared video system. Finally, we discuss how we link behavioral data from model-based tracking to sensory neurophysiology in our studies. Additional supplementary material on making surface models of animals and the temporal and spatial resolution of video is contained in Appendix D.

3.3 Body modeling

Model-based tracking of an animal requires an accurate quantitative representation of its surface morphology. In this section, we describe procedures for making a physical cast of the animal and creating a 3-D model from the cast. Casting objects is a well developed technical craft (Waters, 1983; Parsons, 1973; Boardman, 1950; Gardner, 1974; James, 1989). Below we describe general casting principles, as well as specific details for casting a black ghost

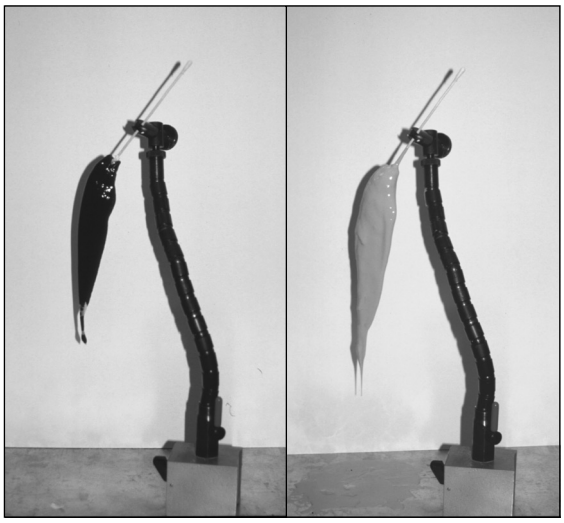

Figure 3.1 Making an RTV silicone mold of a weakly electric fish. (A) The support rod is positioned so that the dorsal curvature of the fish approximates the natural posture in water. (B) During casting silicone is slowly poured on the fish until it covers the entire surface. Several layers of casting compound are added, with enough time between layers for the silicone to partially cure.

knifefish (*Apteronotus albifrons*). The specimen shown in Figs. 3.1 and 3.2 was 190 mm long and weighed 30 grams.

3.3.1 Preparing the specimen

Preparation for casting begins by obtaining a fresh, clean specimen. In our case, an adult *A. albifrons* was euthanized with an overdose of tricaine methanesulfonate (MS-222, Sigma, St. Louis MO USA). The surface of the fish was cleaned with a mild detergent and a soft brush to remove mucus. If accurate casts of the fins are desired they may be fixed with formalin prior to making the mold (McHenry et al., 1995). For our electrosensory research, the sensors of interest are not present on the fins so we were less concerned with this detail.

3.3.2 Posing the specimen

A typical posture of the behaving animal should be selected as the canonical posture in which it is to be cast. Prior to posing the animal for casting, we posed a recently euthanized fish by floating it on its side, directly above a reference grid in water just covering its surface. This allowed us to reproduce the natural dorsal-ventral curvature of the fish's spine. Reference photographs were then taken for correction of distortions created during cast creation (see section 3.3.6).

After taking a set of reference photographs, the animal is posed for creation of the mold. We approximated the natural posture of the knifefish in water by suspending it in mid-air at an appropriate angle to reproduce the natural dorsal-ventral curvature (Fig. 3.1A). To suspend the animal, a section of 3 mm (diameter) wooden dowel was placed into the mouth and 3 cm into the gut. A rapid curing urethane (TC 806 A/B, BJB Enterprises Inc, Tustin CA USA) was injected into the oral cavity to hold the support rod in place.

3.3.3 Selection of moldmaking and casting compounds

Two-component room temperature vulcanizing (RTV) silicone elastomer is often an excellent choice for the moldmaking material because it provides high reproduction accuracy, long mold shelf life, does not normally require the use of mold release agents, and is compatible with a large variety of casting compounds and pouring temperatures. Tests have shown that silicone elastomer can capture surface features of 0.1-0.3 μm reliably (Bromage, 1985). There are many commercial silicone elastomer varieties and additives, giving different setting times,

demolding times, pouring viscosities, cured hardnesses and elasticities. We used Rhodorsil V-1065 with Hi-Pro Blue catalyst (Rhodia Silicones VSI, Troy NY USA) for the flexibility, high tear strength, low shrinkage, and long shelf life of the resultant mold.

There are a larger number of potentially useful casting agents that can be poured into the finished mold to create the cast. Urethanes, silicone elastomers, and molten polyvinyl chloride (PVC) gels can be used for generating rigid and flexible casts. The stiffness of the cast can be controlled through the use of diluents and additives. Flexible PVC casts have been used for biomechanical studies on the role of body stiffness in fish swimming (McHenry et al., 1995). Because we used a contact 3-D digitizer (section 3.3.6 below), our application required a rigid cast. We selected a particular rigid urethane casting material (TC 806 A/B, BJB Enterprises Inc, Tustin CA USA) for its low uncured viscosity, which allowed it to seep into the thin sections of the mold.

3.3.4 Design and construction of the mold

Molds can be made in one-, two-, or multi-part configurations. When the topology of the animal permits it, a one-part mold can be constructed by simply coating the animal with several layers of the mold compound. In general, a one-part mold can be used whenever the object does not contain significant undercuts—indentations that allow the cast surface to get a locking grip on the mold (James, 1989). Because of the streamlined form of knifefish, we were able to use this type of mold.

Prior to coating the fish with the mold compound, Rhodorsil V-1065 silicone elastomer and Hi-Pro Blue catalyst were mixed in a 10:1 ratio, as specified by the manufacturer. Generally, it

is recommended that the mixture be degassed to remove small bubbles trapped in the mixing process, but we did not find this necessary.

The silicone mixture was slowly poured over the fish until it was fully coated. Initially, most of the silicone ran off the surface and had to be recovered and poured over again. This process was repeated over approximately 30 minutes, during which time the compound partially cured. Two additional layers were added in this way at approximately 60 minute intervals. The mold was then allowed to cure for several hours (Fig. 3.1B).

The resulting mold was still quite thin, and needed mechanical reinforcement prior to casting to prevent distortions due to the weight of the casting material. In some cases, a surrounding or "mother mold" can be constructed (James, 1989) for this purpose. For our application, the mold was reinforced by wrapping a section of light cotton cloth once around the coated fish. Mold compound was applied to the cloth before it was draped around the mold.

After the reinforced silicone mold had fully cured, thin slices were cut away from the caudal end with a razor blade until the posterior tip of the caudal fin was seen. This creates a vent hole, preventing air pockets from forming in the thin end section of the mold during casting. An extraction slit was cut along the dorsal edge 2 cm from the snout that was just large enough to remove the fish without tearing the mold. The mold was washed thoroughly and dried.

3.3.5 Making the cast

A sprue (pour hole) must be made in the mold to allow entry of the casting compound. A 3 mm diameter sprue was cut through the mold at the caudal end of the extraction slit for the

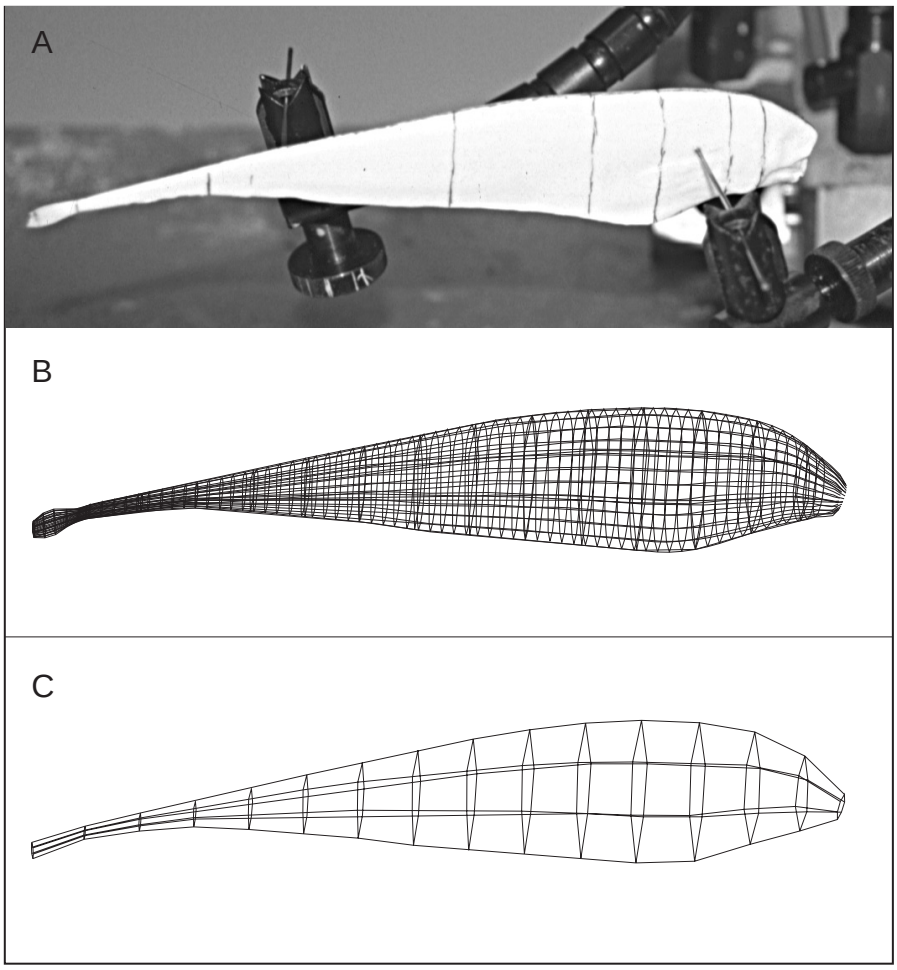

Figure 3.2 Mounting the cast for digitizing its surface and two surface models. (A) Illustration of the mounting of the cast for digitizing. (B) High resolution polygon surface model of *A. albifrons*, 1,540 faces total, 70 longitudinal and 22 around. (C) Low resolution model, 90 faces total, 15 longitudinal and 6 around.

injection of the casting compound with a large syringe. The two parts of the compound were mixed in the 1:1 ratio recommended by the manufacturer. The mixture was not degassed. It was quickly injected into the mold before the material started to set (2 minutes). A small amount of squeezing pressure on the mold was sufficient to prevent cast mixture leakage through the extraction slit. After 4 hours of curing, the cast was carefully removed from the mold, using thin wooden rods pushed along the mold-cast interface to facilitate release. A high quality rigid

reproduction of the fish results (Fig. 3.2A). The surface quality was sufficient to see the lateral line canals and receptor pores (≈ 40 μm diameter) under a light microscope.

3.3.6 3-D digitizing

The next objective is to obtain a quantitative representation of the surface of the cast. The surface representation will serve as the basis for model-based tracking in which the model surface is deformed to match video images of the behaving animal. Obtaining a quantitative representation of a surface involves measuring coordinate values of points on the surface and constructing a best fit surface model that passes near those points. We used a stylus-type contact digitizer with 0.2 mm accuracy (MicroScribe 3DX, Immersion Corp., San Jose CA USA). The digitizer was operated from within a 3-D modeling software package (Rhinoceros 3D v1.1, Robert McNeel & Associates, Seattle WA USA). Prior to 3-D digitizing the cast, it was securely mounted by drilling two small holes in the cast and gluing a short length of music wire in each for external clamping. The resulting setup is shown in Fig. 3.2A.

When using the MicroScribe, the user has to select a set of surface points to be digitized. The selection of these points depends on the requirements of the surface generation functions available in the 3-D modeling software used with the MicroScribe. We used the surface generation function "Sweep2" of Rhinoceros. This function requires two "rail" curves, in our case corresponding to the dorsal and ventral edges of the fish, and multiple cross-sectional curves between the rails to define the conformation of the surface. Fifteen cross-sectional curves were hand drawn on the cast at 2-10 mm intervals depending upon the change in the surface between the cross-sections. Each of the fifteen closed cross-sectional curves

was entered into Rhinoceros by touching the curves with the digitizer stylus, with a point spacing of approximately 1-4 mm depending on the local curvature of the cast. The dorsal- and ventral-edge open rail curves were entered similarly. Following entry, the curves were edited to correct minor distortions due to the moldmaking process, such as unnatural bends in the trunk and abdominal distension due to pooling of fluids. The correction process was facilitated by comparisons to a scaled reference image (see section 3.3.2 above). Information on other approaches for obtaining a quantitative representation of a surface is available at http://soma.npa.uiuc.edu/labs/nelson/model_based_tracking.html.

3.3.7 Creating a polygonal model

The native representation for all objects within Rhinoceros is parameterized nonuniform rational B-spline (NURBs) curves and surfaces (Piegl and Tiller, 1995). While it is possible to develop algorithms to manipulate objects in this format, it is more straightforward to manipulate polygons (Watt and Watt, 1992). We generated two polygonal models from the original parametric representation with two different resolutions. The first polygonal model consisted of 1,540 quadrilateral faces, 70 longitudinal and 22 around (Fig. 3.2B). The second polygon model consisted of 90 faces, 15 longitudinal and 6 around (Fig. 3.2C). The low resolution model was used for tracking where the number of nodes needed to be minimized for usable screen redraw rates, and for initial electrosensory signal reconstructions (see section 3.5.1). The high resolution model is used in some of our electrosensory reconstructions where we need to avoid errors created by the coarse surface discretization of the low resolution model.

3.4 Model-based tracking

Model-based tracking consists of fitting a model of the tracked object to image or sensor data. In our application, we fit the low resolution polygonal model of the fish (Fig. 3.2B) to digitized video images from prey capture sequences. Several aspects of this process will be described: infrared videography, video digitizing, camera calibration, 3-D reconstruction, validation, creation of a parametric fish model, and fitting the model to images. All computations discussed below were performed using MATLAB and the Image Processing, Optimization, and Signal Processing toolboxes (The Mathworks Inc., Natick MA USA), running on a Sun UltraSparc 2 Unix workstation (Sun Microsystems, Inc., Palo Alto CA USA).

3.4.1 Infrared videography

In this section we detail the methods used in video recording the behavior of a nocturnal weakly electric knifefish (*Apteronotus albifrons*) as it hunts for small prey (*Daphnia magna*) in the dark. Fish behavior was observed in an aquarium (383 mm $\times$ 293 mm $\times$ 186 mm) housed within a light-tight enclosure. The aquarium was illuminated with two arrays of 100 high power infrared light emitting gallium arsenide diodes (SIR 333, Everlight Electronics Co. Ltd., Taipei Taiwan). Each diode provides 35 mW of radiant power at a wavelength of 880 nM, which is above the wavelength cutoff for teleost photoreceptors (Fernald, 1988). Fig. 3.3 shows the configuration of the behavioral recording setup. Some aspects of this system are similar to those described by (Rasnow et al., 1997).

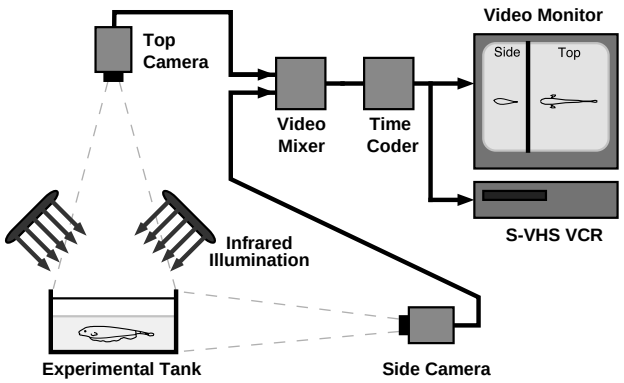

Figure 3.3 Schematic diagram of two-camera infrared video setup. The experimental tank and cameras were housed within a light-tight enclosure.

Activity of the fish and prey was imaged with two black-and-white CCD cameras with infrared blocking filters removed (VDC 2624, Sanyo Fisher Co., Chatsworth CA USA; XC-77, Sony Electronics Inc., Park Ridge NJ USA). These were synchronized with an external signal from a camera adaptor (Sony DC-77RR). A video splitter was used to merge the two signals into one split-screen image (AD1470A, American Dynamics, Pearl River NY USA). A longitudinal time code generator was used to dub a time code display window onto the video (TC-3, Burst Electronics Inc, Corrales NM USA). This provides time-stamping of each field of the behavioral sequence (two fields drawn 16.7 ms apart comprise one video frame). The video signal was recorded on a S-VHS format videocassette recorder (VCR) using S-VHS videotape (AG-7350-P, Panasonic Communications & Systems Co., Secaucus NJ USA; ST-126 videotape, Maxell Corp., New Jersey, USA).

3.4.2 Video digitizing and image processing

Recorded video of animal behavior was played back on an S-VHS player and input to a video digitizing system (Avid Media Composer 1000-7, Avid Technology Inc., Tewksbury

MA USA). Video signals were digitized using the monochrome AVR 77 format and exported as 720 $\times$ 486 pixel 8-bit grayscale TIFF files.

After digitization, a number of image manipulations were performed in order to eliminate motion interlace blur, increase small-object contrast, and resize the image. Motion interlace blur refers to an image distortion created by the way video images are displayed. To reduce flicker, the horizontal scan lines of a video image are drawn in two sets, the first set consisting of the odd-numbered lines, the second set consisting of the even-numbered lines. Thus, there is a brief interval (16.7 ms for video in North America) between adjacent scan lines. Movement within this interval causes motion interlace blur. This artifact was eliminated and the effective frame rate was doubled to 59.94 frames/s by deinterlacing with the missing scan lines interpolated using bicubic interpolation. Each image was then contrast enhanced by subtracting a 2-D median filtering of the image from the original and adjusting intensity values. Finally, the images were resized from 720 $\times$ 486 (non-square TV pixels) to 720 $\times$ 540 pixels. For our studies, video of 120 prey capture events of 1-2 seconds in duration were digitized, resulting in six gigabytes of image data.

Using standard video resolution test patterns we determined the resolving power of the final images to be approximately 1 line/mm along both dimensions, representing the minimum resolvable width of alternating black and white lines. The prey used in our study, 2-3 mm in length, are just resolvable under these conditions. For additional technical information on video resolution see Poynton (1996), Jack (1993), and Young et al. (1995). How to estimate system resolution from camera and recording format specifications and other video information is provided in http://soma.npa.uiuc.edu/labs/nelson/model_based_tracking.html.

3.4.3 Implicit image correction and 3-D reconstruction

Recovering accurate 3-D position information from 2-D camera images is an active topic of research in the field of machine vision. Current methods often employ a model of the camera based on physical parameters such as focal length and principal point (Tsai, 1987). Such methods based on physical parameters of the camera are termed explicit methods. An alternative approach, termed implicit image correction, utilizes a set of non-physical parameters without reference to a camera model. The implicit method is motivated by the observation that the physical parameters of the camera are of little interest when only the relationship between 3-D reference coordinates and 2-D image coordinates is required. Implicit image correction (Heikkilä and Silvén, 1996, 1997) can achieve very high accuracy without the complexity and computational overhead of a rich camera model. We chose to use a simple implicit method, which in our application has the additional advantage that distortions due to water refraction are automatically taken into account.

The geometry of the reconstruction problem for our two-camera system is schematized in Fig. 3.4. The portion of the scene in view for each camera is termed the camera's *window*, while the portion that is finally displayed on the monitor after the video passes through the video splitter is called the *splitter window*. The 720 $\times$ 540 pixel space of the digitized image is the *image coordinate system* (ICS) . We identify two portions of the ICS, the *side viewport* (i, j) and *top viewport* (k, l), corresponding to the area imaged by the the side and top camera splitter windows. The 383 $\times$ 293 $\times$ 186 millimeter space of the tank is the *tank coordinate*

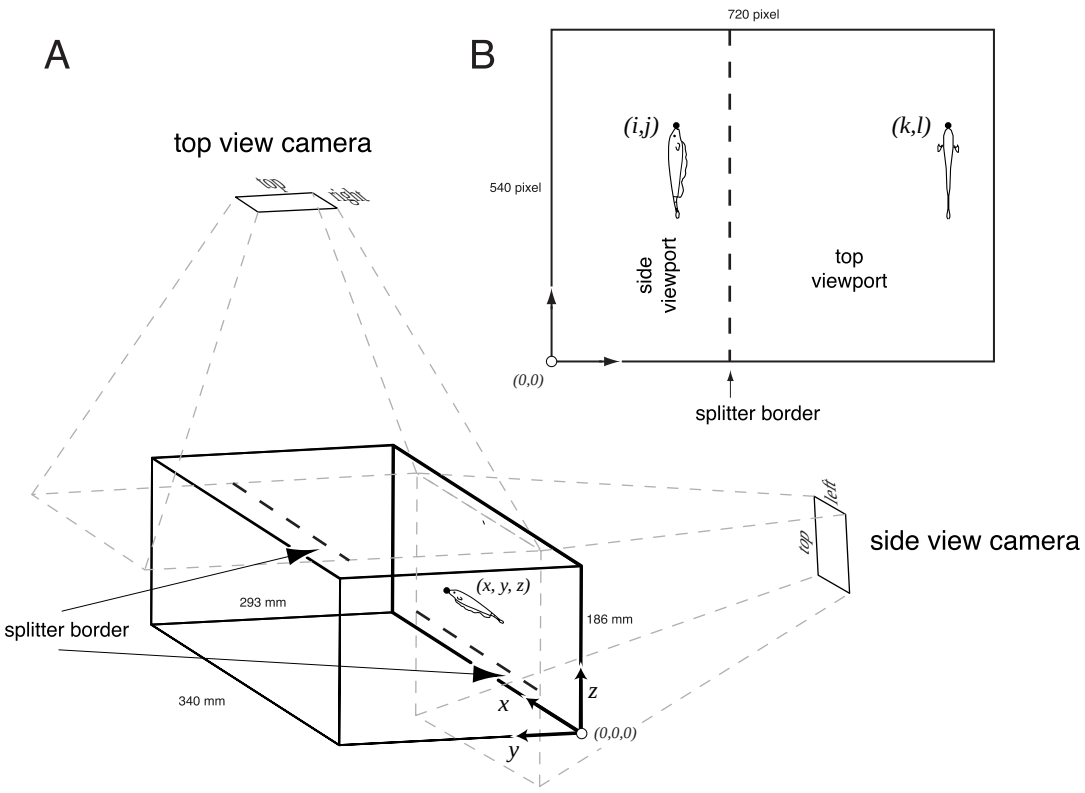

Figure 3.4 The geometry of the 3-D reconstruction problem. (A) The behavioral tank and configuration of the two cameras. (B) Each video image displays two projections of tank objects, as illustrated by the knifefish outline: one in the side viewport and one in the top viewport. The tank (x, y, z) and image coordinate $[(i, j), (k, l)]$ labels for the snout of the fish are shown.

system (TCS). The cameras are positioned so that their sight lines are approximately orthogonal to the face of the tank closest to the camera.

In our implicit image correction method, which does not take into account radial or tangential distortion, the $[(i, j), (k, l)]$ image coordinates are related to the (x, y, z) tank coordinates by the following transformation matrix:

$$\begin{bmatrix} i \\ j \\ k \\ l \end{bmatrix} = \begin{bmatrix} 0 & 0 & -S_i(y) \\ S_j(y) & 0 & 0 \\ 0 & -S_k(z) & 0 \\ S_l(z) & 0 & 0 \end{bmatrix} \cdot \begin{bmatrix} x \\ y \\ z \end{bmatrix} + \begin{bmatrix} b_i(y) \\ b_j(y) \\ b_k(z) \\ b_l(z) \end{bmatrix} \tag{3.1}$$

where $S_{i,j}(y), S_{k,l}(z)$ are scale factors (pixel·/mm), $b_{i,j}(y), b_{k,l}(z)$ are offsets (pixel), $(i, j),\ (k, l)$ are side viewport and top viewport image coordinates (pixel), and (x, y, z) are tank coordinates (mm).

Because of the camera perspective, the scale factors and offsets depend on the distance of the image plane from the camera. Thus the side view parameters (S_i, S_j, b_i, b_j) depend on the tank coordinate y of the imaged point, while the top view parameters (S_k, S_l, b_k, b_l) depend on z.

To measure these distance-dependent scale and offset parameters we populate the proximal and distal planes in both the side and top camera splitter windows with control points using an accurate 1 cm planar grid. The pixel coordinates of the intersection of all grid lines in view within the ICS were measured and recorded semi-automatically using a custom MATLAB script. A constrained optimization function was then called for each of the four sets of digitized and measured calibration points to fit 2-D scaling and offset factors that minimize the aggregate Euclidean distance between the measured and predicted ICS points, where the prediction is obtained by transforming the known TCS coordinates according to Equation 3.1.

Having determined scaling factors at the proximal and distal tank walls in each view, we linearly interpolate to arrive at the appropriate scale and offset factors for intermediate positions. For example, the scale factor $S_i(y)$ for image coordinate i is computed as

$$S_i(y) = S_i^{prox} + (S_i^{dist} - S_i^{prox})\frac{y}{y_{tank}} \tag{3.2}$$

where S_i^{prox} (S_i^{dist}) is the scaling factor for the calibration grid that is proximal (distal) to the camera, y is the coordinate of the point in the TCS, and y_{tank} is the total extent of the tank along the y-dimension. Similar equations apply for other scaling and offset parameters. The model therefore has a total of 16 free parameters: 2 scale factors and 2 offsets for each of four viewplanes (top proximal and distal, side proximal and distal).

3.4.4 3-D reconstruction validation

To validate the calibration and 3-D reconstruction procedures, we digitized 2 s (60 frames) of video of a 150 mm rod being randomly moved through the tank. The (i, j, k, l) image coordinates of a point at each end of the rod were measured. We then inverted Equation 3.1 to numerically solve for the (x, y, z) tank coordinates of each end of the rod. Fig. 3.5 shows a plot of the computed length of the moving rod versus time. The RMS error was 0.48 mm, with a maximum error of 1.0 mm.

The accuracy of the reconstruction is also continually validated during model-based tracking (see section 3.4.5). Correspondence between the two projected polygonal fish models and the position of the real fish provides a cross-check that helps alert the user to unintended

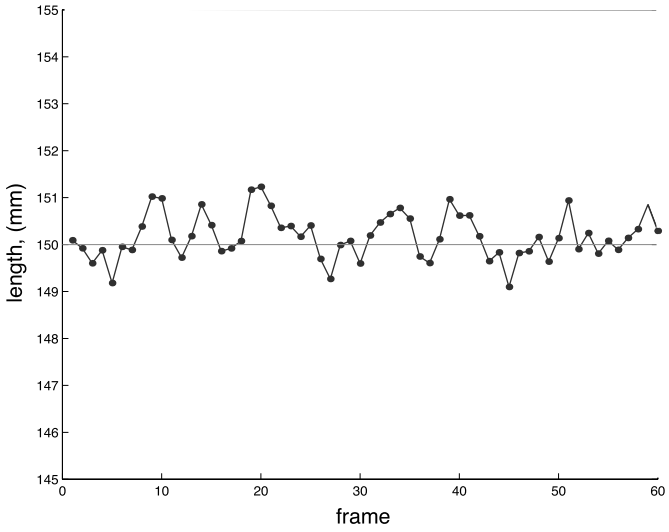

Figure 3.5 Reconstructed test rod length over 60 frames of video. Actual rod length was 150 mm, shown by the horizontal solid line. RMS error: 0.48 mm.

changes in the optical pathway, such as slight shifts in camera position, which necessitate re-calibration of the system.

3.4.5 Creation of a parametric fish model

Having established a method for accurately transforming points between tank and image coordinate systems, we can use the video images to determine the position and shape of the fish during behavioral sequences. Because we are interested in the conformation of a non-rigid object (the fish body) we do not simply digitize key points on the image (e.g. head, tail, fins, etc.). Rather we represent the entire surface of the fish using the polygonal model described earlier. The model is parameterized with suitable degrees of freedom (DOF) to allow it to translate, rotate, and change shape.

We implement six rigid-body DOF: three for position (x, y, z), and three for rotation (roll, pitch, yaw), using standard geometric methods (Mortenson, 1985). Determining the non-rigid

DOF adequate to describe the range of body conformations of interest is an iterative process. In knifefish, locomotion is achieved by generation of traveling waves along the ventral ribbon fin, while the trunk of the fish remains relatively straight or follows a shallow spline-like curve (Blake, 1983; Lighthill and Blake, 1990; Sfakiotakis et al., 1999). We modeled the lateral bend of the trunk with one non-rigid DOF that specified the deviation of the tip of the tail from the midline. The lateral displacement of the body was described by a cubic spline curve, which is widely used in geometric modeling of natural objects (Terzopoulos et al., 1987). The cubic spline was computed with a MATLAB function (de Boor, 1978; Hearn and Baker, 1997). The input points to the spline function were midline points for the non-flexing anterior of the fish body and one point at the tip of the tail. The nodes of the polygonal model were then displaced such that the midline followed the spline curve.

Initial tracking studies using this model revealed that the fish also flexes its spine in a dorsal-ventral plane, a subtle movement we had not previously noticed and which is difficult to see without the visual aid of the overlayed polygonal model. This observation required the use of one additional non-rigid DOF to parameterize the dorsal-ventral bend, modeled and computed in the same manner as the lateral bend. Thus the final model that we used had eight DOF (6 rigid, 2 non-rigid). Using this model we were able to describe the vast majority of the fish's conformations, with rare exceptions such as when the fish briefly enters into an "S" shape. Representing the fish body in this parametric way is compact: rather than save the (x, y, z) coordinates of each node of the polygonal model for each video field, we save only the eight fitted parameters needed to reconstruct the polygonal model's position and shape. When

digitizing prey capture sequences, the 2-3 mm diameter prey (*Daphnia magna*) was modeled using three DOF representing the (x, y, z) coordinates of its center.

3.4.6 Fitting the model to images

Model-based tracking involves determining the position and shape of fish in the tank by manipulating the fish model until its projections are congruent with the imaged fish. First, a representative polygonal model is scaled to the size of the particular individual being studied. Second, a digitized image from the behavioral sequence is displayed on the computer screen within the animal tracking program interface (see Fig. 3.6). The user interface contains eight controls corresponding to the eight DOF of the parametric model. Using the implicit image correction transformation (Equation 3.1), a wireframe visualization of the polygonal model is projected from tank coordinates into image coordinates, resulting in two projected wireframes, one in the side viewport and one in the top viewport. Third, by adjusting the values of the eight DOF, the user moves the polygonal model in the tank coordinate system until the two wireframe projections are congruent with the projections of the real fish on the digitized image. In order to attenuate manual model placement jitter, each adjustment is zero-phase filtered through a digital 5th-order Butterworth filter (6 Hz passband corner frequency). Some aspects of this method are similar to those used by Assad (1997).

In general, it is not necessary to fit the polygon model to every field of the video sequence. In our application, intervals of approximately eight video fields (133.5 ms) are used initially with intermediate positions estimated by cubic spline interpolation of each DOF. A second

Figure 3.6 Snapshot of the animal tracking interface. The sliders adjacent to the image control the (x, y, z) position of the snout; the sliders below control yaw, pitch, roll, lateral bend, and dorsal-ventral bend. The scaling sliders control the subject-specific scaling of the polygonal model. The user navigates through the fields of the behavioral sequence and manipulates the polygonal model so that its top and side viewport projections are congruent with those of the real fish.

pass through the sequence is made to verify the accuracy of the interpolation and set additional fields as necessary.

3.5 Discussion

3.5.1 Linking behavior to neurophysiology

Nocturnal black ghost knifefish (*Apteronotus albifrons*) are able to locate objects without visual cues by sensing perturbations in a weak self-generated electric field (reviews: Bastian,

1986, 1995a; Bullock and Heiligenberg, 1986; Turner et al., 1999). Perturbations in the field caused by objects that differ in impedance from the surrounding water cause changes in the voltage across the skin. These transdermal potential changes are transduced into trains of action potentials by $\approx 10^4$ electroreceptors that cover most of the body surface. By dynamically controlling the positioning of their surface sensory array these fish actively influence the strength and spatiotemporal pattern of the incoming electrosensory signals (Nelson and MacIver, 1999).

In our application, quantitative behavioral analyses of black ghost knifefish and *Daphnia* trajectories allows us to infer properties of the sensory signals reaching the brain through the primary electrosensory afferents during prey capture behavior (Nelson and MacIver, 1999), as detailed in Chapter 5. To characterize the incoming electrosensory signals, fish and prey trajectories were reconstructed at time steps of 16.7 ms. At each time step, we compute the spatial distribution of transdermal voltage changes on the skin based on the physics of electric image formation (Rasnow, 1996). Figure 3.7A shows the resulting pattern of transdermal potential change for a representative prey capture sequence. Note that the electric image is weak and diffuse at the beginning of the sequence and becomes both more intense and more tightly focused as the *Daphni a* comes closer to the electroreceptor array. Based on the estimated transdermal potential change, we then compute the corresponding change in afferent firing rate based on a model of electrosensory afferent response dynamics (Nelson et al., 1997). Figure 3.7B shows the estimated change in afferent firing rate corresponding to the change in transdermal potential shown in Figure 3.7A. These estimates suggested a very low detection threshold of between 0.1-1 μV. Subsequent reanalysis of the afferent spiketrains revealed that the afferents normal-

ize their spike count over behaviorally relevant time windows, an important development that could have implications for other sensory systems (Ratnam and Nelson, 2000).

These electrosensory image reconstructions have also given us a better understanding of the interactions between sensory and motor aspects of active sensory acquisition (Nelson and MacIver, 1999), such as roll behavior (see Chapter 4). We have determined that in the brief period ($\approx$ 600 ms) between the fish's initial reaction to the presence of the prey and the capture of the prey, the fish are able to dynamically change their post-detection posture to compensate for displacement of the prey during the prey strike (MacIver and Nelson, 1999) (see Section 4.5.7). We can conclude that the animal is able to use feedback control of its position during the strike, rather than using a ballistic strike (Gilbert, 1997). Observing and quantifying these behaviors without the use of model-based tracking would have been exceedingly difficult.

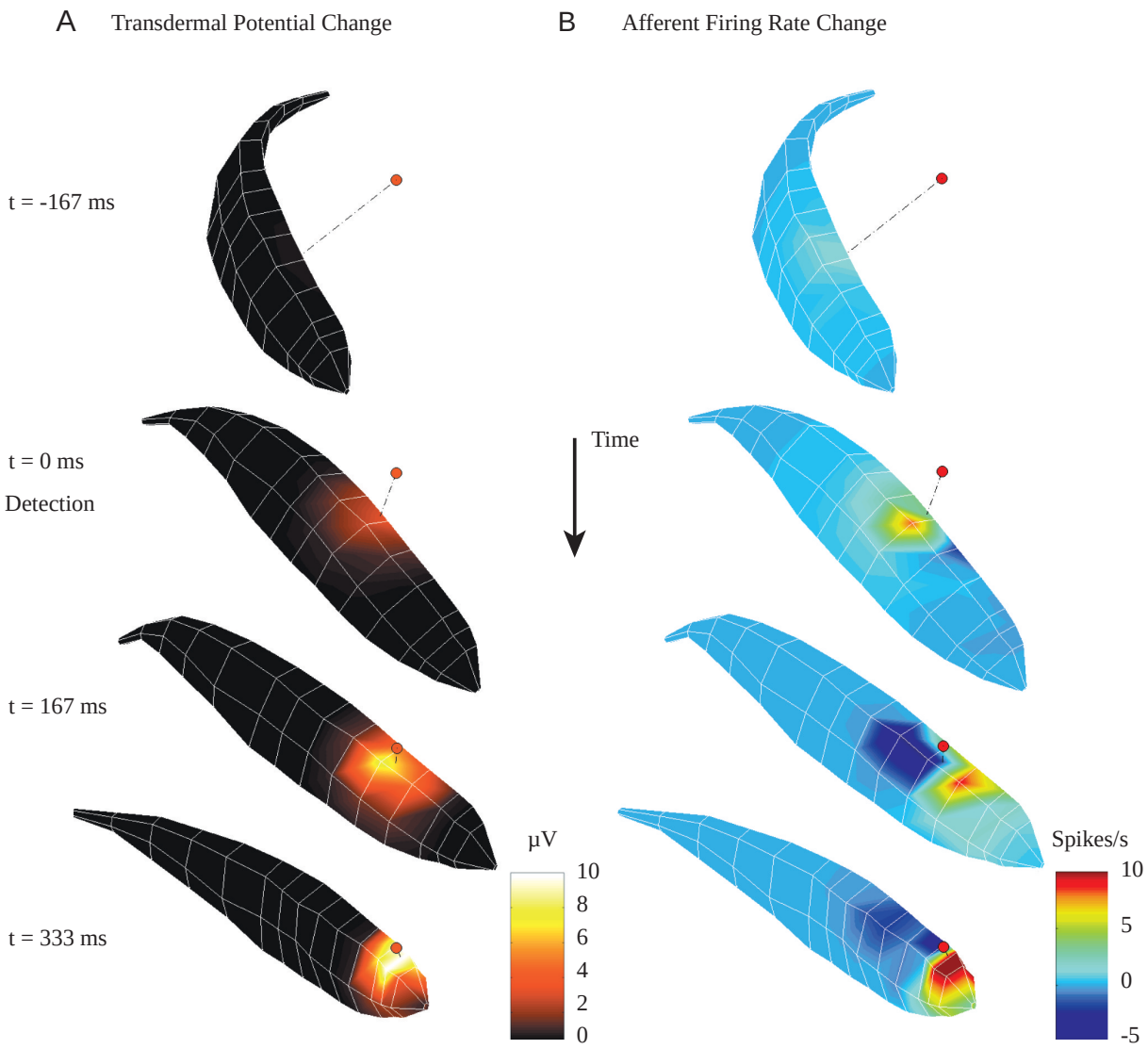

Figure 3.7 False color maps of reconstructed electrosensory images generated from model-based tracking of a single prey capture sequence. The weakly electric fish (*Apteronotus albifrons*) is able to detect prey in the dark by sensing small perturbations in a self-generated electric field. Each column shows 'snapshots' of the polygonal fish model at four different times in the prey capture sequence. The left-hand column (A) shows the voltage change across the skin (transdermal potential) induced by the prey. The right-hand column (B) shows the corresponding change in electrosensory afferent firing rate due to the voltage perturbations shown in (A). The prey (*Daphnia magna*) is shown as a red dot; the dashed line represents the shortest distance between the fish and the prey. Modified from Nelson & MacIver, 1999.

3.5.2 Other Applications

The techniques that we have presented for body modeling and model-based tracking worked particularly well for our application. In part, this can be attributed to three factors: the simple body plan of the knifefish and the corresponding small number of degrees of freedom, the occlusion-free viewing environment of the aquarium, and the relatively short duration (typically less than two seconds) of the behavioral sequences that needed to be reconstructed. While our specific application therefore represents a relatively simple case, the techniques that we have described could be extended to handle more complicated problems including 1) body modeling of animals with more complex body plans and more degrees of freedom, 2) fitting of the model to partially-occluded video images, and 3) reconstructing longer behavioral sequences.

For more complex body plans, it may be useful to build up a body model from multiple components (e.g., head, neck, trunk, limbs, etc.). Using methods similar to those outlined above, a surface representation could be obtained either for the entire animal, or for each body component separately. The rigid and nonrigid degrees of freedom for each component could then be modeled. Finally, the components would need to be linked together, using a technique such as the hierarchical method described in Jung (1997). Also, depending on the requirements of the study, it may be possible to simplify the problem by modeling only a small subset of the body components and degrees of freedom, or by tracking movements in two dimensions rather than three.

In video tracking studies, occlusions can occur either due to objects in the environment or due to self-occlusion when one part of the body overlaps with another part in the projected image. Predictive tracking methods can help in these cases (Jung, 1997), as can the addition of more camera views. These methods typically employ physics-based deformable models (Terzopoulos et al., 1987; Metaxas, 1996; Essa et al., 1993) or active contours (Blake and Isard, 1998) to constrain the placement of the model in images of a scene from multiple perspectives. This is done using computer-automated fitting techniques, rather than manual model placement as described in this study (Jung, 1997; Mochimaru and Yamazaki, 1994; Gavrila and Davis, 1996; Tillett et al., 1997).

Manual model fitting is time consuming and establishes a practical limit for the length of video sequences that can be reconstructed. In our application, reconstruction of a 1-2 s sequence required approximately 45 minutes per sequence. Automatic model fitting techniques reduce the amount of user involvement required and thus have the advantage of enabling longer-term behavioral observations. We are currently exploring the use of automatic model fitting methods in our studies.

3.5.3 Future Directions

The data that we obtain from model-based tracking is rich. One of the challenges we face is the visual display of 3-D data for selection and quantitative analysis of behavioral patterns. In 2-D projections of prey capture sequences, the absence of depth cues makes interpretation of the movements difficult. Thus, we have recently utilized a virtual reality system developed at the University of Illinois (CAVE, Beckman Institute, Urbana IL USA) to visualize prey capture

reconstructions in 3-D. In this facility, a stereo image of the fish and prey is projected onto three walls of a room and the floor using four projectors. Liquid crystal stereo glasses provide the illusion that the fish and prey are floating in space within the CAVE. A computer tracks the user's position and gaze direction and dynamically changes the visual display accordingly. The playback speed, direction, position, and zoom level of the prey capture sequences are controlled by a hand-held joystick. We have used this system to identify subtle aspects of the behavior that were not previously observed while viewing the prey capture sequences on 2-D workstation monitors.

Also, we are in the process of designing a biomimetic robot based on the weakly electric fish in order to test active sensing hypotheses in the electrosensory system. We have utilized a very high resolution (258,609 polygon) version of the fish model discussed above to generate a physical realization of the model using a stereolithography apparatus (SLA-50, 3D Systems, Valencia CA USA). This apparatus consists of a tank of photosensitive resin and a computer controlled laser. The laser scans the tank of resin to build up a rigid model in layers that are 4.2 μm thick.

The sensory acquisition mechanisms of interest in our research are the adaptive control of body posture and the descending control of sensory filtering in the brain. By combining precision behavioral quantification, neurophysiology, neural simulations, and biomimetic robotics we hope to elucidate these mechanisms subserving the remarkable sensory abilities of weakly electric fish. In general, these methods may provide a bridge between analytical methods of studying adaptive behavior and synthetic approaches (Ekeberg et al., 1995; Beer et al., 1998; Terzopoulos et al., 1995, 1997; Chiel and Beer, 1997).

CHAPTER 4

Motion analysis and effects of water conductivity

4.1 Summary

Animals can actively influence the content and quality of sensory information they acquire from the environment through the positioning of peripheral sensory surfaces. This study investigated receptor surface positioning during prey capture behavior in gymnotiform weakly electric fish of the genus *Apteronotus*. Infrared video techniques and 3-D model-based tracking methods were used to provide quantitative information on body position and conformation as black ghost (*A. albifrons*) and brown ghost (*A. leptorhynchus*) knifefish hunted for prey (*Daphnia magna*) in the dark. We found that detection distance depends on the electrical conductivity of the surrounding water. Best performance was observed at low water conductivity (2.8 cm mean detection distance and 2% miss rate at 35 $\mu\mathrm{S} \cdot \mathrm{cm}^{-1}$, *A. albifrons*) and poorest performance at high conductivity (1.4 cm and 11% at 600 $\mu\mathrm{S} \cdot \mathrm{cm}^{-1}$, *A. albifrons*). The observed conductivity dependence implies that non-visual prey detection in *Apteronotus* is likely to be dominated by the electrosense over the

range of water conductivities experienced by the animal in its natural environment. This result provides the first evidence for the involvement of electrosensory cues in the prey capture behavior of gymnotids, but it leaves open the possibility that both the high-frequency (tuberous) and low-frequency (ampullary) components may contribute. We describe an electrosensory orienting response to prey, whereby the fish rolls its body following detection to bring the prey above the dorsum. This orienting response and the spatial distribution of prey at the time of detection highlight the importance of the dorsal surface of the trunk for electrosensory signal acquisition. Finally, quantitative analysis of fish motion demonstrates that *Apteronotus* can adapt its trajectory to account for post-detection motion of the prey, suggesting that it uses a closed-loop adaptive tracking strategy, rather than an open-loop ballistic strike strategy, to intercept the prey.[1]

Key words: computational neuroethology, electrolocation, electroreception, active sensing, conductivity, sensory ecology, nocturnal, nonvisual, orienting behavior, mechanosensory lateral line, backwards locomotion, reverse swimming, motion capture

4.2 Introduction

One universal task carried out by the nervous system is the extraction and enhancement of sensory signals that are relevant to behavior. This sensory acquisition process has both motor and sensory aspects. The motor aspect is related to the positioning of peripheral receptor

[1]Published as: MacIver, M.A., Sharabash, N.M., Nelson, M.E. (2001) Prey-capture behavior in gymnotid electric fish: motion analysis and effects of water conductivity. *Journal of Experimental Biology*, 204(3): 543-557.

surfaces, providing the animal with some degree of control over the content and quality of incoming sensory data. The sensory aspect is related to the adaptive filtering of incoming data for further enhancement of relevant signal components and suppression of extraneous signals. For the electrosensory system, prey detection and localization provides a neuroethological context for studying both sensory and motor aspects of sensory acquisition (MacIver et al., 1997; Nelson and MacIver, 1999).

This study presents a quantitative analysis of the positioning of peripheral receptor surfaces during the detection and capture of small aquatic prey in two species of South American gymnotid weakly electric knifefish, *Apteronotus albifrons* (black ghost) and *A. leptorhynchus* (brown ghost). Weakly electric fish possess an organ that produces an electric discharge (electric organ discharge; EOD). In *Apteronotus*, the EOD creates a quasi-sinusoidal field with a fundamental frequency of $\approx$1 kHz and a field strength of $\approx 1\ \mathrm{mV \cdot cm^{-1}}$ near the fish.

These fish have the ability to sense both the self-generated field and extrinsic electric fields using two submodalities of electrosense, each with a distinct receptor population. The high frequency electrosense, sensitive to fields similar to the fish's own EOD, is mediated by tuberous receptors, whereas the low frequency electrosense, sensitive to fields of $\approx$0-40 Hz, is mediated by ampullary receptors (review: Zakon, 1986). In active electrolocation behavior, the fish uses its high frequency electrosense to detect perturbations in the self-generated field (reviews: Bastian, 1986; von der Emde, 1999). In passive electrolocation behavior, the fish uses its low and high frequency electrosense to detect extrinsic electric fields such as the weak bioelectric field of aquatic prey or the EODs of other electric fish (Kalmijn, 1974; Hopkins et al., 1997; Wilkens et al., 1997; Naruse and Kawasaki, 1998).

Black and brown ghost knifefish are primarily nocturnal hunters that feed on insect larvae and small crustaceans (Marrero, 1987; Winemiller and Adite, 1997; Mérigoux and Ponton, 1998). Such prey may stimulate the high frequency electrosense due to the difference in impedance between their bodies and the surrounding water, and the low frequency electrosense due to their bioelectric fields. The prey may stimulate other nonvisual modalities, such as the mechanosensory lateral line system and the olfactory system.

In weakly electric fish, active electrolocation is often assumed to play a key role in the detection and capture of prey. This assumption is based on the observation that these animals are able to capture prey in the absence of visual cues, as well as the predominance of peripheral receptors and volume of brain tissue devoted to the high frequency electrosense. In an adult *A. albifrons*, for example, there are $\approx$15,000 tuberous receptor organs distributed over the body surface, compared with $\approx$700 ampullary receptor organs and $\approx$300 neuromasts for the mechanosensory lateral line (Carr et al., 1982). Although such indirect arguments for active electrolocation may be compelling, there is currently no direct supporting evidence for electrosensory involvement in prey detection in South American gymnotids, and few studies address this question in African mormyrids (von der Emde, 1994; von der Emde and Bleckmann, 1998).

In this study we used infrared video recording and a model-based animal tracking system (MacIver and Nelson, 2000) to provide quantitative information on the position and conformation of the fish body, and hence of the peripheral sensor array, during prey capture behavior. We manipulated the electrosensory contributions to prey capture behavior by varying water conductivity. Our results provide the first direct evidence for the involvement of electrosensory

signals in the prey capture behavior of gymnotids. We also obtain quantitative data addressing how weakly electric fish orient their sensory surfaces during prey capture behavior, and show that they are able to adaptively change their strike trajectory to compensate for prey movement. The quantitative behavioral data obtained in these studies can provide a link among the motor aspects of sensory acquisition, the adaptive neural processing of electrosensory signals, and the sensory ecology of the animal (Nelson and MacIver, 1999; Ratnam and Nelson, 2000).

4.3 Materials and methods

4.3.1 Behavioral apparatus

Two adult *Apteronotus albifrons* and two *Apteronotus leptorhynchus,* 12-15 cm in length, were housed in a rectangular Plexiglas aquarium with a central area partitioned from the rest of the tank to form a 40 x 30 x 20 cm behavioral observation arena. The arena was imaged by two video cameras that provided top and side views, allowing three-dimensional reconstruction of behavioral trajectories. Video signals from the two cameras were electronically merged and recorded onto videotape for subsequent analysis. To eliminate visual cues, prey capture behavior was observed using infrared (880 nm) illumination provided by high-intensity infrared diodes. The illuminators, cameras, and aquarium were housed within a light-tight enclosure that was maintained on a 12-h light:12-h dark cycle. Water temperature was maintained at $28 \pm 1.0\ ^{\circ}C$ and pH at 7.0 ± 0.1. Animal care procedures were reviewed and approved by the Laboratory Animal Care and Advisory Committee of the University of Illinois at Urbana-Champaign. For details on the behavioral apparatus see MacIver and Nelson (2000).

4.3.2 Experimental protocol

The prey used in these studies were mature *Daphnia magna* (water fleas), 2-3 mm in length, cultured in our laboratory. *Daphnia* are aquatic crustaceans that are similar to the prey typically found in stomach content analyses of *Apteronotus* (Marrero, 1987; Winemiller and Adite, 1997; Mérigoux and Ponton, 1998). Each day, shortly after the beginning of the dark cycle, one fish at a time was allowed into the central observation arena for 15-20 minutes. Prey were introduced one at a time at random locations near the surface of the tank using a thin flexible tube from outside the light-tight enclosure. This method avoided entry of visible light and generated minimal mechanical disturbance. After introduction of the *Daphnia*, its position was observed on the video monitor. If the prey was eaten by the fish or drifted to a corner or bottom of the tank, another individual prey was introduced.

We maintained constant water conductivity during each of four sets of recording sessions, each lasting 10-21 days. Behavior was recorded at four different water conductivities: 35 ± 5, 100 ± 5, 300 ± 40, and 600 ± 40 $\mu S \cdot cm^{-1}$ (sequence: 300, 100, 300, 600, and 35 $\mu S \cdot cm^{-1}$). For each tested conductivity, the behavioral tank water conductivity was established by mixing deionized water with a stock salt solution consisting of $CaSO_4 \cdot 2H_2O$, $MgSO_4 \cdot 7H_2O$, KCl, $NaH_2PO_4 \cdot H_2O$, and NaCl in a weight ratio of 60:4.7:3.0:1.0:0.8 (L. Maler, personal communication; similar to Knudsen, 1975). Changes between different conductivity values were made gradually, over several days, followed by several days at the new conductivity to acclimate the fish before behavioral data were recorded. Conductivity measurements were made using a cal-

ibrated conductivity meter (TDSTestr 40, Cole Parmer Instrument Company, Vernon Hills, IL, USA), and water conductivity was corrected on a daily basis.

4.3.3 Behavioral segment selection

Videotaped recordings of prey capture behavior were visually scanned to identify segments to be digitized for further processing. The criteria for selection of a prey capture event were as follows: a successful capture, or a failed capture attempt where there was an abrupt and directed movement toward the prey; fish and prey visible in both camera views, except for brief occlusions; prey at least 2 cm from the bottom and sides of the tank.

The start of a video segment was typically chosen to begin $\approx$0.5 s prior to the onset of the prey strike. The segment ended with prey capture or, in the rare cases where the fish did not catch the prey, near the time when the fish mouth came closest to the prey.

4.3.4 Behavioral data acquisition, visualization, and analysis

Selected video segments were digitized and stored as 8-bit grayscale image files for analysis. The video sampling rate was 60 images per second, with each video image consisting of one video field with alternate scan lines interpolated. A model-based animal tracking system was developed to accurately determine the trajectory and conformation of the fish's body and prey position for each image of selected sequences (MacIver and Nelson, 2000). In this system, an accurate 3-D wireframe model of the observed fish and prey was overlaid onto digitized images. The fish and prey models were then manipulated by the user to achieve congruence with the side and top view images of the actual fish and prey. Calibrated image transformations

ensured that model-to-image matching resulted in accurate ($\pm$1 mm) recovery of the positions of the animals in the behavioral arena. The fish models were provided with eight degrees of freedom (DOF) (Fig. 4.1). The six rigid-body DOF were position of the snout (x, y, z), yaw, pitch, and roll (θ, ϕ, Ω). The two nonrigid DOF were lateral tail bend and dorsoventral body flexion. The prey was modeled with three DOF, corresponding to the coordinates of its center. The wireframe fish models were scaled to each individual fish. The output of the model-based tracking system was the value of each model parameter for the fish and prey at each image of the sequence. For details see MacIver and Nelson (2000).

Some analyses presented below required fitting the fish and prey model to images in the entire behavioral sequence (full motion analysis), whereas other analyses required only the less time-intensive process of fitting the single frame where the fish changed from forward to reverse swimming (single frame analysis).

Full 3-D reconstructions of selected sequences were displayed on computer monitors using a custom prey-strike browser that simultaneously displayed graphs of movement parameters. However, the limited depth cues provided by monitor projections made interpretation of the movements difficult. In collaboration with Stuart Levy of the National Center for Super Computing Applications (NCSA, Beckman Institute, University of Illinois at Urbana-Champaign, http://virdir.ncsa.uiuc.edu/virdir/), we brought the model-based tracking data into an immersive multi-person virtual reality system (CAVE, Fakespace Systems Inc., Kitchener, ON, Canada) (Cruz-Neira et al., 1992, 1993; Leigh et al., 1995). The prey-strike browser and CAVE were used for identification of patterns of movement that were largely inaccessible in the original video records.

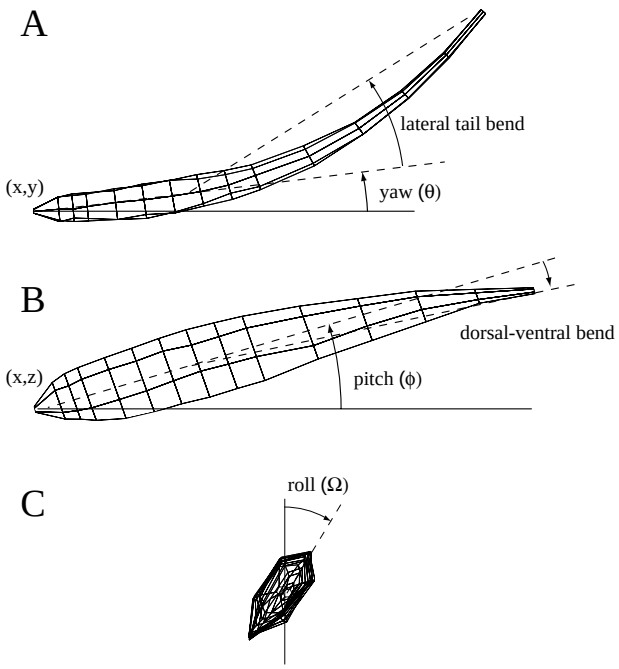

Figure 4.1 Fish body model with eight degrees of freedom. (A) Top view showing four degrees of freedom: (x, y) in-plane position of the snout; yaw angle (θ); and lateral tail bend. (B) Side view showing three additional degrees of freedom: (z) vertical position of the snout; pitch angle (ϕ); and dorsoventral bend. (C) Front view showing roll angle (Ω). Description of axes angles: dotted line indicates the central body axis of the unbent fish; yaw (θ) and pitch (ϕ) measure the angle of the body axis relative to the tank coordinate system. Lateral bend angle is defined as the angle in the dorsal plane between the unbent body axis and a line extending from 1/3 the body length from the head to the tail; dorsoventral bend is defined as the angle in the median plane between the unbent body axis and a line extending from 1/3 the body length from the head to the tail.

Velocities and accelerations were computed using the difference in fitted model positions between successive images. The longitudinal velocity of the fish was computed by taking the vector dot product of the snout velocity vector with a heading vector **u**, taken from the yaw (θ)

and pitch (ϕ) angles:

$$u_x = -cos\ \theta\ cos\ \phi; \tag{4.1}$$

$$u_y = -sin\ \theta\ cos\ \phi; \tag{4.2}$$

$$u_z = -sin\ \phi \tag{4.3}$$

The minimum distance between the surface of the fish and the prey was determined by finding the shortest distance between the prey and each of the 84 quadrilateral faces of the fitted wireframe fish model using a parametric optimization procedure. For depictions of prey position at the time of detection (Figs. 4.5 and 4.6), the fish and prey coordinates were transformed into a coordinate frame in which the fish body was straightened and scaled to unit length. For depictions of the temporal variation in the shortest distance to prey from the fish surface ("prey tracks", Fig. 4.7), a higher resolution fish model was utilized (section 5.3.1). At each time step of behavior, the shortest distance to the vertices of this model was found. For comparison of the prey track across trials, we connect the vertices of each prey track with a line on a straightened fish body scaled to unit length. Population peri-detection statistics were computed by aligning trials at the time of detection (see results), and averaging across trials from 500 ms before the time of detection to 1000 ms after the time of detection. The tails of these peri-detection distributions have reduced N due to differences in start and end times between trials. All post-detection averages are computed by first aligning trials at the specified post-detection time. All computations were carried out using MATLAB and the image processing, optimization, and signal processing tool boxes (The Mathworks Inc., Natick, MA,

USA), running on a Unix workstation. All statistical values are reported as mean ± s.d. unless otherwise indicated. For comparison of receptor surface area and size between *A. albifrons* and *A. leptorhynchus*, the scaled polygonal fish models used for model-based tracking were measured within 3D modeling software (Rhinoceros, Robert McNeel and Associates, Seattle, WA, USA).

4.4 Results

A total of 130 *A. albifrons* prey capture sequences were processed for full motion analysis, with a mean duration of 1.2±0.3 s. In a typical sequence the fish was initially swimming forward and made a rapid reversal in swimming direction to capture the prey. Such rapid reversals were associated with prey capture behavior and were rarely observed during normal swimming when no prey were present in the tank.

Figure 4.2A shows the longitudinal velocity profile for a representative prey capture sequence, illustrating a rapid reversal. The time at which the longitudinal velocity changes sign from positive to negative (Fig. 4.2A, dotted vertical line) is referred to as the "time of reversal." The mean duration of a rapid reversal (from time of reversal to time of forward movement) for all trials was just under half a second (418 ± 141 ms). To obtain a better estimate of the time of prey detection, we used the longitudinal acceleration profile (Fig. 4.2B) to determine when the fish began to slow down. The zero-crossing of the longitudinal acceleration profile prior to the rapid reversal (Fig. 4.2B, solid vertical line) was taken as the "time of detection." The actual time of detection, however, would be prior to this behavioral response due to neu-

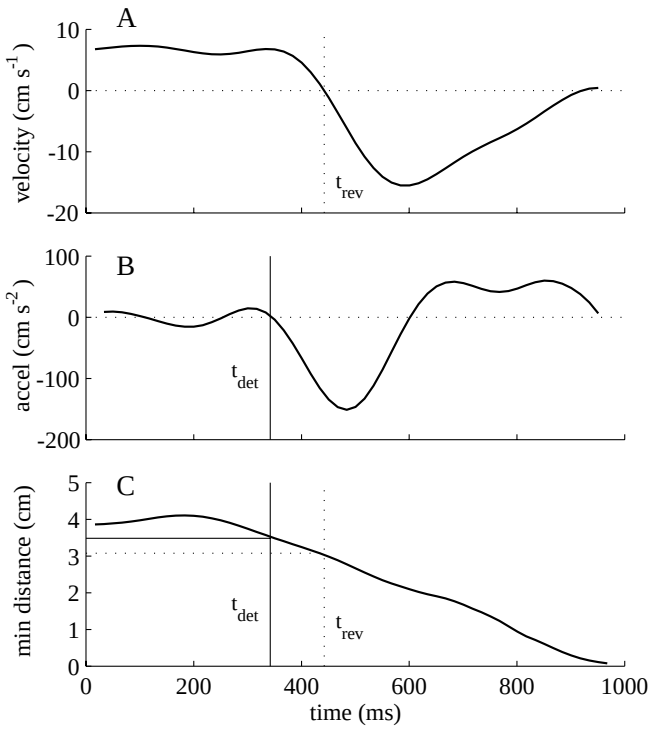

Figure 4.2 Motion parameters for a sample trajectory. Longitudinal velocity, longitudinal acceleration, and shortest distance between prey and fish body surface is shown for a representative trial that ends with a successful capture. (A) Longitudinal velocity, showing the time of reversal. (B) Longitudinal acceleration, showing the time of detection. (C) Shortest distance from fish body to prey, with time of reversal (dotted vertical line), time of detection (solid vertical line), reversal distance (dotted horizontal line), and detection distance (solid horizontal line) indicated for comparison.

romotor output delays. In subsequent analyses, these two time points ("time of reversal" and "time of detection") are used as reference points for comparing distances to prey. Typically, the prey were captured in just over half a second following the time of detection (682 $\pm$ 165 ms). Figure 4.2C shows the minimum distance between the prey and the surface of the fish, computed from the model-based tracking data. At the time of detection, the *Daphnia* was 3.5 cm away from the sensory surface, and at the time of reversal it was 3.1 cm away.

4.4.1 Longitudinal velocity and acceleration

In 14 of the 130 behavioral segments, we could not determine the time of detection, either because there was no rapid reversal or because the deceleration profile was ambiguous. The other 116 behavioral segments had velocity and acceleration profiles similar to those shown in Fig. 4.2.

Figure 4.3 shows a peri-detection plot of the average longitudinal velocity and acceleration for all 116 trials, aligned at the time of detection. At the time of detection, the average forward longitudinal velocity of the fish was 9.6 $\pm$ 4.3 cm $\cdot$ s^{-1}. The peak negative velocity of the rapid reversal occurred on average at 307 $\pm$ 135 ms following detection and had a magnitude of -19.1 $\pm$ 5.2 cm $\cdot$ s^{-1}. The average peak reverse acceleration during the rapid reversal was -172 $\pm$ 75 cm $\cdot$ s^{-2}.

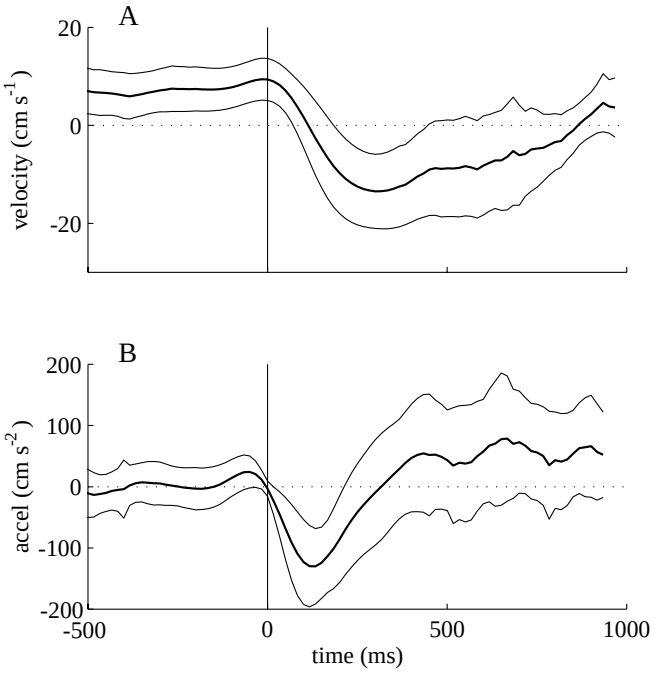

Figure 4.3 Population distribution of peri-detection velocity and acceleration. Mean (thick solid lines) and standard deviation (thin solid lines). Trials are aligned at detection time (t = 0 ms), indicated by vertical line. (A) Longitudinal velocity. (B) Longitudinal acceleration.

We found that the mean longitudinal velocity from the start of the behavioral segment to the time of detection (pre-detection or search velocity) was 8.1 $\pm$ 3.7 cm $\cdot$ s^{-1}(N = 116). At 35 μS $\cdot$ cm^{-1}the mean search velocity was significantly higher (10.4 $\pm$ 3.3 cm $\cdot$ s^{-1}, N = 38) than at all other conductivities, with no significant difference between velocities at 100 μS $\cdot$ cm^{-1} and above ($p \leq 0.01$, t-test).

4.4.2 Detection Distance

In this section we present results for data collected at 35 μS $\cdot$ cm^{-1}, which was associated with the largest mean detection distance. Figure 4.4A shows the peri-detection time course of the distance between the fish and prey, averaged over all 35 μS $\cdot$ cm^{-1} trials (N = 38). The mean distance to the prey at the time of detection was 2.8 $\pm$ 0.8 cm. Figure 4.4B shows the distribution of distances at the time of detection (range 1.2-5.2 cm). Note that the distribution is well separated from the origin, indicating that all detections were noncontact in nature. Figure 4.4C shows the distribution of distances at the time of reversal. The distribution is similar to that shown in Fig. 4.4B, except that the mean is shifted to lower values (1.9 ± 0.6) because the time of reversal occurs $\approx$200 ms after time of detection (see Fig. 4.2C).

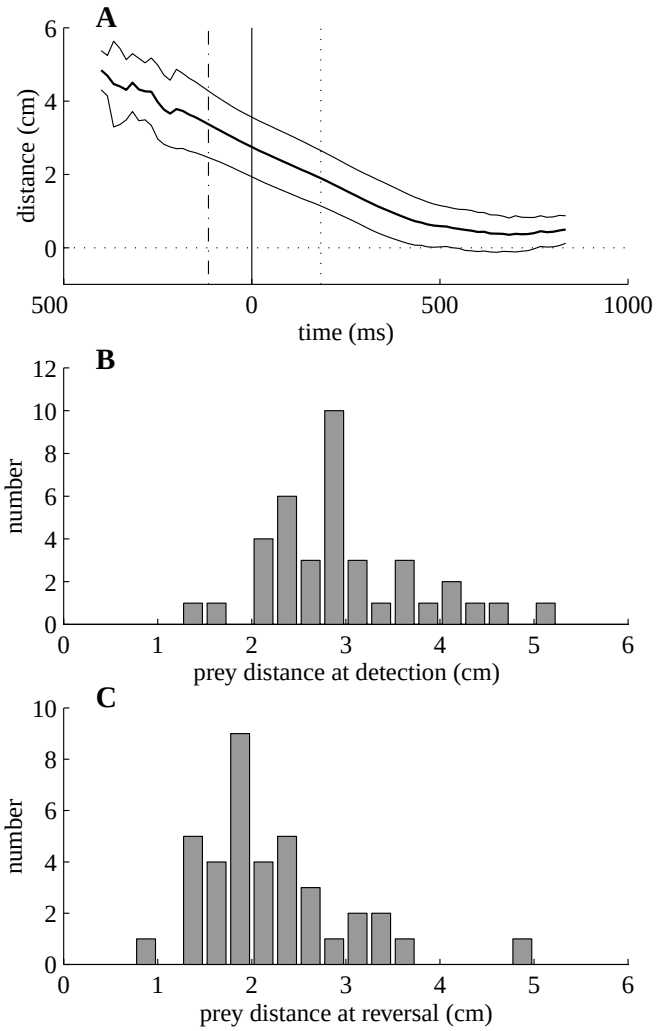

Figure 4.4 Detection distance profile and distributions for 35 μS $\cdot$ cm^{-1} trials (N = 38). (A) Average distance to prey for all trials, aligned at time of detection (t = 0 ms). Vertical solid line indicates the time of detection; vertical dotted line indicates the average time of fish reversal. (B) Histogram showing the detection distance distribution. The mean distance to prey at time of detection was 2.8 $\pm$ 0.8 cm. (C) Histogram showing the reversal distance distribution. The mean distance to prey at the time of reversal was 1.9 $\pm$ 0.6 cm.

4.4.3 Prey position at time of detection

Most detection events occurred when the prey was close to the dorsal surface of the fish. Figures 4.5 and 4.6 illustrate the angular and rostrocaudal distributions of prey at the time of detection for 35 μS $\cdot$ cm^{-1}. As shown in Fig. 4.5A, the prey tended to cluster above the dorsal surface of the fish. All prey but two fell within $\pm 60^{\circ}$ of the vertical midline of the fish (Fig. 4.5B). Mean detection distance did not vary significantly with azimuthal position (Fig. 4.5C). As shown in Fig. 4.6A, prey positions were distributed along the entire rostrocaudal extent of the fish. There was a slight bias in the number of detections favoring the anterior trunk region of the fish (Fig. 4.6B). The mean detection distance did not vary significantly with rostrocaudal position (Fig. 4.6C).

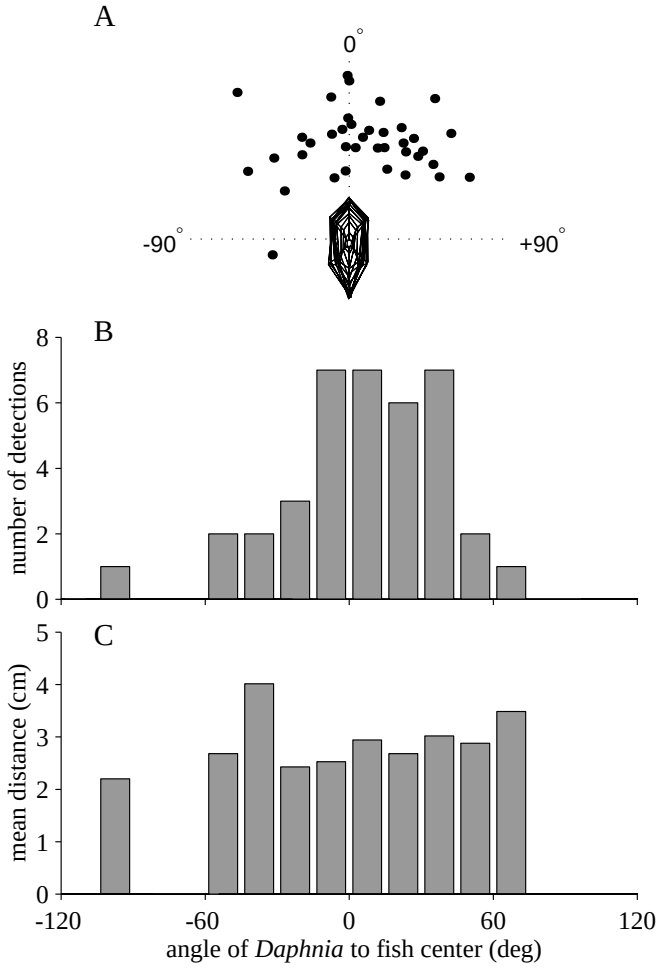

Figure 4.5 Distribution of prey in transverse plane for 35 μS $\cdot$ cm^{-1} trials (N = 38). Dots indicate position of *Daphnia* at the time of detection, positive angles are to the animal's right, negative angles are to the animal's left, 0° is midline above the fish. (A) Tail-on view showing distribution of prey at the time of detection. (B) Number of detections. (C) Detection distance.

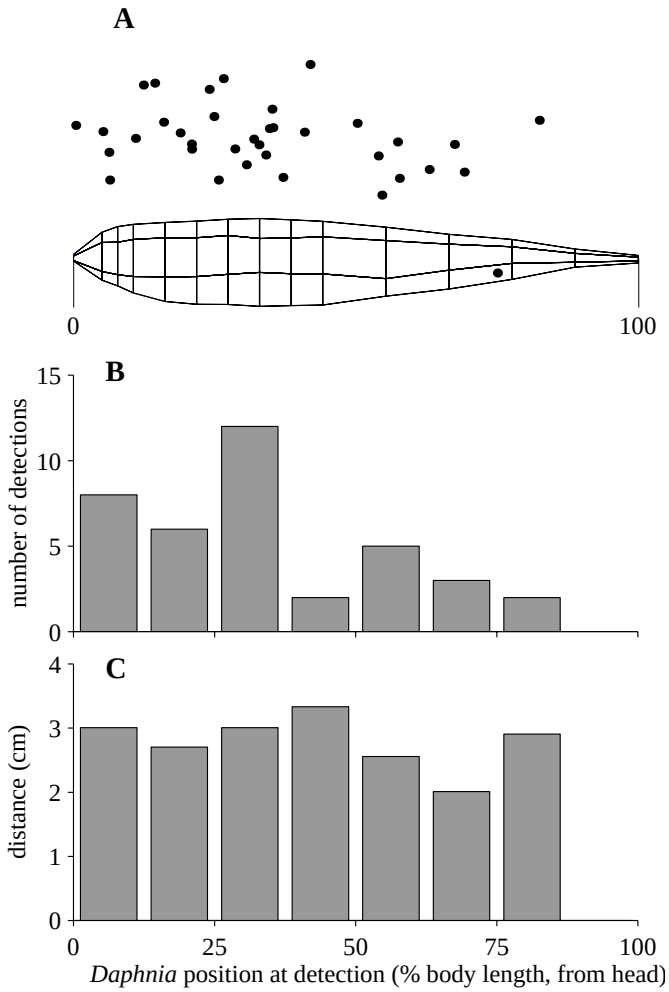

Figure 4.6 Distribution of prey in median plane for 35 μS $\cdot$ cm^{-1} trials (N = 38). Body lengths are normalized to be from 0 (head) to 100 (tail). Dots indicate position of *Daphnia* at the time of detection. (A) Side view showing the position of the prey at detection, projected onto a straightened fish. (B) Number of detections. (C) Detection distance.

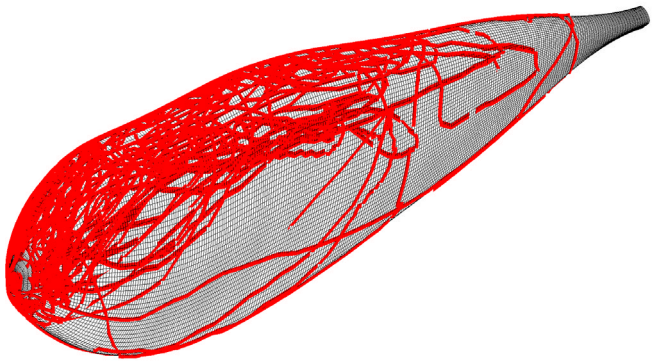

Figure 4.7 Prey tracks on fish surface. Lines connect the closest points on the fish surface to the prey over the course of a prey capture sequence (N = 116). These tracks are concentrated on the dorsal aspect of the fish, where there is a higher concentration of receptors (Fig. 5.3).

4.4.4 Distribution of prey "tracks" on fish surface

The temporal variation in location of the closest point on the surface of the fish to the prey, which will be referred to as the prey "track" for simplicity, is illustrated in Fig. 4.7 for all trials. Both prior to and following detection the location of the prey track is constrained largely to the dorsal aspect. In part, this is the result of active positioning of the dorsum with respect to the prey through rolling behavior (see Section 4.4.6 and Fig. 4.10 below).

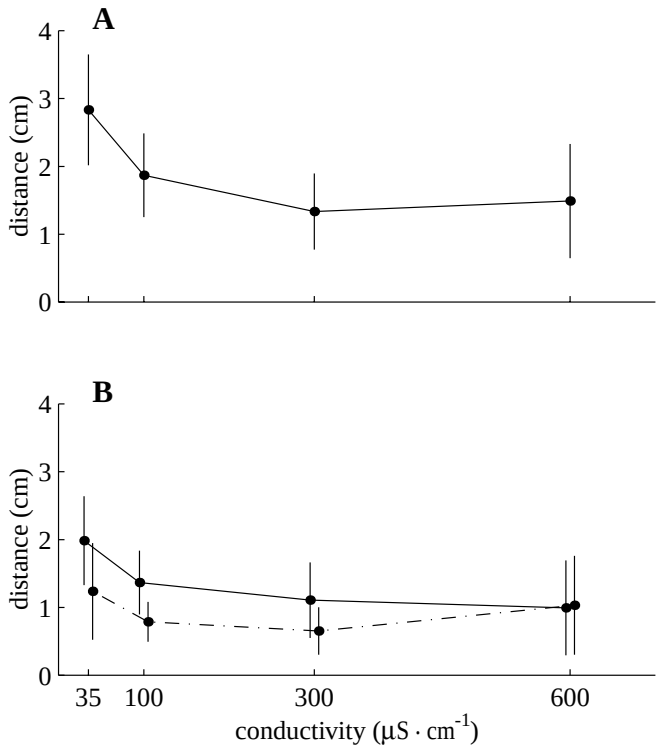

Figure 4.8 Detection distance versus conductivity. (A) Distance to prey at the time of detection for *A. albifrons* from full motion reconstructions. (B) Distance to prey at the time of reversal from single-frame reconstructions; solid line is *A. albifrons*; dashed line is *A. leptorhynchus*. Vertical lines indicate standard deviation.

4.4.5 Detection distance and water conductivity

The mean detection distance increased with decreasing water conductivity. At a conductivity of 35 μS $\cdot$ cm^{-1}, the mean detection distance was approximately a factor of two times greater than at 600 μS $\cdot$ cm^{-1}. Figure 4.8A shows the mean and standard deviation of the detection distance distribution for each of the four conductivities tested. The mean detection distances were not significantly different between 300 and 600 μS $\cdot$ cm^{-1}, but were significantly different between 300 and 100, and between 100 and 35 μS $\cdot$ cm^{-1}($p \leq 0.01$, t-test). Two sets of 300 μS $\cdot$ cm^{-1} trials, collected approximately 10 weeks apart, showed no statisti-

	A. albifrons		*A. leptorhynchus*	
	detection	reversal	detection	reversal
35 µS	2.8 ± 0.8 (38)	1.9 ± 0.3 (54)	NA	1.2 ± 0.7 (34)
100 µS	1.9 ± 0.6 (18)	1.4 ± 0.5 (18)	NA	0.8 ± 0.3 (9)
300 µS	1.3 ± 0.6 (37)	1.0 ± 0.5 (51)	NA	0.6 ± 0.3 (17)
600 µS	1.5 ± 0.8 (23)	1.0 ± 0.7 (23)	NA	1.0 ± 0.7 (20)

Table 4.1 Distance to prey at detection and reversal for *A. albifrons* and *A. leptorhynchus*. Reversal distances include both the full-motion and single-frame data.

cally significant difference in mean detection distance and were pooled for this analysis. The results are summarized in Table 4.1.

The miss rate (misses as a percentage of all capture attempts) decreased monotonically with decreasing water conductivity, from a high of 11 $\pm$ 3% at 600 μS $\cdot$ cm^{-1} to a low of 2 $\pm$ 1% at 35 μS $\cdot$ cm^{-1} (mean $\pm$ s.e.m.) (Fig. 4.9). The miss rate at 35 μS $\cdot$ cm^{-1} was significantly lower than that at 300 or 600 μS $\cdot$ cm^{-1} ($p \leq 0.001$, binomial significance test)

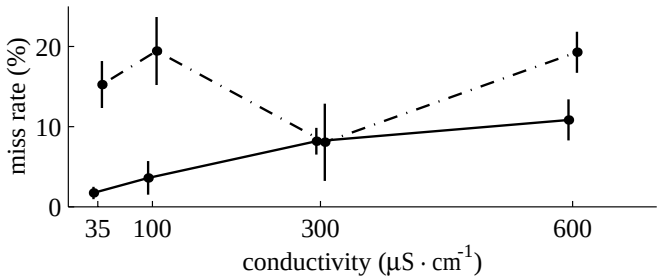

Figure 4.9 Prey strike miss rate versus conductivity. Miss rate is defined as failed prey capture attempts, and is shown as a percentage of all prey capture attempts at four conductivities for *A. albifrons*. Vertical lines indicate standard error of the mean.

4.4.6 Roll and pitch

Prior to detecting prey, fish were typically oriented with close to zero body roll (-3 $\pm$ 16°, N = 116, Fig. 4.10A). At the end of the rapid reversal (onset of the final forward lunge to engulf the prey), $\approx$0.6 s later, the mean roll was still close to zero, but the RMS value had increased significantly, from 17° to 33° (Fig. 4.10A). This post-detection increase in the RMS value is due to rolling movements following detection. A typical rolling movement is illustrated in Fig. 4.13A.

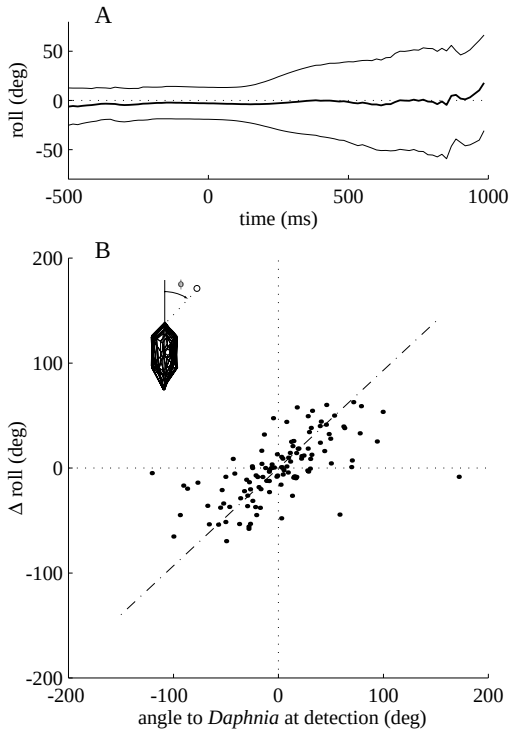

Figure 4.10 Peri-detection population distribution of roll angle and evidence for an electrosensory orienting response to prey. (A) Mean and RMS value of the roll angle, trials aligned at the time of prey detection (t = 0 ms). (B) The change in roll angle from the time of detection to the time of maximum reverse longitudinal velocity versus the initial angle to the prey at the time of detection (α). The angle to the prey is defined as shown in the inset. The dashed line shows the relationship when the roll angle change equals the initial prey angle, and corresponds to a linear regression of the data.

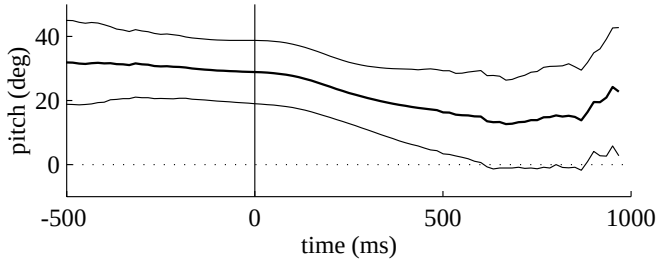

Figure 4.11 Mean and standard deviation of the pitch angle; trials aligned at the time of prey detection (t = 0 ms).

Figure 4.10B compares the change in roll angle (from the time of detection to the time of maximum reverse velocity) to the angle of the prey at the time of detection. The angle to the prey is defined as shown in the inset of Fig. 4.10B. The slope of the regression line is close to unity, indicating that between the time of detection and the time of maximum reverse velocity the fish rolled approximately the same angle as it initially made to the prey (slope=0.93, $p \leq 0.001$). This resulted in the prey being located above the dorsum following the roll movement.

When the fish were searching for prey, they typically swam forward with their bodies pitched slightly downward. At the time of detection, the average pitch angle was $29 \pm 9.8^{\circ}$ (Fig. 4.11). In this posture, the dorsal surface of the trunk forms the leading edge as the fish moves through the water. During the rapid reversal, the pitch angle tended to decrease. At the end of the rapid reversal, $\approx$0.6 s after detection, the mean pitch angle had decreased to $15 \pm 13^{\circ}$.

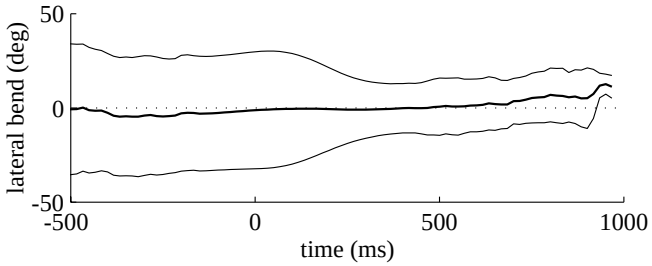

Figure 4.12 Mean and RMS value of the lateral bend parameter; trials aligned at the time of prey detection (t = 0 ms).

4.4.7 Lateral tail bend and bending velocity

Following detection, as the fish executed the rapid reversal, the degree of lateral tail bend tended to decrease. The lateral tail bend angle is defined as shown in Fig. 4.1A. The mean of the lateral bend angle is always near zero (Fig. 4.12), indicating that the fish showed no preference for left- versus right-side body bends. The RMS bend angle, however, dropped significantly following detection. At the time of detection, the RMS value was 31°, whereas at the end of the rapid reversal ≈0.6 s later, it had declined to 16°.

The bend angle analysis provides information about the degree to which the body is bent, but not about how rapidly the bend angle is changing. We examined the lateral bend velocity across all trials and found a mean RMS lateral bend velocity of $107^\circ \cdot s^{-1}$ around the time of detection. There was no significant difference between pre- and post-detection values. For a 14 cm *A. albifrons*, this bend velocity corresponds to a tail tip velocity of ≈ 19 cm $\cdot s^{-1}$. At the end of a rapid reversal there was often a rapid dorsoventral or lateral body bend just prior to capture to close the final gap to the prey (Fig.4.13B).

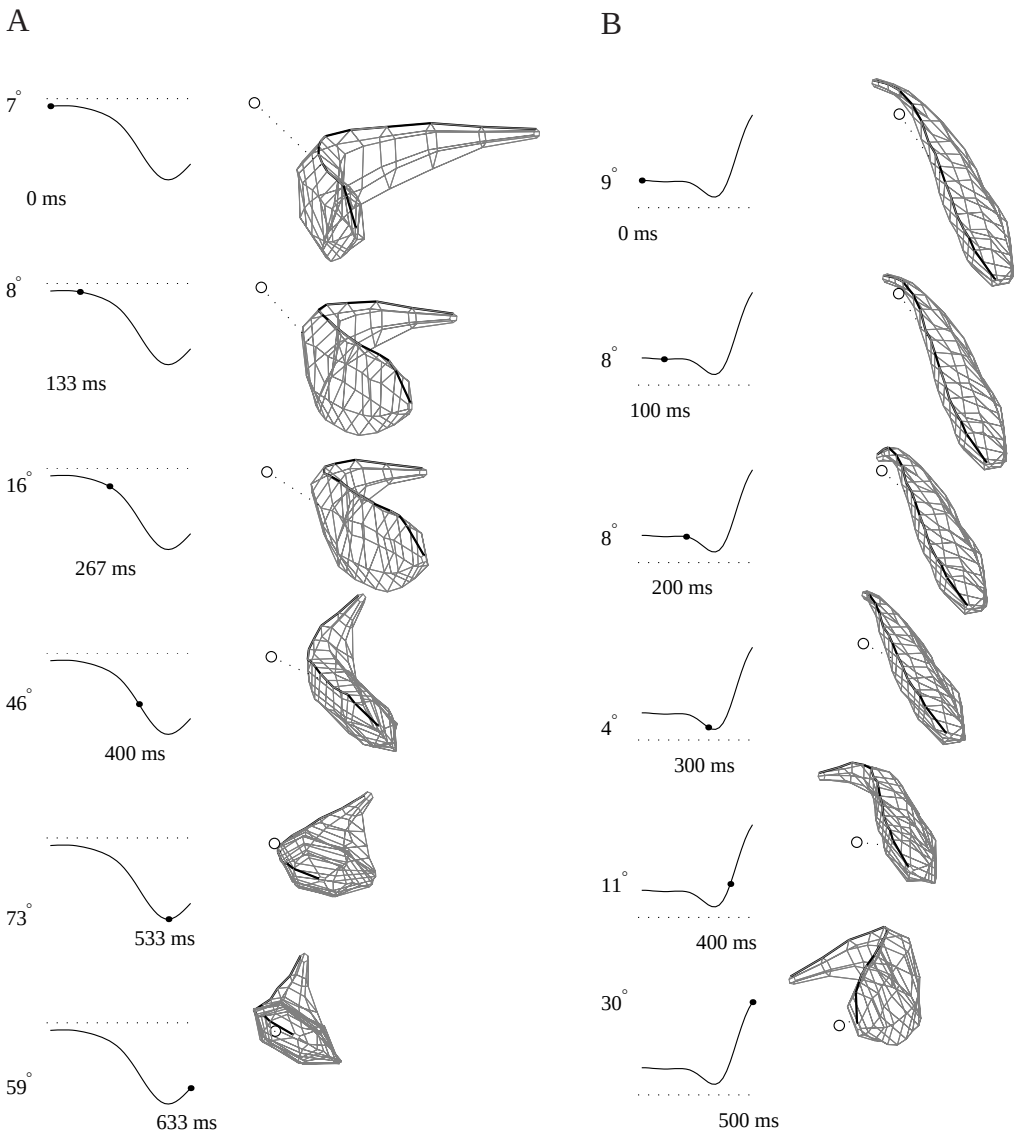

Figure 4.13 Two characteristic post-detection movement strategies, illustrated with two different prey capture sequences. In both panels the top snapshot (t = 0 ms) is at the time of detection, and time increases going down to the last snapshot at the end of the sequence. The heavy line on the fish indicates the dorsum, the open circle marks the position of the *Daphnia*, and the dotted line indicates the shortest line from the *Daphnia* to the body surface. (A) Roll, a possible electrosensory orienting behavior. Inset plot on left shows the roll angle parameter history and current value. (B) Lateral body bending to rapidly swing the mouth to a laterally positioned *Daphnia*. Inset plot on left shows the lateral bend angle history and current value.

4.4.8 Effects of prey displacement on prey capture behavior

To assess whether fish tended to perform ballistic strikes at the place where the *Daphnia* was originally detected, or whether they were able to modify their strike trajectory to compensate for prey displacement, we examined trials where the *Daphnia* moved 2.0 cm or more from the time of detection to capture. The mean *Daphnia* displacement from the time of detection to capture was 1.5 ± 1.0 cm, and the prey was displaced 2.0 cm or more in 25 of the 116 trials. For these trials, we compared two distances at each time step following detection: the distance from the fish mouth to the (changing) position of the prey, and the distance from the fish mouth to the (unchanging) position of the prey at the time of detection. A representative graph of these two quantities and of the corresponding capture sequence is shown in Fig. 4.14. Figure 4.14A shows that the distance from the fish mouth to the prey decreased more rapidly than the distance from the fish mouth to the original position of the prey at the time of detection. If, as shown in Fig. 4.14, the distance between the mouth and the actual prey position dropped below 1.0 cm before the distance between the mouth and the original prey position dropped below 1.0 cm, we categorized the trial as an adaptive strike. The converse condition was counted as a ballistic strike. If neither condition was met (e.g., the prey never came closer than 1.0 cm to the mouth due to a failed strike), the trial was scored as inconclusive. By these criteria, 18 of the 25 trials were categorized as adaptive strikes, 2 trials were categorized as ballistic strikes, and 5 trials were categorized as inconclusive.

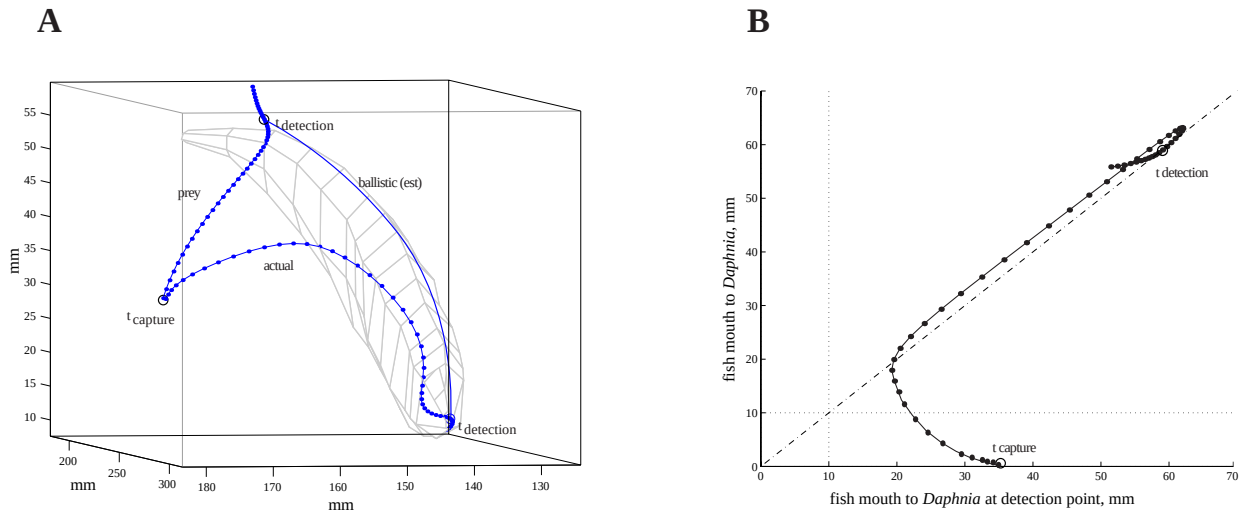

Figure 4.14 Closed-loop control of prey capture, illustrated with a representative trial where the *Daphnia* was displaced ≈4 cm from the time of detection to the time of capture. (A) A parametric plot of the distance from the fish mouth to the (changing) prey position vs. the distance from the fish mouth to the (unchanging) original position of the prey at the time of detection. Each dot on the curve represents the parameter values for the corresponding video image (60 images $\cdot$ s^{-1}; interimage interval 16.67 ms). The lines at 1.0 cm indicate our threshold for categorizing the sequence as adaptive or ballistic. (B) Illustration of the fish and prey original positions and subsequent trajectories for (A). If the fish had made a ballistic strike, the head might be expected to have followed a trajectory to the location of the prey at the time of detection, similar to the hypothetical trajectory shown by the solid line. The actual fish trajectory (dotted solid line) follows the drift of the prey, intercepting the prey trajectory at the time of capture.

4.4.9 Comparison between species

In general *A. leptorhynchus* exhibited poorer detection performance (shorter detection distances, higher miss rates) than *A. albifrons*. However, the key features of their behavior, including forward swimming velocity, reversal velocity and acceleration, pitch, tail bend, tail bend velocity, and post-detection increase in RMS roll angle were similar to those reported above for *A. albifrons* (N = 12, 35 μS $\cdot$ cm^{-1}).

To make comparisons between the distance at which prey are sensed in *A. albifrons* and *A. leptorhynchus*, we performed single-frame analysis of the video records using the time of

velocity reversal as a reference point (see Fig. 4.2A). Figure 4.8B compares the prey distance at the time of reversal for *A. albifrons* (solid lines) and *A. leptorhynchus* (dashed lines). The results are summarized in Table 4.1. The distance to the prey at the time of reversal was generally larger for *A. albifrons* than for *A. leptorhynchus*. These differences were significant at 35, 100, and 300 μS $\cdot$ cm^{-1}, but not at 600 μS $\cdot$ cm^{-1} ($p \leq 0.05$, t-test). The dependence of detection distance on water conductivity was similar for both species. The mean miss rate for *A. leptorhynchus* was more than twice as high as for *A. albifrons*. *A. leptorhynchus* captured approximately half as many *Daphnia* per session as *A. albifrons* (mean 4 and 7 per session, respectively).

There were several qualitative differences that are not reflected in these data. First, *A. leptorhynchus* appeared less motivated to feed on *Daphnia*. A total of $\approx$800 prey captures were recorded for *A. albifrons*, but there were only half as many prey captures recorded for *A. leptorhynchus*. We often observed *A. leptorhynchus* capturing a *Daphnia* and then ejecting it from their mouths, while this was never observed with *A. albifrons*. Although we observed that *A. albifrons* increased general search activity after prey were discovered, this was less apparent with *A. leptorhynchus*. In addition, *A. leptorhynchus* swam backwards more often than *A. albifrons* while searching for prey. Only 4% of the *A. albifrons* trials were excluded because the animal was moving backward at the time of detection (preventing identification of the time of detection), whereas 15% of the *A. leptorhynchus* trials were excluded for this reason.

The surface area and volume of length-matched *A. albifrons* was larger than *A. leptorhynchus*. A 16 cm *A. leptorhynchus* had a surface area of 34 cm^2 and volume of 6 cm^3, whereas

a 15 cm *A. albifrons* had a surface area of 49 cm^2 and volume of 10 cm^3. The percentage differences were similar for a 12 cm *A. albifrons* compared to a 12 cm *A. leptorhynchus*.

4.5 Discussion

The body of the weakly electric fish serves as a dynamic sensory antenna that can be repositioned to improve the reception of signals of interest from the environment. It is often assumed that the high frequency active electrosense provides the key signals for prey capture behavior. However, there is no direct evidence to support this assumption in South American gymnotids, and few studies address this question in African mormyrids (von der Emde, 1994; von der Emde and Bleckmann, 1998). It is possible that other nonvisual modalities, such as the low frequency electrosense and the lateral line mechanosense, may contribute to prey capture behavior. First, we outline candidate sensory modalities that may contribute to prey capture, and provide evidence that electrosensory contributions are likely to dominate over the range of water conductivities encountered by the animal in its natural environment. Second, we discuss our findings concerning the positioning of peripheral electroreceptor surfaces, the functional importance of the dorsal surface, and the evidence for a previously undescribed electrosensory orienting response. Finally, we discuss evidence that *Apteronotus* is able to dynamically modify its trajectory in order to capture moving prey. This finding implies that the nervous system implements a closed-loop control strategy during prey strikes.

4.5.1 Candidate sensory modalities supporting prey capture in *Apteronotus*

These studies were conducted under infrared illumination at a wavelength beyond the range of teleost photoreceptors (Fernald, 1988; Douglas and Hawryshyn, 1990), and our fish did not exhibit a startle response to the infrared illuminators, as they did to visible light. Thus it is unlikely that visual cues were available to aid the fish in prey detection. Tactile contributions can be eliminated because detection always occurred when the prey was well separated from the fish (Figs. 4.5 and 4.6). In principle acoustic cues may contribute, but the small prey used in this study are unlikely to generate pressure waves of sufficient strength to provide whole-body accelerations or stimulate the ear via the swim bladder and Weberian ossicles. Although chemosensory cues may stimulate feeding behavior, it is unlikely that the olfactory system can provide the spatial accuracy required to guide the precise high-efficiency strikes that were observed (Fig. 4.9).

The remaining candidate modalities that may contribute to prey detection are the high frequency electrosense, the low frequency electrosense, and the lateral line mechanosense. These three sensory modalities are all part of the octavolateral system.

4.5.2 Dependence of detection distance on conductivity

The key evidence that the electrosensory system is important for prey capture behavior in *Apteronotus* comes from our observation of better detection performance (longer detection distances and lower miss rates) at lower water conductivities (Figs. 4.4 and 4.9). The mean

detection distance nearly doubled (from 1.4 to 2.8 cm) from high conductivity (300 or 600 μS $\cdot$ cm^{-1}) to low conductivity conditions (35 μS $\cdot$ cm^{-1}), and the miss rate decreased from 11% to 2%.

Natural conductivity ranges for Apteronotus. Conductivities of South American rivers and streams where *Apteronotus* is found (Ellis, 1913) vary from lows of approximately 10 μS $\cdot$ cm^{-1} in electrolyte-poor blackwater regions to typical values of 60-110 μS $\cdot$ cm^{-1} in whitewater regions of Central Amazon (Furch, 1984b; Crampton, 1998). *Apteronotus* is also found in the relatively electrolyte-rich waters of the Western Amazon, with conductivities of 160-270 μS $\cdot$ cm^{-1} (Hagedorn and Keller, 1996). Although seasonal variations in conductivity in areas inhabited by weakly electric fish have been discussed in the literature (Hopkins, 1972; Knudsen, 1974; Kirschbaum, 1979), there does not appear to be significant seasonal variation in water conductivity for the fast flowing waters inhabited by *Apteronotus* (Furch, 1984a; Hagedorn, 1988; Crampton, 1998, Hagedorn personal communication).

In this study, we observed the best detection performance at the lowest conductivity (35 μS $\cdot$ cm^{-1}), which is within the natural range. Reduced performance was observed at higher conductivities (300 and 600 μS $\cdot$ cm^{-1}) that are most likely outside the natural range.

Effects of water conductivity on high frequency electrolocation. Changes in water conductivity can influence high frequency (active) electrolocation performance in three ways: effects on the fish's EOD strength, effects on tuberous receptor sensitivity, and effects on the "electrical contrast" between an object and the surrounding water.

The first effect is due to the constant current source characteristic of the electric organ of *A. albifrons*, which causes the EOD amplitude to increase with increasing water resistivity (Knudsen, 1975). Based on data presented in Knudsen (1975), we estimate that the EOD amplitude was approximately ten times higher at our lowest conductivity (35 $\mu S \cdot cm^{-1}$) compared to our highest conductivity condition (600 $\mu S \cdot cm^{-1}$). The strength of the voltage perturbation induced by the *Daphnia* is proportional to the strength of the fish's own electric field (Rasnow, 1996). Hence, considering only the effect of bath conductivity on EOD amplitude, we expect the intensity of the *Daphnia* image on the skin to increase as water conductivity is decreased. Other studies of weakly electric fish have also established that performance on certain high frequency electrolocation tasks improves with lowered bath conductivities, including the ability to discriminate capacitive targets (von der Emde, 1993) and the distance at which conspecifics are detected (Squire and Moller, 1982; Moller, 1995).

The second effect of water conductivity on high frequency electrolocation is related to changes in tuberous receptor organ sensitivity. Knudsen (1974) found that behavioral thresholds to high frequency stimuli increased with decreasing water conductivity in *Apteronotus*. Based on Knudsen's data (Fig. 7; Knudsen, 1974), we would expect the behavioral threshold to an active electrolocation stimulus to increase by about a factor of three as water conductivity decreases from the highest conductivity used in our study to the lowest. This change in sensitivity is measured in terms of an externally imposed voltage gradient in the water outside the skin, and it is independent of the change in amplitude of the fish's EOD discussed above.

The third effect is related to the electrical contrast of the prey. The magnitude of the active electrolocation stimulus depends on the degree to which the electrical impedance of an

object differs from that of the surrounding medium (Rasnow, 1996). We have found that the resistive impedance of *Daphnia* approximately matches that of the surrounding water at a bath conductivity of 300 μS $\cdot$ cm^{-1} (unpublished data). Considering only the resistive impedance of the prey, we would expect its electrical contrast to increase for conductivities both above and below 300 μS $\cdot$ cm^{-1}.

In summary, as conductivity decreases from 600 to 35 μS $\cdot$ cm^{-1}, we would expect an order of magnitude increase in the strength of the perturbation due to the current source property of the electric organ, a factor of three decrease in the overall sensitivity of peripheral electroreceptors, and an increase in the electrical contrast of the prey. The net result is that lower conductivities should result in better performance for high-frequency electrosense, and thus longer detection distances, to the extent that active electrolocation contributes to prey capture behavior.

Effects of water conductivity on low frequency electrolocation. Aquatic prey such as *Daphnia* generate weak low frequency bioelectric fields (Peters and Bretschneider, 1972; Kalmijn, 1974; Wilkens et al., 1997) that can be sensed by ampullary electroreceptors of weakly electric fish (Dunning, 1973; Zakon, 1986). Although the density of ampullary receptors on the surface of the body of *A. albifrons* is more than an order of magnitude lower than that of tuberous receptors, low frequency electrolocation may well be important in prey capture behavior. For example, Kalmijn and Adelman (reported in Kalmijn, 1974) found that *A. albifrons* and *Gymnotus carapo* will strike at low frequency signal sources designed to mimic the bioelectric field of natural prey.

Changes in water conductivity can influence low frequency electrolocation in two ways: effects on the bioelectric potential of the prey, and effects on the behavioral threshold of the fish. The first effect is due to the current source characteristic of *Daphnia*, resulting in increasing bioelectric field strength with increasing water resistivity. The bioelectric potential of *Daphnia* at 1 mm distance has been measured to be on the order of a few hundred microvolts in low resistivity water (760 μS $\cdot$ cm^{-1}), and several thousand microvolts in high resistivity water (10 μS $\cdot$ cm^{-1}) (Wilkens et al., 1997; Wojtenek et al., 1999, and personal communication). The second effect was studied by Knudsen (1974), who examined behavioral thresholds of *A. albifrons* to externally imposed low frequency (10 Hz) sinusoidal fields at different water conductivities. Threshold values were lowest (approximately 0.6 μV $\cdot$ cm^{-1} peak-to-peak) at 100 μS $\cdot$ cm^{-1}, and they increased modestly both above and below this conductivity to values on the order of 1.0-1.5 μV $\cdot$ cm^{-1} peak-to-peak over the range of conductivities of interest here (35–600 μS $\cdot$ cm^{-1}).

Of these two conductivity effects on low frequency electrolocation, the order of magnitude increase in *Daphnia* field strength is expected to dominate the factor 2-3 increase in behavioral threshold. The net result is that lower conductivity should result in better performance for the low frequency electrosense, just as it did for the high frequency electrosense.

Effects of water conductivity on the mechanosensory lateral line. Several species of non-electric fish use the mechanosensory lateral line for detecting the weak flow fields produced by prey (Kirk, 1985; Bleckmann, 1986; Enger et al., 1989; Montgomery, 1989; Bleckmann et al., 1991; Montgomery and Milton, 1993; Janssen, 1997). Lateral-line mediated detection

distances for *Daphnia* are generally found to be around 1 cm (Coombs and Janssen, 1989; Hoekstra and Janssen, 1986; Janssen et al., 1995), although distances of up to 4 cm have been reported for blind cave fish (*Amblyopsis*), a mechanosensory specialist (Poulson, 1963).

Changes in water conductivity are not expected to influence mechanosensory sensitivity, except at very low conductivities where a low concentration of Ca^{2+} in the bath has been shown to reduce hair cell sensitivity (Sand, 1975; Crawford et al., 1991). We would only expect to see such results at our lowest conductivity (35 $\mu S \cdot cm^{-1}$), where the concentration of Ca^{2+} was 0.11 $mmol \cdot l^{-1}$. Studies with non-electric fish also suggest that lateral line sensitivity should be reduced at this Ca^{2+} concentration (Sand, 1975; Hassan et al., 1992). If mechanosensory cues were dominant in prey detection, we would expect detection performance to be largely insensitive to changes in water conductivity, or perhaps to decrease with lower water conductivity due the effects of low Ca^{2+} concentration.

Summary. The improvement in detection performance that we observed with lower water conductivity strongly suggests that electrosensory cues dominate at the low conductivities. Best performance was observed at conductivities comparable to those experienced by the animal in its natural environment, leading us to conclude that electrosense is the ecologically relevant sensory modality for prey capture.

Our results leave open the possibility that improved prey capture performance for both species at low conductivities could be due to either high or low frequency components of electrosense. To assess whether one component is more likely to dominate, we compared estimated signal strengths with estimated behavioral thresholds. Both the high and low frequency

signal strengths appeared to be of the right order of magnitude to be detectable at the observed prey detection distances. Determining the relative contributions of these two components will therefore require further investigation. We have begun developing a pharmacological method to block the low frequency electrosense and mechanosensory lateral line while sparing the high frequency electrosense to aid these investigations (Appendix A).

4.5.3 Functional importance of the dorsal receptor surface

The dorsal surface of the fish appears to be of particular functional importance during prey capture behavior. When searching for prey the fish typically swam forward with an upright posture (i.e., roll angle near zero) and body pitched downward such that the dorsum formed the leading edge as the fish moved through the tank. on the dorsum. Furthermore, immediately following detection the fish initiated a rolling movement during the reversal, that brought the *Daphnia* more directly above the dorsum. Figures 4.5 and 4.6 show that the active space for prey detection is a wedge of space above the dorsum that extends the entire length of the body. The observed dorsal bias may in part be due to prey drifting downward from the point of introduction near the water surface. If we examine the location of the point on the surface of the fish that is closest to the prey over the course of each trial, for all trials, we see that the resulting "prey tracks" are also clustered on the dorsum (Fig. 4.7), with slightly greater spread in the dorsoventral axis near the snout. This distribution is most likely in part due to the way the fish moves through space, in combination with the near stationarity or slow downward drift of the prey over the time spans of interest for this study. An additional factor is the position of the pectoral fins, which makes it less probable to find tracks passing along the middle of

the body as the prey are typically quite close to the body by the time they are near the head, and this would lead to the prey being buffeted away by the fins. The distribution of prey tracks on the fish surface nicely fits with the receptor density distribution (see Fig. 5.3), including the dorsoventral broadening toward the snout. Previous studies of active electrolocation in gymnotids have often focused on objects placed lateral to the fish's flattened body surface, but our results suggest that the space above the dorsum may have greater functional importance to the animal, at least under the conditions of our study.

The functional importance of the dorsum is also reflected by regional specializations in electroreceptor distribution on the body surface (Carr et al., 1982). Tuberous receptors are two to three times more dense on the dorsal surface of the trunk than on the lateral surface. A similar dorsal bias is also observed for ampullary receptors. In contrast, the mechanosensory system has a more lateral bias, with the majority of the neuromasts on the trunk located in the lateral line; only a few superficial (non-canal) neuromasts are located on the dorsum. Apteronotids also possess a specialized electrosensory structure on the dorsal midline, known as the dorsal filament, that may aid in the detection and discrimination of prey (Franchina and Hopkins, 1996). In *A. albifrons*, this filament extends along the caudal-most third of the dorsum. Given that the EOD field is stronger near the tail (Rasnow and Bower, 1996) and the presence of the dorsal filament, we might expect a bias in the detection point distribution toward this region. However, we do not observe this (Fig. 4.6B & C), perhaps in part because the tail region has a smaller surface area and fewer receptors, and perhaps because the fish was not required to discriminate prey from other objects in this study.

4.5.4 Roll: evidence for an electrosensory orienting response to prey

We observed that following detection the fish would execute a body roll to position the prey more directly above the dorsum (Figs. 4.10 and 4.13A). This roll behavior may have both sensory and biomechanical aspects. The sensory aspect is similar to an orienting response observed in Mexican blind cave fish in which the fish rolls the lateral side of its body, and thus the lateral line canal organs, toward objects (Campenhausen et al., 1981). For *Apteronotus*, in addition to taking advantage of the dorsal electrosensory specializations discussed above, centering the prey above the dorsum may facilitate spatial localization by allowing comparisons between electroreceptor activation on the left and right sides of the body. A balanced stimulus would indicate the prey is located directly above the dorsum, whereas an imbalance could serve as a relative measure of the angular deviation from the dorsal plane. In the weakly electric gymnotid *Eigenmannia virescens*, Feng (1977) observed that the roll component of the substrate orienting response was abolished by sectioning one of the bilateral trunk electroreceptor nerves, suggesting that the roll response may depend on bilateral electrosensory comparisons. Balancing an electrosensory stimulus on two sides of the body has also been reported in *Gymnotus carapo* for spatial localization of an electrical dipole (Hopkins et al., 1997). In general, localization through bilateral comparison of stimulus intensity is a common orienting strategy (Hinde, 1970; Kuc, 1994; Coombs and Conley, 1997).

The biomechanical aspect of dorsal roll is related to hydrodynamic constraints associated with the knife-like shape of the animal and the propulsive capabilities of the ribbon fin. Because of these constraints, the fish cannot perform pure lateral translations. Thus when the initial prey

position has a lateral component, the optimal approach strategy may be a dorsal roll toward the prey, accompanied by a dorsum-leading reversal. Similar hydrodynamic constraints have been noted for movements of the flattened rostrum of the paddlefish during prey capture (Wilkens et al., 1997, and personal communication). The electrosensory specialization of the dorsal body surface in *Apteronotus* may have evolved as a result of these biomechanical and hydrodynamic constraints on movement.

4.5.5 Backward swimming

Historically, backward swimming in electric fish has been a topic of keen interest and speculation, triggering research that led to Lissmann's discovery of active electrolocation in 1958 (Moller, 1995). Our results show that rapid reversals in swimming direction play a key role in the behavioral strategy used by *Apteronotus* for prey capture (Fig. 4.3), as has been reported previously for several gymnotids (Heiligenberg, 1973; Lannoo and Lannoo, 1993; Nanjappa et al., 2000).

For fish that detect prey using the electrosense, there are two general body designs and two corresponding behavioral strategies that permit efficient prey capture. The first design has the mouth located subterminally, with receptors in front, allowing prey to be scanned across the receptor array before reaching the mouth during forward swimming. This is observed in many elasmobranchs and in paddlefish (Montgomery, 1991; Wilkens et al., 1997). The second design has the mouth positioned terminally, with receptors located behind the mouth. This design is complemented with a behavioral strategy of backward swimming to scan the image across the receptor array, as observed in *Apteronotus* and other gymnotids (Heiligenberg, 1973; Lannoo

and Lannoo, 1993; Nanjappa et al., 2000). In *Apteronotus*, tuberous and ampullary electroreceptor densities are about 5-10 times higher on the head than on the trunk (Carr et al., 1982); the head can thus be considered the "electrosensory fovea." By executing a rapid reversal, the fish scans the electric image of the *Daphnia* across a receptor array of increasing density and provides the nervous system with a progressively stronger and sharper electrosensory percept.

4.5.6 Tail bend

Swimming modes that utilize propagated waves along an elongated ventral (gymnotiform mode) or dorsal (amiiform mode) ribbon fin effectively decouple locomotion from trunk movements (Breder, 1926). Lissmann (1958, 1961), among others, has speculated that ribbon fin locomotion, when performed with a rigid trunk, may help electric fish avoid electrosensory reafference caused by tail bending (von Holst and Mittelstaedt, 1950; Bastian, 1995b). Tail bends cause large modulations of the transdermal potential due to movement of the electric organ in the tail (Bastian, 1995b; Assad, 1997). It is also possible that by decoupling propulsion from trunk movement, trunk movement can be utilized to aid sensory acquisition. For example, gymnotids are known to execute nonlocomotory tail bends during exploration of novel objects (Heiligenberg, 1975; Assad et al., 1999). Lannoo and Lannoo (1993) noted that *A. albifrons* arched their bodies toward *Daphnia* during prey capture behavior. The gymnotid *G. carapo* similarly bends its body to conform to the curvature of electric field lines when approaching dipole sources (Hopkins et al., 1997).

We examined tail bend in *A. albifrons* during prey capture behavior to address some of these issues. We observed that the fish does not keep its body straight prior to detection (Fig. 4.12),

arguing against the need to minimize electrosensory reafference by maintaining a straight trunk. It is now known that fish can compensate for electrosensory reafference in the central nervous system (Bastian, 1995b, 1999). We did note that the RMS value of the bend angle dropped significantly following detection (Fig. 4.12), which implies a straightening of the body during the rapid reversal. This may have sensory relevance or may be due to hydrodynamic constraints on rapid backward movements.

In addition to examining the magnitude of tail bend, we quantified the velocity of tail bend. Our results show an average RMS bending velocity close to $90^{\circ} \cdot s^{-1}$, corresponding to an arc velocity of about 15 cm $\cdot s^{-1}$ at the tip of the tail. The tail bending behavior we observed is different from the slow, large amplitude "tail probing" that occurs during exploration of novel objects (Assad et al., 1999). In general, the tail bends we observed were fast, small amplitude adjustments of body posture. It is possible that these postural adjustments facilitate active electrolocation by modulating the spatiotemporal properties of the *Daphnia* electric image.

4.5.7 Closed-loop control of prey capture

Our results show that following prey detection, *Apteronotus* is able to adaptively modify its trajectories to intercept prey that are drifting or being buffeted away. Closed-loop control of prey capture is rather remarkable given how rapidly the behavior is executed, with a mean time from detection to capture of 665 ± 165 ms. Thus it appears that the fish continues to process incoming electrosensory data and update estimates of current prey position on a relatively fast time scale. Another possibility is that the fish is able to predict the trajectory of the prey and use this prediction for feed-forward control of the prey capture strike. We believe this is unlikely

in this case, as the majority of the movement of the prey appears to be due to turbulance caused by the fish's rapid reversal, the effects of which could be quite difficult to predict in principle. The real-time demands of closed-loop tracking of prey sets limits on the integration times that the nervous system uses for prey localization and therefore constrains neural models of electrosensory target acquisition. Such a closed-loop strategy is similar to nonvisual prey pursuit strategies observed in echolocating bats (Kalko, 1995), and it contrasts with open-loop, ballistic strike strategies such as those observed in the tiger beetle and mottled sculpin (Gilbert, 1997; Coombs and Conley, 1997).

CHAPTER 5

Sensory signal estimation

5.1 Summary

In order to understand the nature of the signal processing that the brain has to perform in order to detect an object in the environment, and then estimate features of that object that are relevant to the current behavioral goal, we need to know about the signals reaching the brain that are correlated with the presence of the object. With regard to the specific behavior we are concerned with in this study, the prey capture behavior of weakly electric fish, we have developed a computational approach to estimating the afferent activity of a key sensory modality that the fish uses to hunt for, detect, and capture *Daphnia*. In the previous chapter, we established that electrosense plays a role in the prey capture behavior of *Apteronotus*. The vast majority of the electroreceptive afferents are tuberous units, and almost all of the tuberous units in the trunk region of *Apteronotus* where prey detection typically occurs (Fig. 4.6) are the P-type amplitude coders (Hagiwara et al., 1965; Szabo and Yvette, 1974). By coupling the tracking data presented in Chapter 4 to a model of

the P-type sensors, and a model of how the energy that these sensors are tuned to is modified by the presence of prey, we are able to estimate the full sense data stream (≈14,000 afferent spiketrains) reaching the brain during behavior. At the time of prey detection, the signal to these afferents is approximately 0.1% of the steady state signal level. At the time of detection, the number of receptors stimulated by the presence of the prey is on the order of a few thousand. These receptors supply a change in the total spikecount across all afferents of only approximately 0.05%. Due to the regularization of the spikecount over behaviorally relevant time windows found in the electrosensory afferents (Ratnam and Nelson, 2000), this small change is over three standard deviations above the baseline spikecount, and thus may be detectable by the animal. Using a 3σ threshold, we derived a neural detection time which we then compared to the behaviorally estimated detection time. For the trials where the detection distance was highest, and where we believe that the electrosense is most strongly contributing to the behavior, the difference between the neural and behavioral detection times was not statistically significant. These results will be useful for ongoing efforts toward understanding the information processing principles underlying adaptive sensory acquisition in vertebrates.

Key words: computational neuroethology, afferent spiketrain, sensory reconstruction, electrolocation, detection, signal processing, electric field

5.2 Introduction

In order to understand the nature of the signal processing that the brain has to perform in order to detect an object in the environment, and then estimate features of that object that are relevant to the current behavioral goal, we need to know about the signals reaching the brain that are correlated with the presence of the object. With regard to the specific behavior we are concerned with in this study, the prey capture behavior of weakly electric fish, we have developed a computational approach to estimating the afferent activity of a key sensory modality that the fish uses to hunt for, detect, and capture *Daphnia*. In the previous chapter, we established that electrosense plays a role in the prey capture behavior of *Apteronotus*. The vast majority of the electroreceptive afferents are tuberous units, and almost all of the tuberous units in the trunk region of *Apteronotus* where prey detection typically occurs (Fig. 4.6) are the P-type amplitude coders (Hagiwara et al., 1965; Szabo and Yvette, 1974). By coupling the tracking data presented in Chapter 4 to a model of the P-type sensors, and a model of how the energy that these sensors are tuned to is modified by the presence of prey, we are able to estimate the full sense data stream ($\approx$14,000 afferent spiketrains) reaching the brain during behavior. In what follows we detail the methods used to accomplish this, and the results of our analysis.

5.3 Methods

There are six sections: development of the high resolution fish surface model, populating this model with electroreceptors, estimation of the electric field at the prey, measurement of

prey impedance, estimation of the transdermal voltage, and estimation of the afferent spiking activity.

5.3.1 The high resolution fish surface model

The original model-based tracking and analysis discussed in Chapters 3 and 4 were performed with a fish model that consisted of fifteen cross-sectional (transverse plane) irregular polygons, each with six vertices. The ninety vertices of these fifteen polygons were utilized to make eighty-four quadrilateral faces when visualizing the fish model. The distance between each cross-sectional polygon varied, with less distance between polygons near the head than between polygons in the trunk, where the surface of *A. albifrons* linearly tapers similar to a cone. In earlier estimations of the electrosensory consequences of movement during prey capture sequences (Nelson and MacIver, 1999), we found that the low spatial resolution of this model led to artifacts. In addition, the earlier estimates did not take into account the distribution of electroreceptors, which is clearly relevant to motor aspects of sensory acquisition such as rolling behavior where a region of higher electroreceptor density is oriented towards the prey (Fig. 4.10). However, the low resolution of the ninety-vertex model made it less suitable for population with the full complement of $\approx$14,000 electroreceptors estimated for this species (Carr et al., 1982). A simple method for populating the model with electroreceptors is to regenerate and restructure the fish surface such that the distribution of vertices leads to there being around one receptor per associated quadrilateral. As there is a $1:1$ relationship of quadrilaterals to vertices for all but the vertices on the terminal cross-section, this thereby allows the coordinates of each vertex to serve as the coordinates of a receptor where needed.

To regenerate and restructure the low resolution model, it was brought into a 3D modeling package (Rhinoceros, Robert McNeel & Associates, Seattle, WA, USA). The cross-sectional polygons were used to build a smooth non-uniform rational b-spline (NURBS) surface and the surface was then adjusted using the package's surface rebuilding functions. The new surface was then used to generate a new set (267) of cross-sectional polygons with a fixed spacing of less than 1 mm, and each of these polygons was made to consist of the same number of vertices (99). The resulting model contained 26,433 vertices, a ≈300-fold increase over the low resolution model. As a result of the constant number of vertices per cross-section, the vertex density increases in the head region where the body tapers, roughly in step with the receptor density increase (Fig. 5.1, see section below). This is interesting in light of the observation that tuberous receptor pores are located on the rostral end of the cycloid scales on the surface of the fish (Suga, 1967), as illustrated in an image of a tuberous receptor pore I acquired using an environmental scanning electron microscope (Fig. 5.2). As with the number of receptors, the number of fish scales does not change with age. In addition, as the body tapers, the fish scales also decrease in size (personal observation), just as the inter-vertex distance of the fish model does. However, the face appears to be scaleless in *A. albifrons*; thus, if there is a relationship to between receptor density and scale dimension, perhaps it stems from common dermatomal determinants.

5.3.1.1 Using the model-based tracking data with the new model

In order to reconstruct the position of the originally observed fish, the eight fitted fish model parameters must be applied to the high resolution model at each time step. The eight parameters

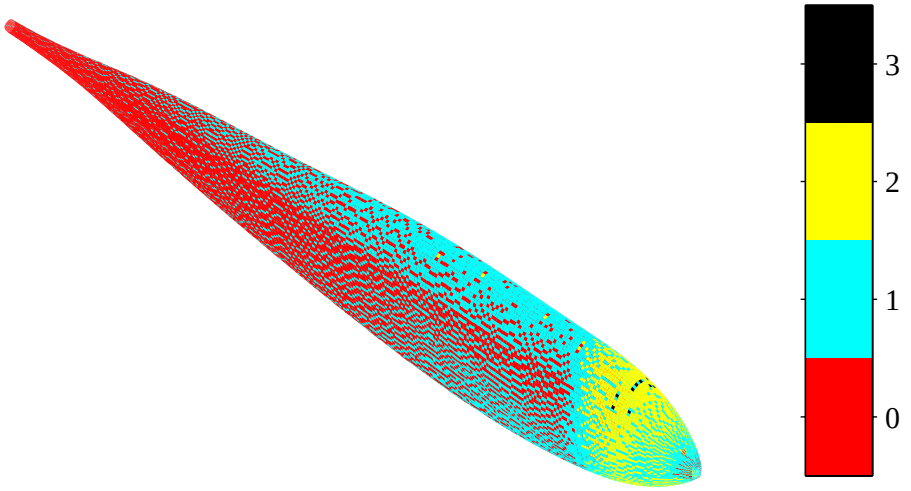

Figure 5.1 Tuberous receptor count by surface model facet. While there is an order of magnitude increase in the density of receptors at the head compared to the trunk, the number on each facet stays close to between 0 and 2 throughout. The ribbon and pectoral fins do not possess electroreceptors.

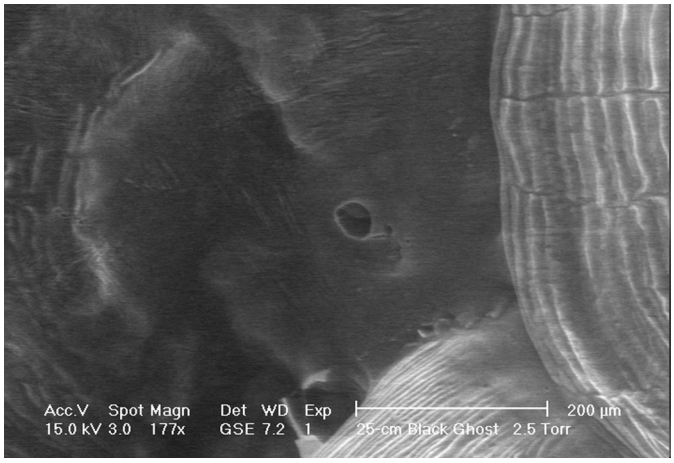

Figure 5.2 Environmental scanning electron micrograph of tuberous receptor pore. The pore is located on the rostral edge of the fish scale (the anterior of the fish is to the right), as observed by Suga (1967).

were the three-axis position of the snout, in-plane rotations of yaw, pitch, and roll, and non-rigid deformation parameters for lateral and dorsoventral trunk bend (see Fig. 4.1). To apply these parameters, the fifteen cross-sections in the high resolution model that were closest to the cross-sections in the low resolution model were identified. The fish positioning algorithm was then run on only the vertices of these fifteen cross-sections. Thus, these cross sections, each containing 99 vertices, were placed into their correct position in the world coordinate system utilizing the same algorithm as was used for the low resolution model during the original fitting of the data to the video images. The location of the vertices for the remainder of the 267 cross-sections was obtained through spline interpolation. Following this procedure minimized the disparity between the original low-resolution fish model position that was fit to the video data and the high resolution model position. The results of this procedure was checked across all time steps of all trials by computing the distance between the low resolution model vertices and the closest corresponding high resolution model vertices.

5.3.2 Populating the fish model with electroreceptors

There are approximately 14,000 tuberous electroreceptor organs on the surface of *A. albifrons*, with each organ innervating one afferent (Carr et al., 1982; Zakon, 1986). In order to assess the neural signal going to the fish's brain during prey capture behavior, we populate the surface of the fish model with electroreceptors according to prior measurements of their density along the body (Carr et al., 1982).

First, we scaled the high resolution *A. albifrons* model described in the preceding section to be the same size of the fish whose electroreceptor density was sampled by Carr et al.

(1982). This was necessary, as measurements on several other fish indicated that the number of electroreceptor organs does not change with changes in fish size (Carr et al., 1982); thus, the receptor density decreases as the fish grows. With a model of *A. albifrons* the same size as that used in the study, we then identified the locations of the body landmarks that were used as reference points for the density measurements. In the Carr et al. (1982) study, the receptor density was measured at 21 such points per side. With these points registered on the model fish, we then used interpolation to generate a density estimate for each of the 26,334 quadrilaterals on the surface. Starting with the dorsalmost quadrilateral at the snout and proceeding in a clockwise fashion down the fish, the area of each quadrilaterals was computed and multiplied by the receptor density for that quadrilateral. The whole number portion of this computation was subtracted off and the corresponding quadrilateral labeled as possessing that number of receptors. The remainder was carried forward to be added to the next computation. At the end of this procedure, a total of 13,953 receptors had been positioned on the quadrilaterals, in excellent agreement with number of receptors experimentally estimated and the number of cells in the ganglion where the afferent cell bodies reside (Carr et al., 1982). The resulting density distribution is shown in Fig. 5.3. A total of 11,954 quadrilaterals had one or more electroreceptors, of which 1,990 quadrilaterals had one additional electroreceptor and 9 quadrilaterals had two additional electroreceptors. Thus, 14,380—over half–of the quadrilaterals of the fish had no associated electroreceptor.

To determine the receptor distribution for each subject used in our behavioral studies, the receptor count for each quadrilateral determined above is retrieved. Thus, fish smaller than the mapped fish will have higher receptor densities and larger fish will have lower densities.

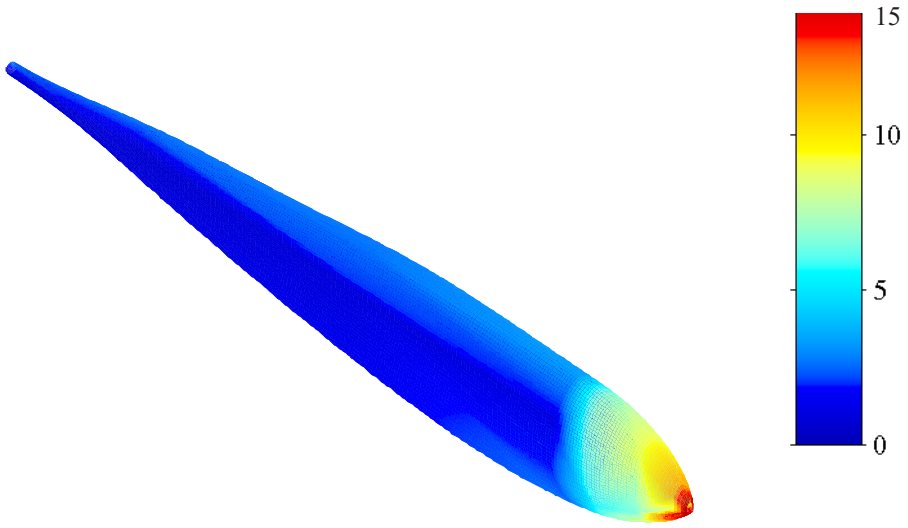

Figure 5.3 Tuberous receptor density on the surface of *A. albifrons*, reconstructed from data presented in Carr et al. (1982). There is an order of magnitude increase in density rostral of the operculum, a region sometimes referred to as the electrosensory "fovea". There is also an increase in the density at the dorsal and ventral edges of the body. The ribbon and pectoral fins do not possess electroreceptors.

5.3.3 Estimating the electric field at the prey

The analytic model we use for computing the input for each electroreceptor requires the magnitude and direction of the electric field vector at the location of the prey. The electric field around a fish varies with a number of factors, including fish size, conductivity of the water, deformation of the body such as tail bending, and objects in the environment. We will make several simplifying assumptions in light of these sources of variation. First, we will use detailed measurements of the electric field around a 10 cm *A. albifrons* obtained from other researchers (B. Rasnow, C. Assad, P. Stoddard, 1993 unpublished measurements, collected as detailed in Rasnow and Bower 1996). The magnitude of the field is shown in Fig. 5.4. The length of the fish that was mapped was similar to the 13 cm mean length of the subjects in this study. Second, we will neglect the effects of body deformation, and utilize measurements of the field around a straight fish. Measurements of afferent activity indicate that large amplitude ($\pm$ 45°) tail

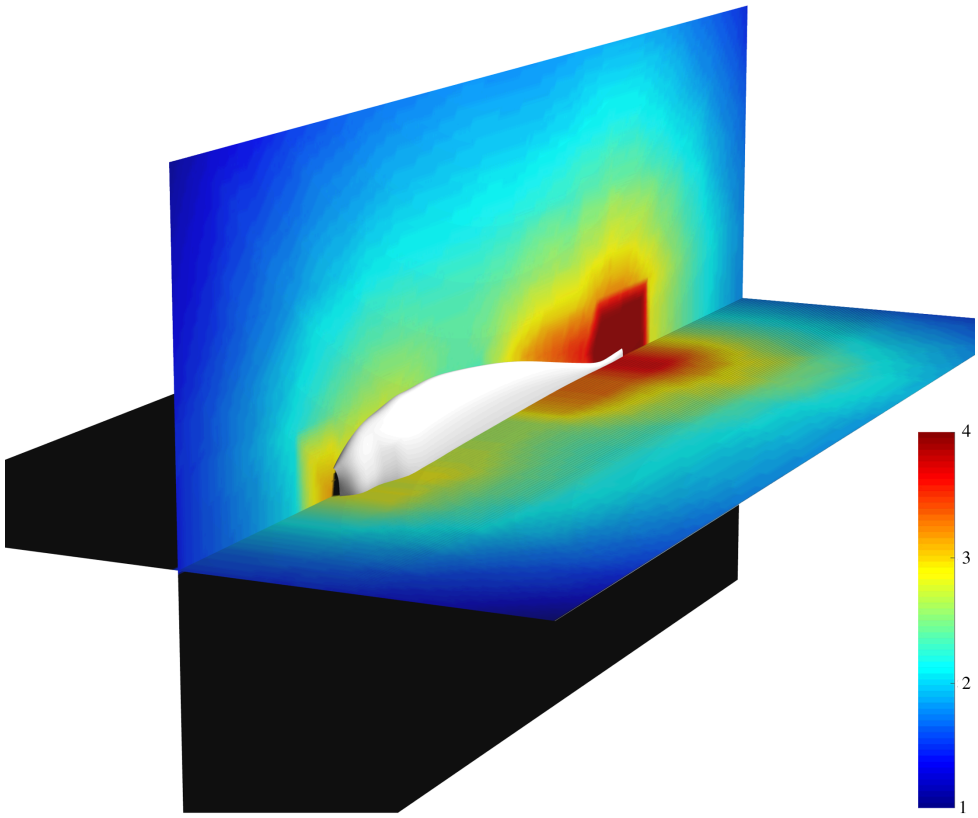

Figure 5.4 The magnitude of the dorsal and median plane electric field vectors for a 9.8 cm *A. albifrons* in 210 μS $\cdot$ cm^{-1} water, log μV of the RMS value over one electric organ discharge cycle (B. Rasnow, C. Assad, and P. Stoddard, 1993 unpublished measurements collected as detailed in Rasnow and Bower 1996). A surface model of the mapped fish is also shown.

bends, which concentrate the field on the concave side of the body, can change afferent firing rates by 10-20% (Bastian, 1999). However, the tail bends that we observed during our studies were more commonly small amplitude rapid bends (see Chapter 4, sections 4.4.7 and 4.5). Third, we assume that the electric organ is a constant current source, and thus linearly scale the measured field strength by the ratio of the conductivity of the bath during the measurement of the map to the conductivity of the bath during the behavioral recording. For the conductivity ranges treated here, this approximation is in good agreement with measured variation of field strength with water conductivity for this species (Knudsen, 1975).

In order to compute the value of the field vector at the prey by use of the map for the 10 cm *A. albifrons* we must first find the location of the prey relative to the fish used in the mapping study, and then estimate the field at that point based on the nearest measured values. At each time step of behavior, a coordinate frame is established at the transverse section of the original fish that has the shortest distance to the prey, using as basis vectors the vector from the center of the section to the center of the next caudal section, the vector from the ventral edge to the dorsal edge, and the vector from the midline to the left lateral aspect. To find the equivalent transverse section in the straight-bodied mapped fish, we first scale the field mapped fish to the same length, width, and height as our source fish, and find the transverse plane the same distance from the snout as the transverse plane previously chosen. The prey is then placed at the same point relative to a coordinate frame erected at that section.

Having found the location of the prey in the reference frame of the field-mapped fish, the next step in computing the field at the prey is to scale the coordinates of the field measurements using the same length-width-height scaling factors used for the fish in the previous step. As

noted, we do not attempt to correct for the effects of fish size on the field here, thus we do not scale the field measurements themselves. However, this procedure does result in an implicit scaling of the field values. If the (x, y, z) (length, width, and height) fish scaling factors are greater than unity, by scaling the field measurement coordinates we may be slightly overestimating the field gradient around the larger fish (if we consider the fish body as roughly interchangeable with a dipole, greater fish length is equivalent to larger dipole separation, which results in weaker field gradients). Conversely, if the scaling factors are less than unity, we may be slightly underestimating the field gradient. Given that the mapped fish's length is close to the length of fish used in our studies, we expect that this scaling will result in negligible error.

The mapping data contains measurements in the median and dorsal planes of the fish, extending roughly six centimeters out rostral, caudal, dorsal, and ventral of the fish, with sampling interval of 1 cm distal to the fish and 0.5 cm or less proximal (closer than 2 cm). Given the detection distances we found, the data therefore spans the volume of space of interest. Roughly speaking, the field is radially symmetric about the central axis of the fish (Rasnow, 1994). Thus, in principle the field at locations away from the dorsal and median planes could be estimated from measurements on one side of any plane containing this axis. In order to obtain a more accurate estimate, we retrieve field vectors on both the median and dorsal planes, rotate these field vectors to the location of the prey, and weight the contribution from each plane by the plane's angular proximity to the prey in the transverse plane (Fig. 5.5).

The appropriate field vector to rotate on the median and dorsal plane is computed by locating the transverse plane containing the prey. For our data, this plane normally includes a cross section of the fish, except in those instances where the prey is rostral or caudal to the body of

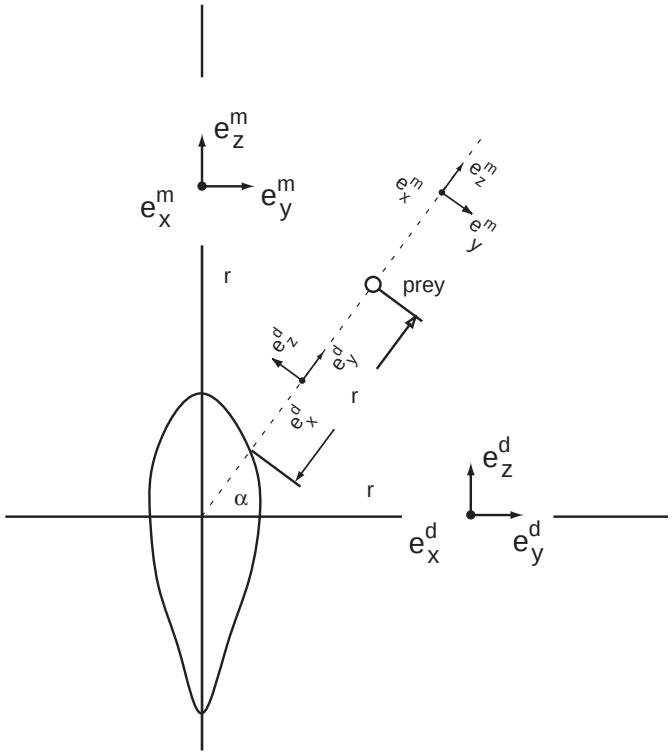

Figure 5.5 The computation of the field at the position of the prey. The figure shows the transverse plane containing the center of the prey that has been placed into the field-mapped fish coordinates. The field vectors the distance r of the prey to the fish surface are found on the median and dorsal plane, and rotated to the prey. The are then combined by weighting their value by the angle the vectors were rotated through.

the fish. A simple approach would be to rotate the vector from the central axis to the prey to the dorsal and median planes, and use the field vectors at these two locations. However, the laterally compressed geometry of the body of these knifefish fish could result in errors for prey locations close to the fish near the dorsal plane. Thus, we instead take the distance between the prey and the surface of the fish at the transverse section and lookup the on-plane field vectors at this distance away from the fish surface, as shown in Fig. 5.5. When the transverse section does not contain the fish, we take the central axis of the fish as the point at which to rotate the radius vector. Once the correct locations on the dorsal and median planes are found, we estimate the field at these locations by linear interpolation of the nearest neighboring measurements.

The result of this procedure is two field vectors, e^d from the dorsal plane, and e^m from the median plane. These two field vectors are then rotated to the position of the prey, and weighted by their angular distance to the prey. The equations for performing this two-plane interpolation are as follows for the case shown in Fig. 5.5; the equations are very similar for other prey quadrants:

$$e^p_{dx} = e^d_x \tag{5.1}$$

$$e^p_{dy} = cos(\alpha)e^d_y - sin(\alpha)e^d_z \tag{5.2}$$

$$e^p_{dz} = sin(\alpha)e^d_y + cos(\alpha)e^d_z \tag{5.3}$$

$$e^p_{mx} = e^m_x \tag{5.4}$$

$$e^p_{my} = cos(90 - \alpha)e^m_y + sin(90 - \alpha)e^m_z \tag{5.5}$$

$$e^p_{mz} = -sin(90 - \alpha)e^m_y + cos(90 - \alpha)e^m_z \tag{5.6}$$

$$e^p = ((90 - \alpha)/90)(e^p_{dx}e^p_{dy}e^p_{dz}) + (\alpha/90)(e^p_{mx}e^p_{my}e^p_{mz}) \tag{5.7}$$

where ${e^p}_{dxyz}$ are the components of the field at the prey from the dorsal plane following rotation, ${e^p}_{dxyz}$ are the components from the median plane, and e^p is the field after the contribution from each plane has been weighted appropriately.

Finally, consistent with our idealization of the electric organ as a constant current source, we scale e^p by the ratio of the field mapping conductivity to the test conductivity, leading to field scaling factors of 6.0, 2.1, 0.7, and 0.3 for water conductivities of 35, 100, 300, and 600 $\mu\text{S} \cdot \text{cm}^{-1}$ respectively.

5.3.4 Measurement of prey impedance

The strength of the high frequency component of the electrolocation stimulus is proportional to the contrast between the impedance of the object and the impedance of the surround-

ing water (see the following section). Thus, to estimate the strength of this signal for the prey, we undertook measurements of the impedance of live *Daphnia*. A test cell was constructed of glass tubing (2 mm ID) embedded in a Plexiglas block. Brass cylindrical electrodes (2 mm OD) were gold plated, then plated with platinum black by applying 36 C/cm^2 at a 10 mA/cm^2 current density (Schwan, 1963). The electrodes were attached to micromanipulators to accurately set the electrode spacing to 3 mm. The leads of the electrodes were connected to a precision LCR Meter (HP 4245A, Agilent Technologies Inc., Palo Alto, CA, USA) and the magnitude and phase of the impedance of live *Daphnia magna* was measured over a range of frequencies (0.03, 0.10, 0.3, 1, 3, 10, 30, 10, and 30 kHz) and water conductivities (100, 300, and 1000 μS). The water used for these measurements had the same relative ionic concentrations as the water used during the recording of fish behavior.

5.3.5 Estimating the transdermal voltage

Given an electric field vector $\vec{E}_{fish}$ at the location of the prey, the perturbation (Δ) of the dipolar field (ϕ) as a function of location ($\vec{r}$) from the center of a spherical object (in this case, the *Daphnia*) is given by Rasnow (1996):

$$\Delta\phi(\vec{r}) = \left(\frac{\vec{E}_{fish}\cdot\vec{r}}{r^3}\right)\left(a^3\frac{1-\rho_p/\rho_w}{1+2\rho_p/\rho_w}\right) \tag{5.8}$$

where a is the radius of the prey, ρ_p is the resistivity of the prey (obtained from the prey model, section 5.4.1), and ρ_w is the water resistivity. We idealize the *Daphnia*, which have a length of 3 mm on average, as a 3 mm diameter sphere.

Computing the electrosensory image for a single "frame" of a reconstructed prey-strike trajectory involves evaluating this equation for a fixed value of $\vec{E}_{fish}$ (i.e., a fixed prey position relative to the fish) and with $\vec{r}$ corresponding to the vector from the center of the *Daphnia*to the vertices of the high resolution fish. Computing the full spatiotemporal image pattern during a complete prey strike involves evaluating the equation with $\vec{E}_{fish}$ and $\vec{r}$ taken as functions of time. Given our behavioral data, this results in a spatiotemporal image resolution of approximately one estimate per 0.2 mm^2 of electroreceptor surface per 16.7 ms of behavior.

The last term of the equation varies in magnitude from unity for a perfect conductor, to -0.5 for a perfect insulator. To quantify the spatiotemporal pattern of the signal, we initially ignore the effects of the measured impedance of the prey, and idealize the *Daphnia*as a perfect conductor. We consider the effects of including the measured resistive component of the prey impedance and the water conductivity in a separate section. As we are not considering the phase-sensitive electrosensory pathway in this study (mediated by T-units, see Zakon 1986), we do not here consider the effects of the capacitive component of the prey impedance.

5.3.6 Estimating the afferent activity

We have recently developed a linear adaptive threshold model of P-type electroreceptors (Brandman and Nelson, 2001). The model captures some special statistical properties that we believe are crucial to the weak signal detection ability of this animal (Ratnam and Nelson, 2000). The model is described by five update rules, which are evaluated in the following order at each time step n:

$$u[n] = exp(-1/\tau_m)u[n-1] + [1 - exp(-1/\tau_m)]gi[n] \tag{5.9}$$

$$v[n] = u[n] + w[n] \tag{5.10}$$

$$\theta[n] = exp(-1/\tau_\theta)\theta[n-1] + [1 - exp(-1/\tau_\theta)]\theta_0 \tag{5.11}$$

$$s[n] = H(v[n] - \theta[n]) = \begin{cases} 1 & \text{if } v[n] \geq \theta[n], \\ 0 & \text{otherwise.} \end{cases} \tag{5.12}$$

$$\theta[n] = \theta[n] + bs[n] = \begin{cases} \theta[n] + b & \text{if } s[n] = 1, \\ \theta[n] & \text{otherwise.} \end{cases} \tag{5.13}$$

where u is the value of a low pass filter, v is the afferent intracellular voltage, θ is the action potential threshold, and s is a binary spike train, H is the Heaviside function, defined as $H(x) = 0$ for $x < 0$ and $H(x) = 1$ for $x \geq 0$.

The voltage v is a product of the input resistance g and the instantaneous input current i, plus random noise w, where w is zero-mean Gaussian noise with variance σ^2. When the voltage v crosses the threshold level θ, a spike is generated and the threshold level is elevated by an amount b. Then, the threshold decays exponentially with a time constant of tau_theta until the next spike is generated.

For the results presented in this chapter, we used the following parameters: $\tau_m = 8$, $\tau_\theta = 60$, $b = 0.052$, $\theta_0 = bR$, where R is a random number from a uniform distribution on the interval (0.0,1.0), $\sigma^2 = 0.0004$, $g = 0.25$.

To compute the activity of the afferent population of the fish, we take the transdermal voltage history of each quadrilateral possessing one or more electroreceptors as input $i[n]$ to this model. The model generates steady-state spike rates of 300 spike s^{-1} with an input $i = 1$, which is approximately what we measure in *A. albifrons*. Thus, the computed transdermal perturbation is added ($i[n] = \Delta\phi[n] + 1$) prior to the signal entering the model.

When there is more than one receptor on a quadrilateral, the model is independently run with the same $i[n]$. Because the Gaussian random noise is different for each afferent, the spiking activity is also different. An alternative approach to a quadrilateral possessing more than one receptor would be to randomly place each receptor on the surface of the quadrilateral, and then compute the perturbation with a correspondingly different $\vec{r}$. However, given the very small size of the quadrilaterals (on average ≈ 0.2 mm^2), the computed difference in perturbation would likely be masked by the added Gaussian noise.

The effect of the prey on the fish appears to be too small to be observed on a single-afferent basis. Thus, we sum the spiketrains over all 13,953 afferents at each time step. We then filter the summed activity with a 100 ms sliding boxcar. We define the afferent detection time to be the time when the filtered summed activity passes over a threshold of 3σ, where σ is the standard deviation of the filtered spikecount from 100 ms to 150 ms (the first 100 ms are unusable as this is the initialization period of the boxcar filter).

5.4 Results

5.4.1 Prey impedance

The results of our measurements of the impedance of live *Daphnia magna*, the first such measurements of a live small animal we know of, are shown in Fig. 5.6.

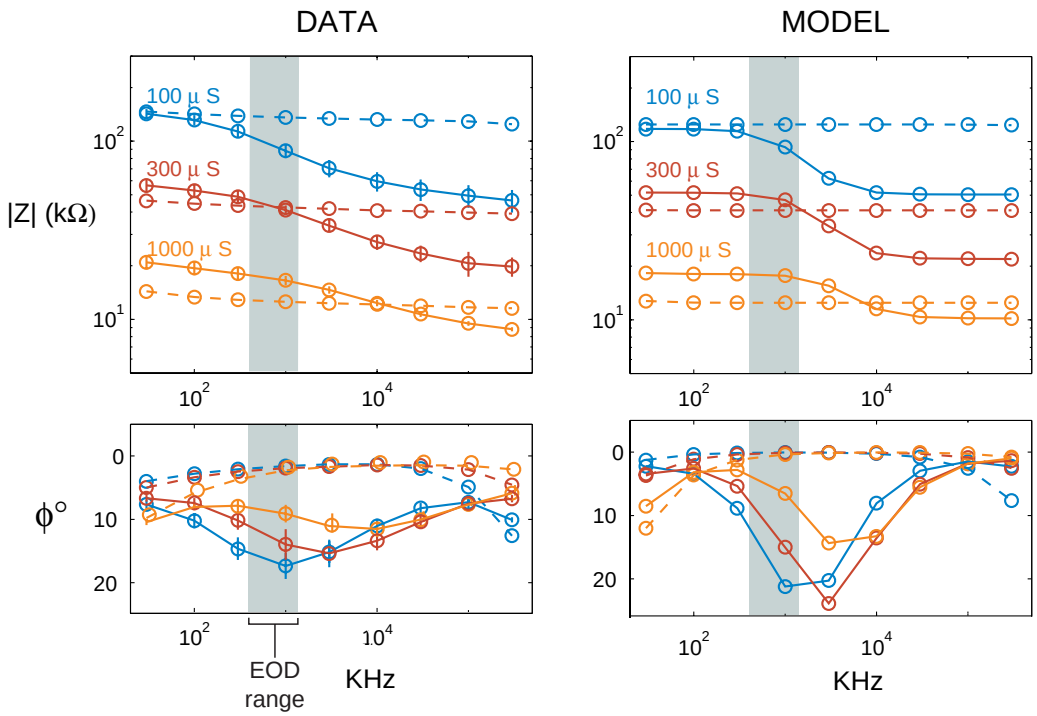

Figure 5.6 Measured and modeled impedance of live *Daphnia* at three water conductivities and nine test frequencies. These three conductivities bracket the natural range found in the fish's habitat. Dashed lines are the impedance of the cell without *Daphnia* (volume replaced with water of test conductivity); solid lines are the impedance with live *Daphnia* in the test chamber. The light green bands show the range of electric organ discharge frequencies for individual *Apteronotus*.

Fig. 5.6 shows both the magnitude of the impedance and its phase as a function of test frequency. The impedance of the test cell containing only the test solution is shown as dashed lines, while the test cell with *Daphnia* is shown with solid lines. We observe that the conductiv-

ity of the empty cell is fairly constant across the tested frequencies; once a *Daphnia* is added, it varies in a frequency-dependent manner. The impedance decreases with increasing frequency, indicating that it is primarily capacitive.

Note that for a bath of 300 μS and a frequency near the mean EOD rate of *Apteronotus*, the empty cell and *Daphnia* $|Z|$ graphs intersect, indicating the prey may provide less stimulus to the P-type electrosensory afferents at this conductivity. A small population of tuberous receptors are phase locked (T-receptors) to the animal's own EOD, which could be used for detecting capacitance. It has been shown that in mormyrids, African weakly electric fish, capacitances of several hundred picofarads to several hundred nanofarads can be discriminated from pure insulators and conductors (von der Emde, 1990). We estimate the capacitance of *Daphnia* to be approximately 2 nF (see below), well within this range. While *Apteronotus* is not related to mormyrids, it is possible that they have comparable discriminative abilities. During electrophysiological studies of the afferents in another South American gymnotid, Feng and Bullock (977b) found that external shunts of less than 50 nF had a clear effect on T-receptor afferent firing.

Examining the phase results, we can see that the empty cell has a phase lag with little variation over the test frequencies, while with *Daphnia* in the chamber, the phase lag increases from approximately -2°in the empty cell to -18°with the lowest conductivity solution at 1 kHz. It is interesting to note that this variation is concentrated in the region of the typical EOD of this species.

In a previous study with mormyrids, von der Emde (1993) showed that at 50 μS, the smallest detectable capacitive value was below 0.5 nF, increasing to 20 nF in water of 800 μS. At

1000 μS, the highest value used in these measurements, he found that fish were unable to make discriminations on the basis of capacitance; he hypothesized that this was due to a reduction in EOD amplitude at high conductivities (the EOD becomes effectively shorted at higher conductivity). We can see from Fig. 5.6 that the extent of the phase lag with *Daphnia* in the cell also decreases with increasing conductivity of the external milieu. This may thus contribute to the failure to discriminate capacitance in high conductivity water.

5.4.2 Prey electrical equivalent model

Several possible electrical equivalent circuits for the *Daphnia* in series with the electrode impedance and in parallel with the surrounding water were tested. We obtained the best match with empirical data with the configuration shown in Fig. 5.7.

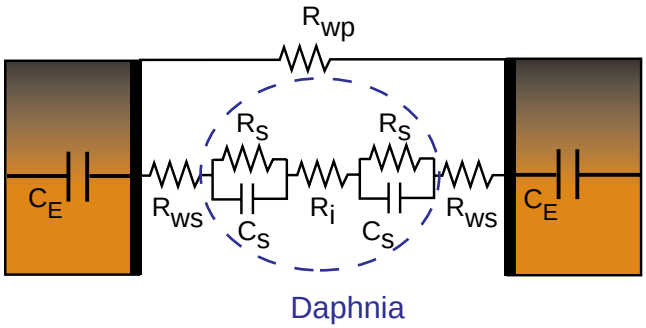

Figure 5.7 Electrical equivalent model of *Daphnia* and the test cell. Abbreviations: C_E, test cell electrode capacitance; R_{wp} resistance of parallel water path; R_{ws}, resistance of series water path; R_s resistance of one face of *Daphnia* exoskeleton; C_s the capacitance of one face of the exoskeleton; R_i the internal resistance of *Daphnia*.

The circuit is a resistor for the internal specific resistance for its body cavity $(550\Omega \cdot cm)$, in series with an identical leading and following circuit for the exoskeleton of the crustacean, consisting of a capacitor in parallel with a resistor $(C_s = 1.2\ nF,\ R_s = 230\ k\Omega)$. Our best

estimate of the electrode capacitance, C_E, was 2 μF per electrode. These values were obtained by utilizing a constrained optimization algorithm to minimize the χ^2 error between the simulated $(|Z|, f)$ and the measured $(|Z|, f)$ across all tested frequencies and water conductivities. Fig. 5.6 shows there is good agreement between the measured and modeled impedance. With this electrical equivalent circuit, we can interpret the pattern of frequency-dependent impedance changes shown in Fig. 5.6. At the lower measurement frequencies, capacitors approximate an open circuit, placing the high resistance of the exoskeleton in series with the lower internal resistance of the body fluids. In low conductivity water, this effect will be minimal as the exoskeleton resistance will be close to the water resistance, but at higher conductivities, the exoskeleton resistance causes the placement of the *Daphnia* in the test cell to increase the impedance relative to the empty cell, as shown by our measurements.

At the higher measurement frequencies, the contribution from the *Daphnia* will be almost entirely from the low resistance body fluids. Since we can see that the impedance of the empty cell is higher at the maximum test frequency for a test solution of 100 μS, and lower for a test solution of 1000 μS, we can infer that the internal resistance of the *Daphnia* is in this range, as our model confirms.

The appearance of the "notch" in the phase graph can also be interpreted with our equivalent circuit. As the capacitive reactance of the *Daphnia* exoskeleton decreases with increasing frequency, at some point it will transition from appearing as an open to sharing the current flowing through the serial water resistance with the resistive branch of the exoskeleton parallel circuit. This occurs at roughly the same point in the measurements as in the model, at around

1 kHz. At higher frequencies, the capacitive reactance approaches zero, so the phase lag does as well.

5.4.3 Effect of the prey impedance on stimulus strength

With the results presented above, we are able to estimate the factor of a in the last term of Equation 5.8 for the four different conductivities used for our behavioral trials. They are 0.7, 0.4, 0, and -0.2 for conductivities 35, 100, 300, and 600 μS $\cdot$ cm^{-1}, respectively. Thus, the transdermal potentials will be accordingly scaled at the different water conductivities, which will then effect the resulting afferent activity.

5.4.4 Signal strength at the time of detection

In this section we consider the magnitude of the perturbation caused by the *Daphnia* when it is considered an ideal conductor. The perturbation magnitude is maximal for perfect conductors (the factor of a in the last term of Equation 5.8 is unity); therefore, this estimate can be considered to be an upper bound.

Across all trials, the peak perturbation at the time of detection had a median of $1.1 \pm 1.6\,\mu$V (Fig. 5.8A), with no statistically significant difference between the values for each conductivity (Fig. 5.8B). As shown in Fig. 5.8A, the data does not have a normal distribution. Thus, in this and several following sections we use the median as an estimate of the center of the distribution, and the interquartile-range derived standard deviation (equal to $0.7413IQR$) as a measure of the spread.

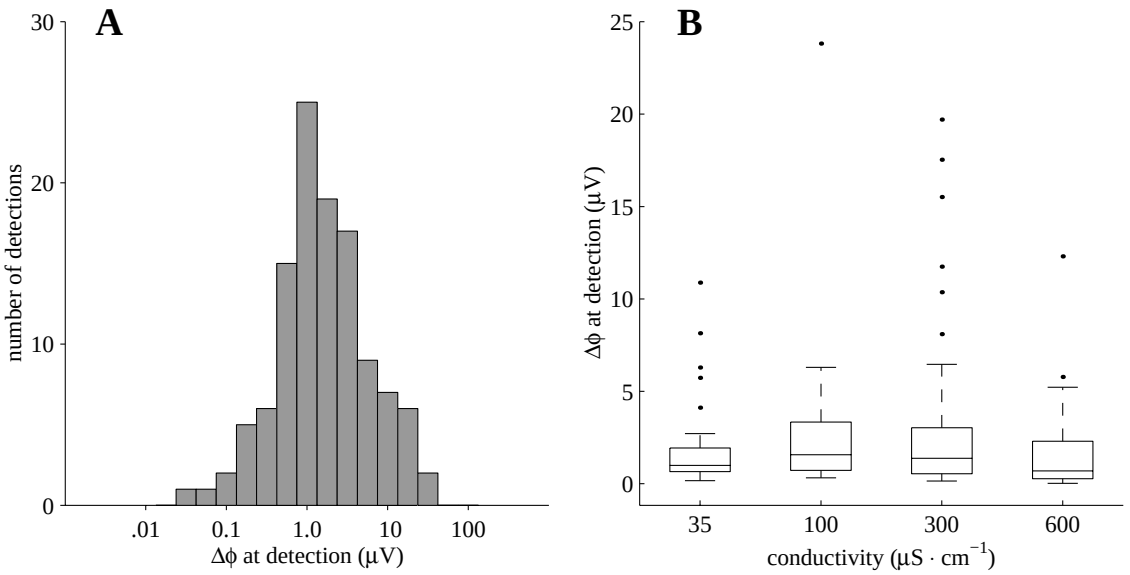

Figure 5.8 Peak magnitude of the prey stimulus at detection. (A) Histogram of the peak transdermal potential change caused by the prey at the time of detection, μV, log scale (N=115). (B) Box plot of the peak transdermal potential change caused by the prey at the time of detection by water conductivity (N=115). The bottom edge of the box shows the lower quartile (25%) value, the top edge of the box the upper (75%) quartile value, and the line within the box indicates the median value. The whiskers extend from the end of each box to show the extent of the rest of the data, to a maximum of 1.5 times the interquartile range. Outliers beyond this point are shown by dots.

5.4.5 Electric image area and receptor count

We will refer to a defined zone of electroreceptor activation on the fish surface as an 'electric image' (Assad et al., 1999). We will examine both the time course of the image and its distribution at our behaviorally determined detection time (see Section 4.4). We have selected two different image metrics, one proportionate and one fixed. Using the proportionate metric, we measured the image by summing the area of the surface that has a transdermal potential greater than or equal to 50% of the maximum transdermal potential at the current time step. For the fixed metric, we measured the image by summing the area of the surface that has a transdermal potential greater than or equal to 0.5 μV. For this analysis, we will focus only on

the trials where we found the highest detection distance, 35 μS $\cdot$ cm^{-1}(N=38), which is likely to be closest to the conductivity of water that the animal lives in (see Section 4.5.2).

5.4.5.1 Properties of the proportionate threshold image

The distant prey casts a diffuse electric image on the surface. The resulting area of the image at half-peak is large, but as the fish zeros in on the *Daphnia*, there is a dramatic narrowing of the width of the image. Four-tenths of a second prior to detection, the image area was 25 $\pm$ 8 cm^2, close to half the entire fish surface area (Fig. 5.9A). At the time of detection ($t = 0$ in Fig. 5.9A), the area had decreased to less than half of that, 9 $\pm$ 4 cm^2 (Fig. 5.9B). Four-tenths of a second post-detection, the area had more than halved again, to 1.4 $\pm$ 2.3 cm^2.

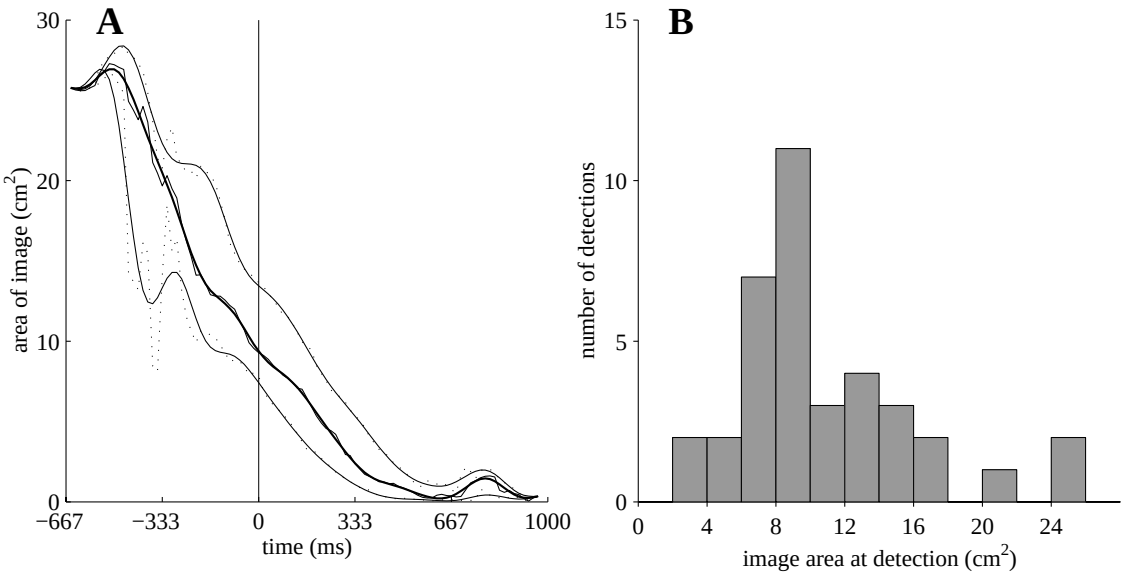

Figure 5.9 Area of proportionate threshold electric image, 50% of peak signal. (A) Peri-detection image area, 25th percentile, median, and 75th percentile (N=38). Smooth lines are the low-pass filtered data, indicated for readability. The peri-detection trials were aligned at the time of detection (t=0). Thus, the tails of the distribution have reduced N due to differences in trial length. (B) Image area distribution at the time of detection.

If we count all the receptors within the proportionate threshold image, we find a similar pattern as was found with the image area. At four-tenths of a second prior to detection, the total receptor count was 8.2 $\pm$ 3.6 thousand; at detection it had dropped to less than half of that, 3.1 $\pm$ 2.4 thousand. Four-tenths of a second post-detection, there was 0.7 $\pm$ 1.2 thousand receptors activated, again a drop of over half the preceding total. An important difference between the area and total receptor profiles, visible in Fig. 5.10A at around t=100 ms, was the decrease in the slope of the total receptor profile from around the time of detection onward. The peri-detection area rapidly decreases, approximately linear with the distance to the prey (Rasnow, 1996), but while this is occurring the prey is being brought toward the region of high electroreceptor density near the head. The brief rise in both the area and receptor count profiles near the end of the trials was due to a brief increase in distance to the prey just prior to capture. As the fish rapidly reverses, it brings the prey into a region of head where the body tapers inward to the snout.

5.4.5.2 Properties of the fixed threshold image

The fixed threshold image area rapidly increased from zero shortly before detection (when the receptors are subthreshold of 0.5 μV), to 36 $\pm$ 7 cm^2, the majority of the surface area of the fish, four tenths of a second post-detection (Fig. 5.11A). The threshold of 0.5 μV was selected in part to avoid rapid saturation of the area profile, but this results in most trials being subthreshold at four tenths of a second prior to detection. At the time of detection, the median image area was 10 $\pm$ 16 cm^2 (Fig. 5.11B).

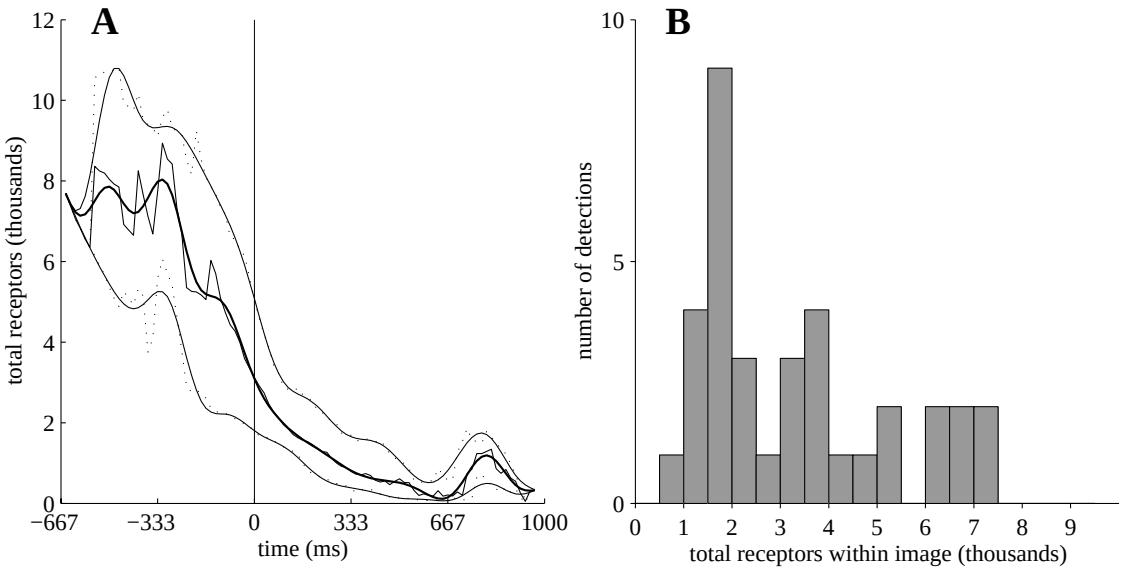

Figure 5.10 Total receptor count for proportionate threshold electric image, 50% of peak signal. (A) Peri-detection receptor count. (B) Receptor count distribution at the time of detection.

Similarly, the total receptors within the image rapidly rose from zero shortly before detection to 3.6 $\pm$ 3.2 thousand at detection (Fig. 5.12B), to 12 $\pm$ 1.5 thousand four-tenths of a second post-detection (the total number of receptors is just under 14 thousand) (Fig. 5.12A). In both the area and count profiles there was a small dip in the profiles corresponding to the prey distance briefly increasing prior to capture.

5.4.6 The receptor-weighted net perturbation

As an approximation of the net sensory stimulation, we developed the receptor-weighted perturbation measure. The receptor-weighted perturbation is the sum of all the voltage perturbations at all the receptors within an image. We have chosen to present this data for the two image types, proportionate and fixed, together with the nonthresholded receptor-weighted perturbation (the sum over all the receptors on the body). The receptor-weighted perturbation at

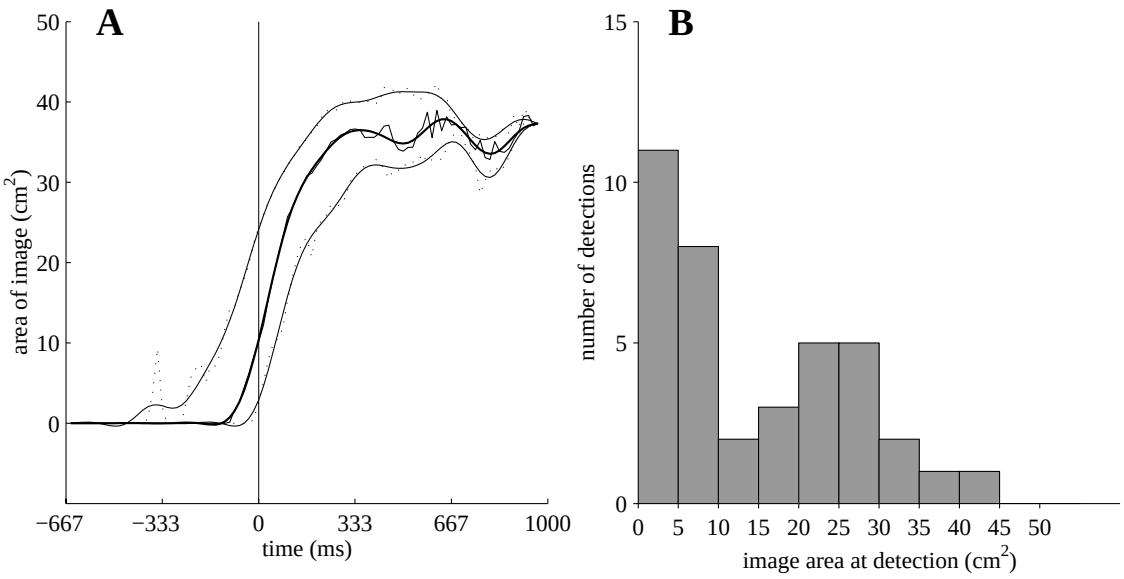

Figure 5.11 Area of fixed threshold electric image, 0.5 μV. Figures include trials where the image area was zero (subthreshold) at the time of detection (N=8). (A) Peri-detection image area. (B) Image area distribution at the time of detection.

detection for the proportionate image was 0.9 $\pm$ 0.3 mV, while it was approximately four times higher for the fixed threshold image, 4.0 $\pm$ 3.2 mV (Fig. 5.13A & B). Four-tenths of a second following detection, the proportionate receptor-weighted perturbation rose to 12.1 $\pm$ 18.6 mV, and the fixed weighted perturbation rose to 53.2 $\pm$ 86.9 mV.

Fig. 5.14A shows the nonthresholded net perturbation. At the time of detection, it was slightly higher than the fixed image net perturbation, at 5.3 $\pm$ 2.9 mV, and similarly four tenths of a second post-detection, 53.8 $\pm$ 86.6 mV. As shown in Fig. 5.14B, there was substantial similarity in the receptor-weighted perturbation at detection across conductivities. There is a weak but significant negative correlation between net perturbation at detection and conductivity (r=-0.4, $p \leq 0.001$).

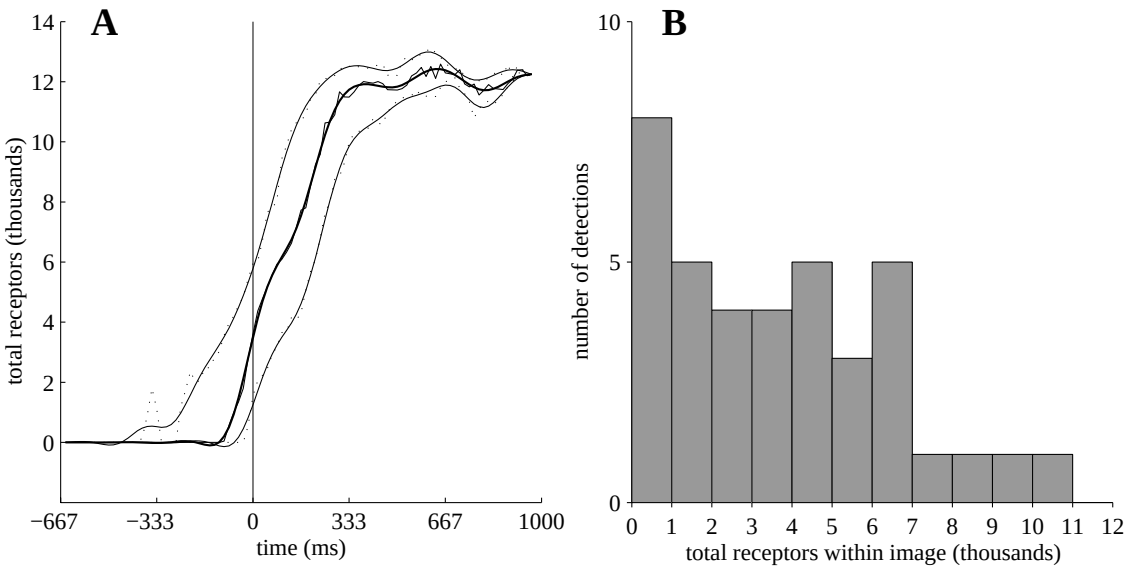

Figure 5.12 Total receptor count for fixed threshold electric image, 0.5 μV. Figures include trials where the image area was zero (subthreshold) at the time of detection (N=8). (A) Peri-detection receptor count. (B) Receptor count distribution at the time of detection.

5.4.7 Afferent response

At the time of detection, the filtered sum of spikes added over baseline (mean 4,567 $\pm$ s.d. 0.55 spike/ms) was 2 $\pm$ s.d. 0.2 spike/ms (N=38). A sample trial 35 μS $\cdot$ cm^{-1} trial is shown in Fig. 5.15A. An afferent detection time, defined as the time when the summed afferent activity passed over a threshold of three times the standard deviation of the baseline, was not statistically different from the behavioral detection time ($p \leq 0.001$). The mean difference (afferent-behavioral) between the two times of detection was -80 $\pm$ 240 ms (Fig. 5.15B). If we then examine the corresponding detection distances, we find very close agreement between the afferent and behavioral detection estimates: the afferent detection distance was 3.0 $\pm$ s.d. 0.8 cm, while the behavioral detection distance was 2.8 $\pm$ s.d. 0.8 cm (N=38). The difference in the means was not statistically significant (t-test, $p \leq 0.001$).

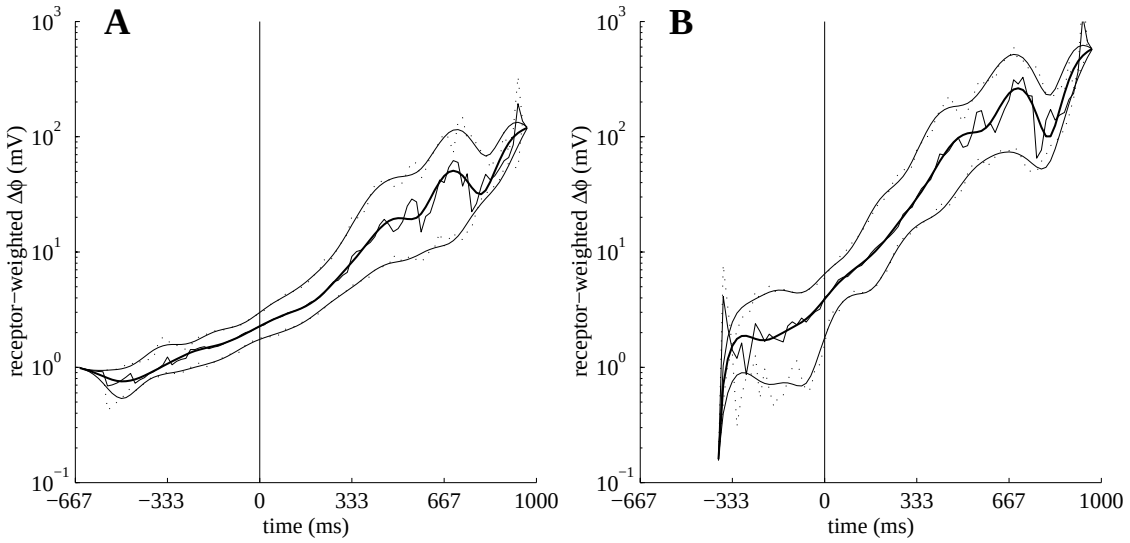

Figure 5.13 The timecourse of the receptor-weighted net perturbation for the two image types. (A) Proportionate threshold. (B) Fixed threshold. The onset of the plot occurs with the first trial where there is one receptor or more above threshold in any of the trials; this occurs at $t = -383$ ms for the 35 μS $\cdot$ cm^{-1} trials, many of which feature large pre-detection prey distances and thus correspondingly small perturbation magnitudes.

5.5 Discussion

Effect of prey impedance. We found that the impedance of the prey was approximately equal to the surrounding water at 300 μS $\cdot$ cm^{-1}. Thus, detection of the prey at this conductivity may be mediated by some combination of T-unit (phase-coder), ampullary unit, and mechanosensory lateral line inputs (see Section 4.5.1). In Chapter 4, we found detection distances of 2.8 $\pm$ 0.8, 1.9 $\pm$ 0.6, 1.3 $\pm$ 0.6, and 1.5 $\pm$ 0.8 cm for 35, 100, 300, and 600 μS $\cdot$ cm^{-1}, the profile of which is roughly consistent with our prey-impedance perturbation scaling factors of 0.7, 0.4, 0, and -0.2. Examination of the effect of the prey impedance on the transdermal potential and afferent activity awaits further analysis.

Electric images. The proportional and fixed image metrics give very different image properties. Neither is likely to be the same as the image metric used by the fish, whose surface

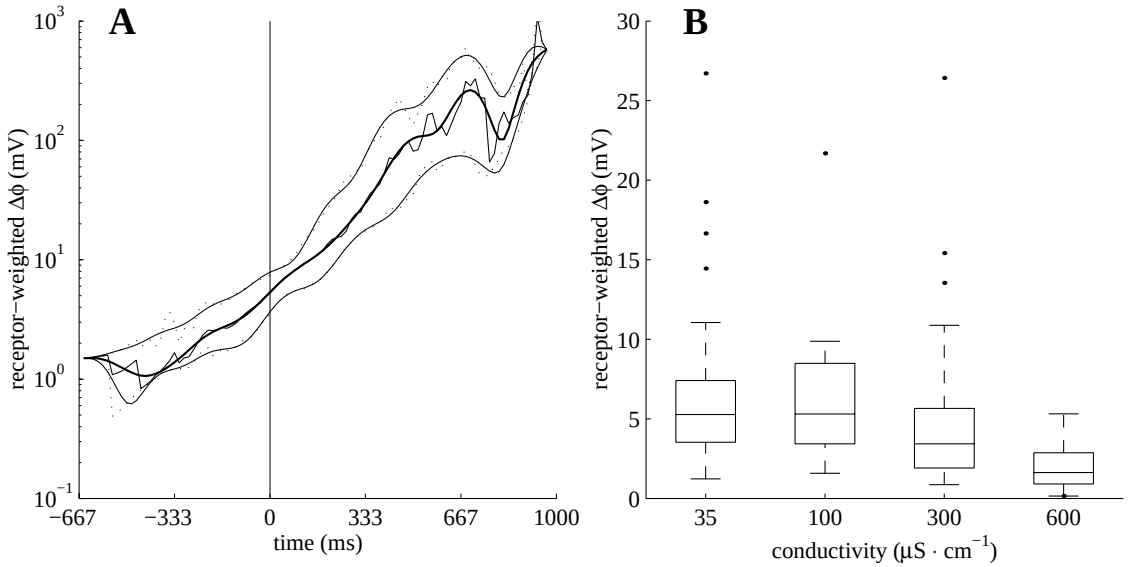

Figure 5.14 The nonthresholded net perturbation. (A) Time course of nonthresholded receptor-weighted perturbation for 35 μS $\cdot$ cm^{-1}. (B) Distribution of the net perturbation at the time of detection across all conductivities.

is covered with receptive fields with excitatory centers and inhibitory surrounds (Shumway, 1989a,b). Given this, it is all the more surprising that our afferent-derived detection time is not statistically different from the behavioral detection time. We expect the performance of the fish to be better than our analysis suggests, because we are averaging out important differences between the post-excitation off-response of the afferents and the on-response. Thus, if we examine the prey tracks depicted in Fig. 4.7, we can imagine a zone of heightened afferent activity on each track just leading the point of closest approach (because the afferents act as high pass filters, and thus are differentiators), and a trailing zone of inhibited afferent firing. If we were to examine the difference in the spatially integrated activity of these two zones, the net afferent contrast, we would most likely come up with an earlier detection time. Given Bastian's 90 ms estimate of the neuromotor latency of these fish (Bastian, 1987), we would hope to find an afferent detection time $\approx$ 100 ms earlier than the behavioral estimate. The diameter of the

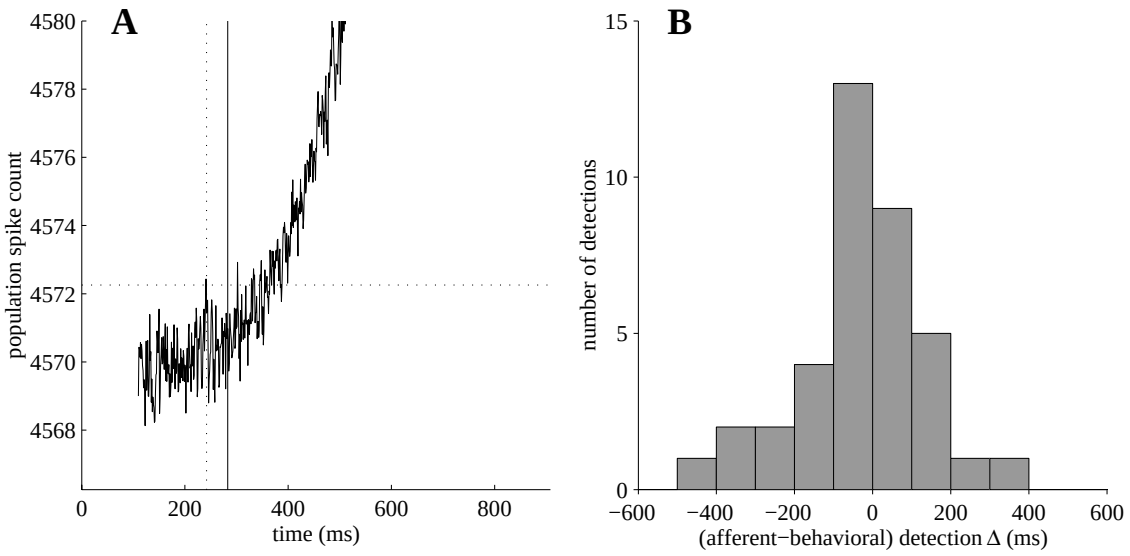

Figure 5.15 Estimated neural versus behavioral detection time. A representative 35 μS $\cdot$ cm^{-1}trial's summed peridetection spike activity, and the population distribution of the difference between the estimated neural and behavioral detection times. (A) Sample population spike activity summed across all 13,953 afferents. Horizontal dotted line shows the 3 σ threshold, and the vertical dotted line shows where the filtered spike count crosses the threshold. The 100 ms intialization time of the filter is not shown. The trial ends at 913 ms, at which time there was a total of 170 spike/ms over baseline due to the prey. (A) Distribution of the difference between the estimated neural and behavioral detection times. Negative values mean the afferents detected the prey before the behavioral detection time. The difference between the means of the corresponding detection distances was not statistically significant (t-test, $p \leq 0.001$).

proportionate image has been shown to be linear with the distance of the prey (Rasnow, 1996), a result we have confirmed (results not shown). Thus, a neural mechanism for assessing the spatial extent of some percentile of the activated electroreceptors may provide the animal with a very simple algorithm for detecting the distance to the prey.

Afferent activity. At baseline, there are approximately 4,500 spikes arriving from the $\approx$ 14,000 afferents per millisecond. Because of spiketrain regularization in these afferents (Ratnam and Nelson, 2000), a property discovered following initial estimates of the strength of the prey stimulus that showed it was an very weak signal (Nelson and MacIver, 1999), an increase of only approximately 2 spike/ms is three standard deviations above the mean spike count. The

coincidence of detection times based on this threshold with behavioral detection times is quite an exciting discovery, and may both validate the accuracy of our models and corroborate our hypothesis that the fish primarily relies on its high frequency electrosense at low water conductivities. More importantly, we have developed a method for observing the spatiotemporal profile of the neural signals correlated with a natural behavior. This information will be important for the next step in our research program, where we will utilize information regarding the typical spatiotemporal profile and magnitude of a natural stimulus towards experimental and modeling efforts to uncover principles of adaptive sensory processing in the brain.

CHAPTER 6

Summary, speculative remarks, and future research

To highlight some of the contributions of this work, I will summarize the primary findings. Following this, I will speculate on what this work suggests about the central processing of prey-related electrosensory signals. Finally, I will briefly discuss future work.

6.1 A summary of the primary results

- The development of a model-based tracking system of animal movements that does not require the use of external markers. This is a key component to investigations into the motor strategies for sensory acquisition.

- The first direct confirmation that the electrosense plays a role in the prey capture behavior of *Apteronotus*. This motivates further investigation into the neural processing of the electrosensory signals that arise during prey capture behavior.

- The discovery of the dorsal roll, a novel electrosensory orienting response. A key claim of the active sense approach is that animal's actively engage their environment in pursuit

of sensory signals; dorsal roll behavior in this organism, which brings a region of higher receptor density toward the prey, is an example of a motor strategy for enhancing signal acquisition.

- The discovery that the animal utilizes a closed-loop adaptive tracking strategy, rather than an open-loop ballistic strike such as used in the mottled sculpin and tiger beetle (Coombs and Conley, 1997; Gilbert, 1997), to intercept the prey. This provides fundamental constraints on the signal processing return time in the animal's hindbrain.

- The reconstruction of the complete neural input for the sensory modality transduced by the P-type afferent population during natural behavior. The simulation of the input, and resulting afferent response, for all ≈14,000 receptors of this animal shows: 1) the peak perturbation at the time of prey detection is ≈0.1% of the baseline signal level, and 2) that this leads to a potentially detectable change in the total spikecount of only ≈0.05%. This result clearly situates the animal's sensory condition as one of extracting a very weak signal from a large baseline, and points the way forward for examining the properties of the background signal that the nervous system will have to filter out in order to extract this weak signal.

- The discovery that despite the low increase in the spikecount, the estimated neural detection time is the same as the behaviorally estimated detection time within statistical uncertainty.

6.2 Some speculative remarks

Figure 6.1 shows the hindbrain structure where all electrosensory afferents terminate, the electrosensory lateral line lobe (ELL). As illustrated in Fig. 6.1B, each map receives identical information from the trifurcating tuberous afferents. The lateral map has high sensitivity and low resolution, the centromedial has low sensitivity and high resolution, and the centrolateral map has sensitivity and resolution somewhere between these two. This arrangement may be well suited to the types of signals I have shown are present at the various stages of prey capture (Chapter 5). At the time of detection, the signal is around a tenth of a microvolt, and excites several thousand receptors above threshold. This very weak signal results in a change of only $\approx$2,000 spike $\cdot$ s^{-1}, out of a total of $\approx$4,500,000 spike $\cdot$ s^{-1} that are arriving at the brain at baseline. The lateral map, with its high sensitivity, seems well suited to play a role in mediating detection at this time, and since all the animal needs to know is roughly where to orient towards, the low spatial resolution of this map does not pose a significant problem for directing subsequent behavior. As the peri-detection perturbation figures of Chapter 5 show, the signal rapidly increases in strength, in part because of behaviors that enhance sensory acquisition, such as the dorsal roll. The centrolateral map may then start to contribute to further behavioral decisions. Finally, the prey reaches the head region, sometimes referred to as the electrosensory fovea because of the order of magnitude increase in receptor density. At this time, the signal is quite strong, so the low sensitivity and high resolution properties of the centromedial map are suited to the prey-related electrosensory signals reaching the ELL in the terminal phase.

A central point of the active sense approach is that a temporal image sequence should be easier to process than a single image, because the images in the sequence are not mutually independent (Blake, 1995). Theoretical approaches to prediction and estimation suggest that correlations between sequences of electric images can be made much stronger through the use of a model of how the the image will change through time. The Kalman filter uses such a model to weight a sensor map by the expected signal to noise ratio, resulting in superior weak signal detection and better noise rejection. We know that the descending inputs to the ELL, which form the vast majority of inputs to this structure, modulate the gain of the pyramidal cells that the sensory afferents terminate on. The action-perception cycle that emerges from these considerations is something like the following: 1) activation of some cells in the lateral map occurs after a suitable number of afferents are modulated by the presence of a target; 2) because of the somatotopy of the ELL, the place of activation on the body surface, and its direction of movement, are simple to extract by higher order structures that modulate the ELL through descending control; 3) the fish increases the strength of the signal by generating motor signals that result in the alignment of the sensory system to the stimulus (such as a roll command) and by closing the gap to the target; 4) the descending projections increase the gain of the parts of the map where the prey is expected to be (the prey "tracks" shown in Fig. 4.7), based on signals regarding self-movement, and, in the case of prey that are moving a significant distance within the brief ($\approx$600 ms, see Chapter 4) period of the strike, a prediction of where the prey will be next; 5) now having obtained a clearer electrosensory percept, the fish manipulates its position further, reversing to bring the prey into the region of highest receptor density and where it can engage depression of the hyoid to bring the prey into the mouth through suction. As this

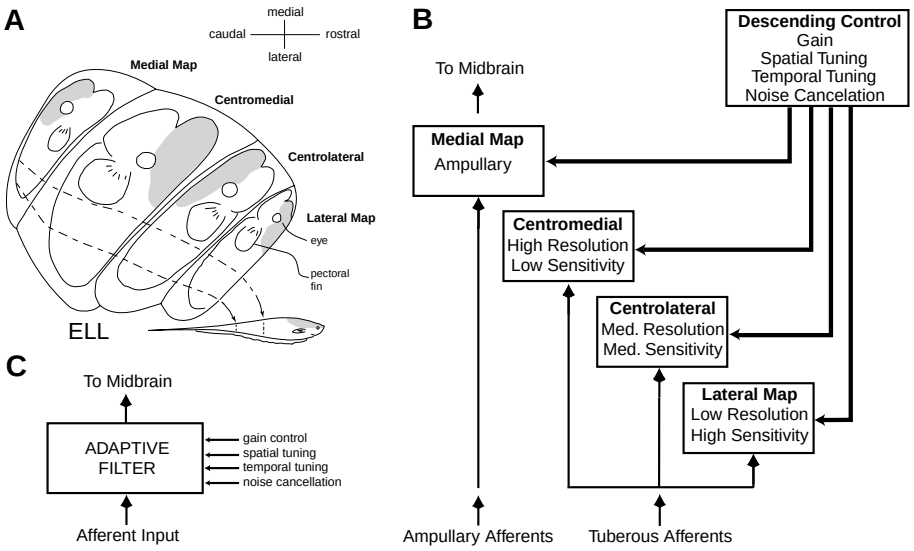

Figure 6.1 Schematic of the ELL as a multiresolution adaptive filter array. (A) Dorsal-ventral projection of the right ELL showing the four somatotopic maps of ampullary and tuberous electrosensory input (shaded area was out of water and not mapped). Modified from Heiligenberg and Dye, 1982. (B) Each map receives essentially identical afferent input, but processes that input with unique spatiotemporal filtering characteristics. (C) Each map can be thought of as an adaptive filter module with descending signals providing gain control, spatiotemporal tuning, and suppression of certain types of background noise.

action-perception cycle iterates, the fish obtains a clearer behavioral agenda in step with the clearer electrosensory percept.

6.3 Future work

In future work, we will be characterizing the background signal that the animal has to filter out in order to extract the weak signal of the prey. For sensory systems, the “backgroundness” of irrelevant signals is something to be continually determined, not given. How it is determined is likely through some appreciation of the statistics of natural electrosensory scenes, which include such things as the reafference noise caused by tail bending. We will also be pursuing some behavioral investigations to ascertain the relative contributions of the high and

low frequency electrolocation systems in prey capture. Finally, we will consider what the optimal processing strategy for the activity of the afferent population would be. We hope that an integrative framework that unites behavioral, physiological, computational, and, more recently (Appendix B) robotic approaches to understanding how the brain and body acquire sensory information will continue to prove fruitful.

APPENDIX A

Receptor blockade with Co^{++}: Physiology and behavior

A.1 Introduction

Chapter 4 provided strong evidence for the involvement of electrosense in prey capture behavior, but left open the question of the relative contributions of the low frequency or passive electrosensory system and the high frequency or active electronsensory system. As a step toward addressing this issue, I adapted a pharmacological approach to blocking the mechansensory lateral line in fish (Karlsen and Sand, 1987) for our use, and performed single-unit electrophysiology in order to assess the effect of the treatment on three different classes of afferents: the ampullary receptor afferents, the tuberous receptor afferents, and mechanosensory lateral line receptor afferents. Finally, some behavioral experiments were performed on the treated fish.[1]

[1] A conference abstract of this work is published as: MacIver M.A., Nelson M.E. (1997) Cobalt blocks modulation of ampullary and mechanosensory lateral line units but not tuberous units in the weakly electric fish Apteronotus leptorhynchus. *Society for Neuroscience Abstracts* 23(1): 247.

A.2 Methods

A.2.1 Pharmacological blockade of sensory input

To test the physiological effects of cobalt exposure in *Apteronotus leptorhynchus* (brown ghosts), we recorded single-unit activity from electrosensory and mechanosensory afferent nerve fibers in the corresponding branches of the lateral line nerve that innervates trunk receptors. We monitored response sensitivity of these units, in a total of 12 different fish, under three conditions: (1) no Co^{++}, (2) 24-hour exposure to 0.1 mM Co^{++}, and (3) one week exposure to 0.1 mM Co^{++}. The surgery and data acquisition protocol for electrosensory afferent data are detailed in Nelson et al. (1997) and Ratnam and Nelson (2000). The mechansensory nerve underlies the electrosensory nerve; thus the protocol is identical except for the removal of a 3 mm section of pALLN nerve to expose the underlying mechanosensory nerve.

A.2.2 Electrosensory afferent analysis

Tuberous units were tested using a transverse 10 Hz AM sinusoidal stimulus (amplitude modulated EOD signal); ampullary units were tested using a transverse 10 Hz sinusoidal stimulus applied directly to the bath (direct-coupled, non-AM). Electrosensory gains were determined by fitting sinusoids to peristimulus rate histograms as detailed in Nelson et al. (1997) and Ratnam and Nelson (2000).

The posterior branch of the left anterior lateral line nerve (pALLN), which innervates trunk electroreceptors, was exposed approximately 1 mm rostral to the insertion of the pectoral fin. In all cases, spontaneous activity of the primary afferents remained, even after cobalt expo-

sure. Tuberous and ampullary afferents could thus be distinguished based on differences in spontaneous interspike interval distributions; identification of mechanosensory afferents was unambiguous because they were recorded in a separate nerve branch.

A.2.3 Mechanosensory afferent analysis

Mechanosensory units were tested using a hand-held vibrating mechanical stimulator with a frequency near 50 Hz. The stimulus amplitude was uncalibrated, so we report the relative response to a constant (but uncalibrated) stimulus. Mechanosensory units typically responded by phase-locking to the stimulus. To analyze the data, we first performed a Fourier time-frequency analysis of the afferent spike train and looked for a response at the fundamental frequency of the stimulus. The mechanosensory response amplitude was determined from the power in the stimulus frequency band relative to the background level.

A.2.4 Behavior with sensory blockade

Adult weakly electric fish of the species *A. leptorhynchus* 12 to 16 cm in length, were maintained in water of 300 $\pm$ 25 mS conductivity at 27 $\pm$ 1.0 °C, and pH 6.9 $\pm$ 0.2, on a 12-hour light/dark cycle. For prey we used *Artemia* (brine shrimp). The control group was maintained under these conditions; the treatment group was exposed to 0.1 mM Co^{++} in a Ca^{++}-free solution (identical to that used for the physiology experiments) for one week under similar water conditions. For this preliminary study detection distances for the two groups were estimated from the 2D projection of the point of fish orientation to the prey. The more

accurate analysis based on 3D reconstruction from digitized two-camera video images will be used in the follow-up studies.

A.3 Results and Discussion

A.3.1 Afferent activity under Co^{++} blockade

Previous studies have shown that a 0.1-1.0 mM Co^{++} bath is effective in blocking the mechanosensory lateral line system in several species of fish (Karlsen and Sand, 1987; Hassan et al., 1992; Coombs and Conley, 1997). It has also been shown that Co^{++} and other calcium channel blockers interfere with transduction in ampullary receptors of catfish and skates (Roth, 1982; Lu and Fishman, 1995). Here, we examine the effects of cobalt on both electrosensory and mechanosensory transduction in weakly electric fish.

We have discovered that in *Apteronotus*, chronic exposure to a 0.1 mM Co^{++} solution selectively blocks both ampullary electroreceptors as well as lateral line mechanoreceptors, while tuberous electroreceptors are relatively unaffected (MacIver and Nelson, 1997). The differential effect on ampullary and tuberous electroreceptors is presumably due to the distribution of Ca^{++} channels, which are found on the apical face of ampullary electroreceptors (and are thus exposed to the cobalt solution), but are on the basal face of tuberous electroreceptors (and thus isolated from the cobalt solution) (Zakon, 1986).

Figure A.1 summarizes our findings and shows that the gains of ampullary and mechanosensory units decreased dramatically while the tuberous gain was relatively unaffected (it

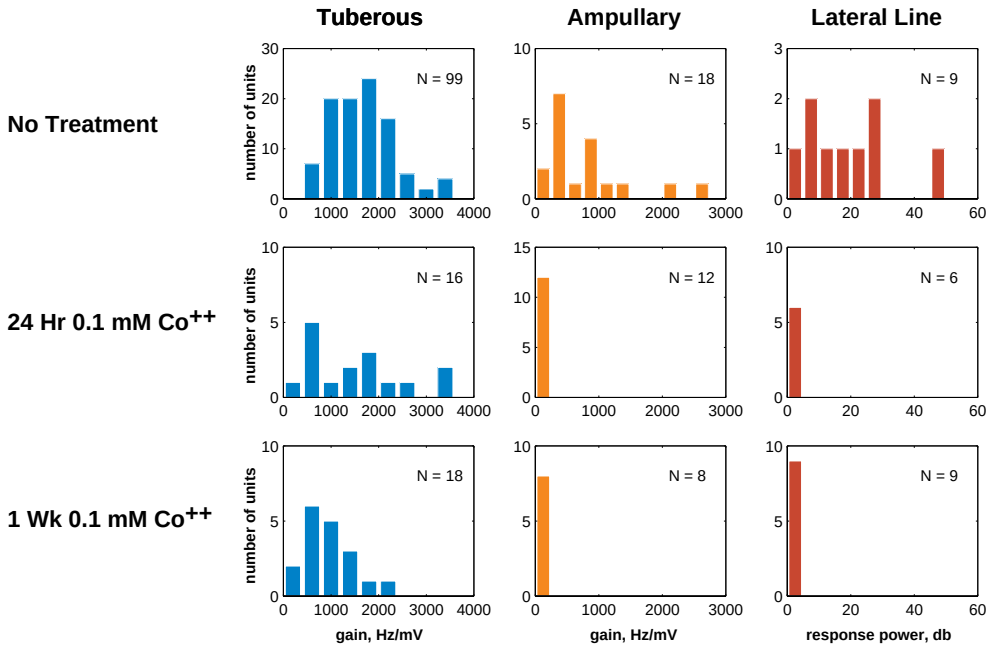

Figure A.1 Effect of cobalt on response properties of electrosensory and mechanosensory afferents.

appears that there could be some decrease in tuberous gain after 1 week, but we need to collect more data to determine whether this effect is significant).

For the tuberous afferent control data, previously collected for other studies (Nelson et al., 1997), the gain was 1,490 $\pm$ 730 Hz/mV; after 24 hours in 0.1 mM Co^{++} week it was 1,310 $\pm$ 1,030 Hz/mV. In comparison, the gain for untreated ampullary afferents was 620 $\pm$ 620 Hz/mV, while after 24 hours in 0.1 mM Co^{++} it dropped to 3 $\pm$ 1 Hz/mV. Similarly, the uncalibrated response power for untreated mechanosensory units was 17 $\pm$ 14 dB; after 24 hours in 0.1 mM Co^{++} it dropped to 0 dB.

We have collected a limited amount of behavioral data with cobalt treated fish. Such fish showed no overt signs of systemic disruption at the low concentration of Co^{++} used, in agreement with behavioral and physiological measures made by (Karlsen and Sand, 1987) in a dif-

ferent species. However, in more recent work with the black ghost knifefish (*A. albifrons*) we have had greater difficulty keeping the animals healthy with chronic treatments. Thus, we have tested the duration of the effectiveness of acute (24-48 hour) treatments with cobalt in *A. albifrons*. We have found that ampullary and mechanosensory units are recovering within approximately 48 hours of the acute treatment, even under the low Ca^{++} concentrations in the post-treatment bath that has been found to extend the effectiveness of acute treatments in another species (S. Coombs, personal communication).

We found that the mean distance of detection is reduced following treatment with cobalt, suggesting that the active electrosensory system is sufficient to mediate prey capture, but that the ampullary and mechanosensory systems may contribute as well. However, the variance is high, and the N is low, so we need to collect further data before resting any conclusions on this data.

A.3.2 Conclusion

With the sensory blockade technique we are on the way to developing a powerful tool to investigate the relative contributions of several sensory systems to the animal's behavior. Our preliminary results provide evidence that cobalt blockade is effective and restricted to the targeted modalities. We have observed some difficulties with the health of *A. albifrons* during chronic treatments, which may necessitate a different approach with this species. Our preliminary behavioral results indicate that the gross behavior of *A. leptorhynchus* is not disrupted by the sensory blockade and that the tuberous system is able to mediate prey capture, but that the passive electrosensory and mechanosensory systems may contribute as well.

APPENDIX B

A robotic approach to understanding electrosensory signal acquisition in weakly electric fish

B.1 Summary

Weakly electric fish hunt and navigate without visual cues by sensing perturbations of a self-generated electric field. In the neuroscience community the electrosensory system has become a leading model system for the investigation of biological sensory acquisition. Previous studies in our laboratory have shown that black ghost knifefish are able to detect small aquatic prey at extremely weak signal levels ($\approx 1\mu$V, 0.1% of baseline). We are pursuing empirical and theoretical approaches to understanding the principles of weak signal detection, estimation, and active sensor positioning during prey capture behavior. In order to explore these issues under more controlled conditions, we have developed a simple robotic platform for controlling the movement of a target object relative to a submerged

artificial electrosensory array. This system allows us to acquire and analyze electrosensory signals similar to those obtained by electroreceptors on the surface of electric fish.[1]

Key words: biorobotics, biomorphic, biomimetic, neuromechanical, biosensor, signal processing, computational neuroethology, electroreceptor, electrosensory, electrolocation

B.2 Introduction

One universal task carried out by the nervous system is the extraction and enhancement of sensory signals that are relevant to behavior. This sensory acquisition process has both behavioral and neural aspects. The behavioral aspect is related to the positioning of peripheral receptor surfaces, providing the animal with some degree of control over the content and quality of incoming sensory data. The neural aspect is related to the adaptive filtering of sensory data for further enhancement of relevant signal components and suppression of extraneous signals.

Weakly electric fish from South America and Africa have the ability to sense their environment using an active electric sense. These nocturnal fish hunt for prey and navigate through tropical rivers at night in turbid waters by emitting weak (millivolt-level) electric fields. Unlike strongly electric fish, the discharges of weakly electric fish are far too weak to stun prey or fend off predators. However, these weak electrical discharges allow these fish to perceive their surroundings in the dark using an electric sense (Bastian, 1994, 1995a; Turner et al., 1999; Wickelgren, 1996).

[1]To appear in print as: MacIver, M.A., Nelson, M.E. (2001) A robotic approach to understanding electrosensory signal acquisition in weakly electric fish. *Autonomous robots*.

In the neuroscience community, weakly electric fish are a leading model system for the investigation of biological sensory acquisition. Wave-type weakly electric fish emit a continuous weak electric field around their body, called the electric organ discharge. Nearby objects that differ in conductivity from the surrounding water perturb the fish's self-generated electric field. Approximately 14,000 specialized electroreceptor organs embedded in the skin of the fish transduce these electric field perturbations. By processing data from the electroreceptor array, weakly electric fish can detect, localize, and discriminate objects in their environment. This ability is referred to as electrolocation. Because the strength of the electric field falls off rapidly with distance, the electric sense is a short-range sense with an effective range that varies from a few centimeters for small prey to tens of centimeters for larger objects.

By controlling the velocity and orientation of their body, and by adjusting the gain and filtering properties of neurons in the electrosensory processing pathway, these fish actively influence the strength and spatiotemporal pattern of the incoming electrosensory signals. Previous studies have shown that the weakly electric black ghost knifefish (*A. albifrons*) are able to detect small water fleas (*Daphnia*) at a distance of a few centimeters (MacIver et al., 2001). At this distance, the voltage perturbation at the skin is estimated to be on the order of 1 μV (Nelson and MacIver, 1999). This represents a change of approximately 0.1% in the RMS voltage level established by the electric organ discharge. We are interested in understanding the behavioral strategies, neural mechanisms, and information processing principles that allow the animal to reliably detect, localize, and categorize objects in the environment based on these extremely weak sensory signals.

In order to explore these issues under more controlled conditions, we have developed a simple robotic system for controlling the movement of a target object relative to an artificial electrosensory array. This system allows us to acquire and analyze electrosensory signals that are similar to the transdermal potential modulations experienced by the electroreceptor array on the surface of a weakly electric fish.

B.3 Materials and methods

A linear electrosensory array was constructed using seven silver-silver chloride EKG electrodes (1 cm diameter) and spaced 1.5 cm apart. The array was mounted along one side of a small water tank (25 x 14 x 10 cm). One of the terminal EKG electrodes was used as a signal source to generate an oscillatory electric field representing the electric organ discharge (EOD). A 1 kHz sine wave was applied across the signal source electrode to approximate the 1 kHz quasi-sinusoidal discharge of the weakly electric knifefish (Assad et al., 1999; Rasnow and Bower, 1996). A 10 kΩ series resistor was attached to each of the other EKG electrodes to represent the skin resistance of the fish. The other end of each resistor was tied to a common voltage reference representing the internal body space of the fish. The voltage across each of the six skin resistors was continuously monitored by the data acquisition system. Signals were acquired using a data acquisition card (National Instruments Corp. DAQCard-AI-16E-4, Austin, TX, USA) and the MATLAB data acquisition toolbox (The MathWorks Inc., Natick, MA, USA) with a laptop PC (Inspiron 5000, Dell Computer Corp., Round Rock, TX, USA). As illustrated in Fig.B.1, electrosensory targets (1 cm diameter metal and plastic spheres)

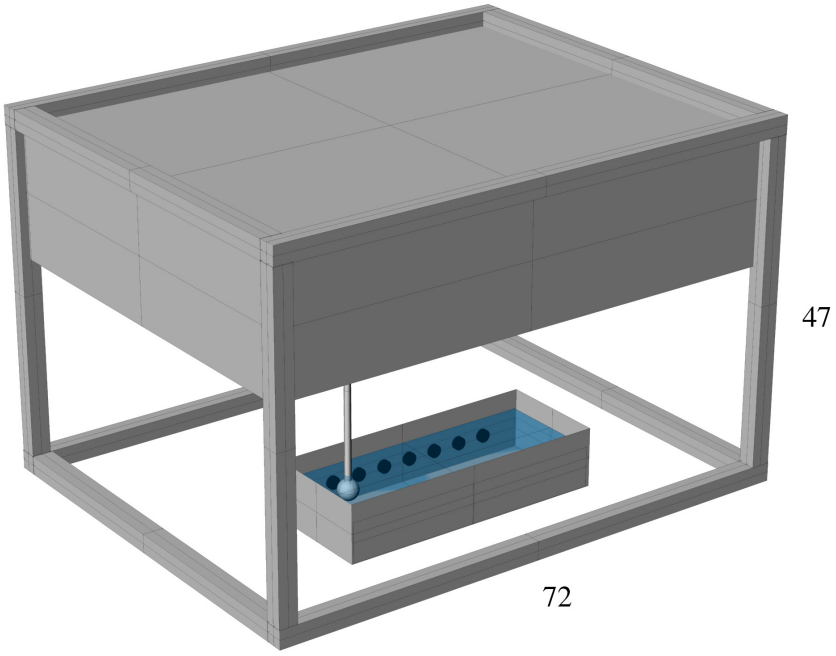

Figure B.1 Schematic of the robotic workcell, test object, and sensors. Outer dimensions of the workcell are indicated in cm.

were moved past the electrosensory array using a three-axis robotic workcell (RW-18B, Arrick Robotics, Hurst, Texas, USA). The position and velocity of the target object was controlled using custom motion control software.

B.4 Results

For a preliminary assessment of the system, we wanted to determine whether the signals from the sensor array were qualitatively similar to the transdermal potential modulations observed when a small object is placed near a weakly electric fish. Studies by Rasnow (1996) have shown that the electrosensory image of a small spherical object is spatially broad and weak for distant objects, and become sharper and stronger as the object approaches the fish. To

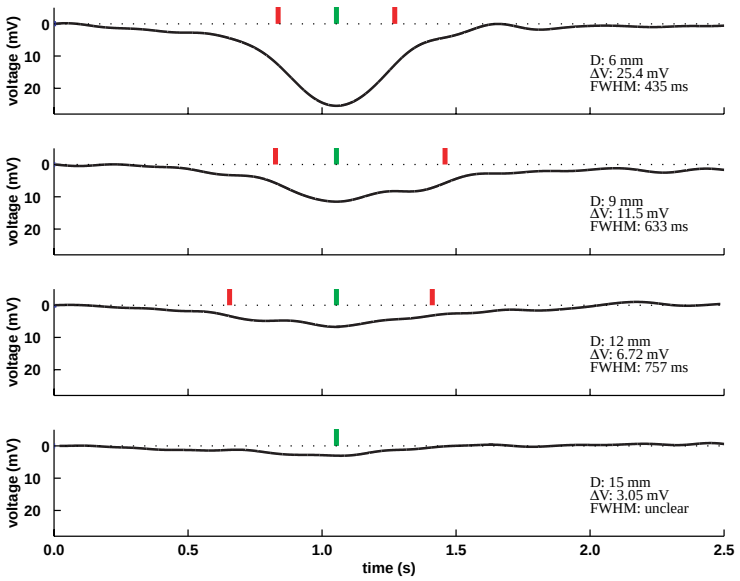

Figure B.2 Voltage change induced by a 1 cm diameter plastic sphere at four different distances as it is scanned past the sensor. The center of the perturbations and the edges of the full width at half maximum (FWHM) are indicated above each line. The FWHM for the bottom plot was ambiguous. The EOD carrier amplitude was 1 V.

examine whether our artificial active electrosensory system exhibited similar voltage patterns, a test object (a 1 cm diameter plastic sphere) was scanned parallel to the sensor array at four different distances from the array (6, 9, 12, and 15 mm). Distances were measured from the array to the center of the test object. As illustrated in Fig. B.2, we determined that the spatial profiles from the voltage sensors were qualitatively similar to those measured in electric fish. The voltage signal is strong and narrow when the object is close to the array, and becomes weaker and broader as the target distance is increased. Future studies will explore these relationships for the artificial array in more quantitative detail.

We have also begun to use the artificial electrosensory array to explore issues of neural information processing. Based on experimental studies of the response properties of electrosensory afferents (Xu et al., 1996; Nelson et al., 1997; Ratnam and Nelson, 2000), we have

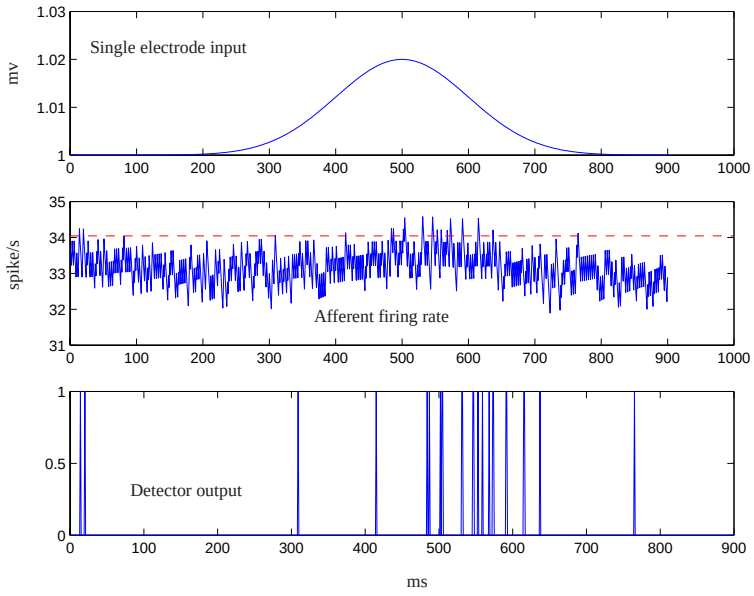

Figure B.3 Sample Gaussian voltage perturbation, afferent response, and detection. The afferent response is processed by a neural detection algorithm based on a simple integrate-and-fire mechanism.

a good understanding of the relationship between the transdermal voltage and the change in firing activity of the afferent nerve fibers. Using a computational model of electrosensory afferent spike generation (Brandman and Nelson, 2001, presented in Chapter 5) we can predict the changes in spike activity due to a change in transdermal voltage. As an illustration of this, Fig. B.3 shows a sample of a Gaussian bump, similar in shape to those shown in Fig. B.2 (but with sign flipped to simulate the effect of a conductive test object), along with the output of the afferent model. The afferent signal is subsequently processed by a biologically plausible detection algorithm to assess the detection efficiency and false alarm probability for detecting weak sensory signals.

B.5 Discussion

The robotic platform described above for studying electrosensory signal acquisition is still in the early stages of development. Initial results have been encouraging and demonstrate that the system is capable of providing signals that are qualitatively similar to those observed in electric fish. In the future, we intend to carry out quantitative studies using this system to explore neurally inspired algorithms for optimal target detection and estimation, including, for example, estimation of target size, range and conductivity. We are also interested in using the robotic platform to explore behavioral strategies for positioning the sensor array during target acquisition. We have carried out detailed studies of how electric fish control the position of their sensory surface while hunting for prey in the dark (MacIver and Nelson, 2000; MacIver et al., 2001). These studies provide us with precise information regarding the relative position between the prey and the sensor array prior to and following prey detection in the biological system. In future work we will be able to use the robotic workcell to play back actual prey trajectories acquired during our behavioral experiments, and explore the impact of behavioral strategies on sensory acquisition performance. Finally, a long term goal is to develop neurally-inspired algorithms for closing the sensory-motor loop, eventually allowing the development of an autonomous robotic electric fish that can detect, localize, discriminate, and "capture" electrosensory targets in its environment.

Acknowledgements: We would like to thank Shaun Law for his help in construction and testing of the sensor array and robotics. This research was supported by grants from the National Science Foundation (IBN-0078206) the National Institute of Mental Health (R01-MH49242), and a University of Illinois Research Board grant.

APPENDIX C

A biomorphic minor carta

C.1 What we are trying to do

Evolution has populated diverse ecological niches with biological systems that are exquisitely adapted to the demands of their environments. Biomorphic engineers seek to emulate the performance and efficiency of these systems by synthesizing artifacts that are isomorphic to the biological system at some level of description. The goal of this approach is to provide a powerful tool for scientific understanding of these complex systems, and to develop new technology that features some of their significant advantages.

C.2 The importance of synthesis

Neuroethology has taught us that adaptive behavior is the result of the tight coupling between the nervous system, its biomechanics, and environment. Reductionist approaches allow us to characterize the role of isolated components of these systems. Synthetic approaches, such

as computational neuroethology and biomorphic engineering, allow us to build on the successes of the reductionistic approach to close the loop between organism and environment. In this way we can explore the interaction of body, nervous system, and environment in adaptive behavior.

C.3 Why we do physical implementations

As the role of the environment and body is key in the synthetic approach, an integrative simulation approach requires accurate models of both. This involves several difficulties, including assumptions about the environment and simplifications for computational tractability. In addition, there are a large number of constraints on physical systems that are imposed by their embodiment which are rarely considered in simulations. The biomorphic approach is sensitive to real-world constraints, such as real-time performance, low power consumption, compactness, autonomy, adaptation, and robustness, and avoids the need to model and simulate complex environments.

C.4 Life: The ultimate technology

Organisms offer us a technological paradigm in some ways far more advanced than our own. They operate on low power, they are robust to damage, and have compact designs while maintaining the real-time performance on which their survival depends. The biomorphic engi-

neering approach aims to emulate this technology to both better understand the basic science underlying living systems, and create technology that is beneficial to humanity. [1]

[1] Composed and edited by M. A. MacIver, K. Boahen, and T. Horiuchi at the 1999 Neuromorphic Engineering Workshop in Telluride, Colorado, USA (MacIver et al., 1999). This document arose from the "How much do you morph?" discussion group, formed by K. Boahen at the workshop.

APPENDIX D

Supplementary material for body modeling and video tracking

This appendix provides supplemental material for developing surface models of animal bodies, and an introduction to the temporal and spatial resolution of video. Additional supplemental information, including links to suppliers listed in Chapter 3 and video resolution charts, is available online at http://soma.npa.uiuc.edu/labs/nelson/model_based_tracking.html.

D.1 Methods for making a surface model of an animal

Obtaining a quantitative representation of a surface involves measuring coordinate values of points on the surface and constructing a best fit surface model that passes near those points. One approach is to coat a cast of the object with a mold release agent and embed it in a rectangular block of rigid casting compound. The block containing the embedded cast is then sliced with a thin-kerf bandsaw, and the cast slices are pushed out. The resulting cross-section negatives are scanned on a flatbed scanner. The images are then imported into a drawing program that allows

extraction of 2-D coordinates of points on the edge of the cross-sections. The outline of the embedding block is used for registration between cross-sections. Knowledge of the thickness of each slice allows reconstruction of the longitudinal dimension for a 3-D surface model.

Another option is to build a model of the organism from a set of photographs. 3-D modeling software, such as Rhinoceros, often allow you to put an image in the background as you construct the model. You build the surface by generating construction curves based on the photograph. By carefully controlling the position of the camera and photographing with scale bars, an adequate model can be made for simple body forms.

A more flexible and precise technique is to use 3-D digitizers. There are two common types of 3-D digitizers, optical and contact. Optical scanners, such as the Cyberware Model 15 (Cyberware Inc., Monterey CA USA), compute the (x, y, z) position of a dense grid (20 microns) of surface points as a laser beam is rapidly scanned and reflected from the target object. Optical scanners are significantly more expensive but can be easier to use for objects with complex surfaces. Additionally, they do not require the surface of the object to be rigid. Since optical scanning requires little user interaction, laser digitizing can be outsourced to commercial scanning services. Contact digitizers, such as the MicroScribe 3DX (Immersion Corp., San Jose CA USA), consist of a stylus at the end of a multi-joint rigid arm that is touched to selected points on the surface of the object being digitized. Each joint of the digitizing arm contains sensors that measure the angle of the joint, allowing the software to compute the (x, y, z) location of the stylus. They have an accuracy of around 0.2 mm. Generating a model with a contact digitizer requires knowledge of the surface generation functions of the software

it is connected to, and is aided by marking the rigid object with a lattice of transverse-sectional and cross-sectional lines to guide what points on the object are touched with the stylus.

D.2 The temporal and spatial resolution of video

An understanding of technical specifications for video resolution is required for determining whether the resolution of a video system will be adequate to meet the needs of a particular animal behavior study. In this appendix we provide a general technical background on video resolution and show how technical specifications are applied to estimate the spatial resolution of our infrared video system. We will restrict our discussion to the video format used in North America, often referred to as National Television Systems Committee (NTSC) video, but the discussion applies to other formats with minor variations. For additional technical information outside the scope of this discussion, see (Poynton, 1996; Jack, 1993; Young et al., 1995).

The resolution of digitized video images is determined by contributions of each device or transformation interposed between the imaged scene and the final digitized image. This includes the CCD sensor and camera electronics, recording and playback device and media, digitizing resolution, and any post-digitization image processing such as deinterlacing.

The temporal resolution of video is nominally the frame rate, which is 29.97 frames/s for NTSC video. In the NTSC video format each video frame has 525 horizontal scan lines divided into two fields, consisting of 262.5 even and 262.5 odd scan lines. To reduce flicker the odd lines are drawn on the screen first, then the even lines are drawn. This creates an interval of 16.7 ms between an odd scan line and its adjacent even scan line. An image artifact termed motion

interlace blur results from this interlacing. For example, a fish moving at 15 cm/s parallel to the scan line drawing direction will move 2.5 mm in the 16.7 ms inter-field interval. Given the scaling of our system, this results in a 3-4 pixel blurry fringe at the leading and trailing edges of the fish. Thus we deinterlace our digitized images, which eliminates interlace blur and doubles the effective frame rate to 59.94 frames/s but also reduces vertical resolution.

Because of the scanning system used in video, vertical and horizontal spatial resolutions are determined by different factors. In general, video resolution is defined in terms of the number of black and white line pairs resolvable on the display, termed luminance resolution. It is most often specified in terms of the total number of lines (L), rather than number of line pairs. The implied spatial scale is the height of the display. Therefore, when lines of resolution is quoted it means lines per picture height (H). Thus, vertical resolution is specified as the total number of resolvable horizontal lines per picture height. For NTSC, the picture width (W) is 4/3 times the picture height. To maintain the same spatial scale for vertical and horizontal resolution, horizontal resolution is also specified as lines per picture height (L/H) rather than lines per picture width (L/W). Horizontal resolution in lines per picture height (L/H) is thus equivalent to the total number of resolvable vertical lines across the width of the display divided by the 4/3 aspect ratio.

Maximum vertical resolution is limited by number of scan lines in the video format. Although there are a total of 525 raster lines in NTSC, no more than 485 carry picture information. The subjective vertical resolution of a video image is consistently found to be less than the resolution predicted on the basis of the number of visible scan lines, in part because of the small gap between neighboring scan lines. This deviation is specified as the ratio of perceived

vertical resolution (L/H) to visible scan lines (485), and is called the Kell factor. A commonly quoted value is 0.7, but this is based on non-interlaced displays. For the 2:1 interlace scanning system in NTSC video, the value is between 0.4-0.7, depending upon a number of factors including movement of the image. For details on the Kell factor and difficulties of establishing resolution specifications, see Hsu (1986).

Maximum horizontal resolution is limited by the total bandwidth of the video system. Typical horizontal resolutions (L/H) obtainable from commercial VCRs are 700 (Betacam), 400 (Super-VHS), and 220 (VHS).

In general, the S-VHS recording format is the best practical choice because of the high cost of Betacam recorders. In S-VHS, VHS, and some other recording formats, the luminance signal is kept separate from the hue and color saturation signal. However, standard video signals are composite, combining color and luminance signals together. This requires that the composite signal be decoded prior to recording or display using what is termed a comb filter. Comb filters are only activated when color information is detected. As comb filtering degrades the signal bandwidth to a degree that is noticeable with S-VHS (but not VHS), it is preferable to use S-video or component cabling with color video. These cabling systems have separate wires for luminance and chrominance.

When choosing a CCD camera, the higher the resolution the better the recorded signal will be, even if the resolution of the CCD exceeds that of the recording device. For example, when recording to S-VHS, better results are obtained with a camera that has higher horizontal resolution than 400 L/H. This is because the depth of modulation of the video signal is greater

with a higher resolution camera. Studio cameras have horizontal resolutions of over 1,000 L/H, despite the 333 L/H limit of NTSC broadcast video.

Using standard resolution test patterns (available at the web site listed at the start of this appendix) we measured the resolution of our system including digitization and deinterlacing to be approximately 355 L/H horizontal and 325 L/H vertical with optimal lighting. To calculate the vertical spatial resolution in L/mm, we take the vertical resolution in L/H and divide by the vertical field of view in mm. To determine the horizontal spatial resolution, we multiply the horizontal resolution (L/H) by 4/3 to obtain the L/W resolution, and divide this by the horizontal field of view in mm. Using this procedure we obtain a spatial resolution of approximately 1 L/mm in both dimensions. In our application, the 2-3 mm diameter *Daphnia magna* prey are representative of the minimum feature size of interest, and are just barely discriminable at this resolution under experimental lighting conditions.

BIBLIOGRAPHY

Assad, C. (1997). *Electric field maps and boundary element simulations of electrolocation in weakly electric fish*. PhD dissertation, California Institute of Technology. UMI, Ann Arbor MI.

Assad, C., Rasnow, B., and Stoddard, P. K. (1999). Electric organ discharges and electric images during electrolocation. *J. Exp. Biol.*, 202(10):1185–1193.

Bass, A. H. (1986). Electric organs revisited. In Bullock, T. H. and Heiligenberg, W., editors, *Electroreception*, pages 13–70. Wiley.

Bastian, J. (1986). Electrolocation: behavior, anatomy, and physiology. In Bullock, T. and Heiligenberg, W., editors, *Electroreception*, pages 577–612. Wiley, New York.

Bastian, J. (1987). Electrolocation in the presence of jamming signals: behavior. *J. Comp. Physiol. A*, 161(6):811–824.

Bastian, J. (1994). Electrosensory organisms. *Phys Today*, 47(2):30–37.

Bastian, J. (1995a). Electrolocation. In Arbib, M., editor, *The Handbook of Brain Theory and Neural Networks*, pages 352–356. MIT Press, Cambridge, Mass.

Bastian, J. (1995b). Pyramidal-cell plasticity in weakly electric fish: a mechanism for attenuating responses to reafferent electrosensory inputs. *J. Comp. Physiol. A*, 176(1):63–78.

Bastian, J. (1999). Plasticity of feedback inputs in the apteronotid electrosensory system. *J. Exp. Biol.*, 202(10):1327–1337.

Beer, R. D., Chiel, H. J., Quinn, R. D., and Ritzmann, R. E. (1998). Biorobotic approaches to the study of motor systems. *Curr Opin Neurobiol*, 8:777–782.

Bennett, M. V. L. (1971). Electric organs. In Hoar, W. S. and Randall, D. J., editors, *Fish physiology*, pages 347–491. Academic Press, New York, NY.

Bennett, M. V. L. and Obara, S. (1986). Ionic mechanisms and pharmacology of electroreceptors. In Bullock, T. H. and Heiligenberg, W., editors, *Electroreception*, pages 157–181. Wiley.

Blake, A. (1995). Active vision. In Arbib, M., editor, *The Handbook of Brain Theory and Neural Networks*, pages 61–63. MIT Press, Cambridge, Mass.

Blake, A. and Isard, M. (1998). *Active Contours*. Springer-Verlag, New York, NY.

Blake, A. and Yuille, A., editors (1992). *Active Vision*. MIT Press, Cambridge, MA.

Blake, R. W. (1983). Swimming in the electric eels and knifefishes. *Can. J. Zool.*, 61:1432–1441.

Bleckmann, H. (1986). Role of the lateral line in fish behaviour. In Pitcher, T. J., editor, *Behaviour Of Teleost Fishes*, Fish and Fisheries Series, pages 177–202. Chapman & Hall, London, 2nd edition.

Bleckmann, H., Breithaupt, T., Blickhan, R., and Tautz, J. (1991). The time course and frequency content of hydrodynamic events caused by moving fish, frogs, and crustaceans. *J. Comp. Physiol. A*, 168:749–757.

Boardman, E. T. (1950). Techniques of life casting of small vertebrates. *Musm News Wash*, 28(11):7–8.

Brandman, R. and Nelson, M. E. (2001). Refractoriness and long-term spike train regularization. *Submitted*.

Breder, C. M. (1926). The locomotion of fishes. *Zoologica (N.Y.)*, 4:159–297.

Bromage, T. G. (1985). Systematic inquiry in tests of negative/positive replica combinations for SEM. *J Microscopy*, 137, Pt 2:209–216.

Bullock, T. H. (1973). Seeing the world through a new sense: Electroreception in fish. *Amer Sci*, 61(3):316–325.

Bullock, T. H. and Heiligenberg, W., editors (1986). *Electroreception*. Wiley, New York.

Campenhausen, C. v., Riess, I., and Weissert, R. (1981). Detection of stationary objects by the blind cave fish *Anoptichthys jordani* (Characidae). *J. Comp. Physiol.*, 143:369–374.

Carr, C. E., Maler, L., and Sas, E. (1982). Peripheral organization and central projections of the electrosensory nerves in gymnotiform fish. *J. Comp. Neurol.*, 211(2):139–153.

Chiel, H. J. and Beer, R. D. (1997). The brain has a body: Adaptive behavior emerges from interactions of nervous system, body, and environment. *Trends Neurosci*, 20:553–557.

Cliff, D. (1995). Neuroethology, computational. In Arbib, M., editor, *The Handbook of Brain Theory and Neural Networks*, pages 626–630. MIT Press, Cambridge, Mass.

Coombs, S. and Conley, R. A. (1997). Dipole source localization by mottled sculpin. I. Approach strategies. *J. Comp. Physiol. A*, 180:387–399.

Coombs, S. and Janssen, J. (1989). Peripheral processing by the lateral line system of the mottled sculpin (*Cottus bairdi*). In Coombs, S., Gorner, P., and Münz, H., editors, *The mechanosensory lateral line: Neurobiology and evolution*, pages 299–319. Springer-Verlag.

Crampton, W. G. R. (1998). Electric signal design and habitat preferences in a species rich assemblage of gymnotiform fishes from the Upper Amazon Basin. *An. Acad. Bras. Ci.*, 70(4 Part 2):805–847.

Crawford, A. C., Evans, M. G., and Fettiplace, R. (1991). The actions of calcium on the mechano-electrical transducer current of turtle hair cells. *J. Physiol.*, 434:369–398.

Cruz-Neira, C., Sandin, D. J., DeFanti, T. A., Kenyon, R. V., and Hart, J. C. (1992). The CAVE: Audio Visual Experience Automatic Virtual Environment. *Commun. ACM*, 35(6):65–72.

Cruz-Neira, C., Sanding, D. J., and DeFanti, T. A. (1993). Surround-screen projection-based virtual reality: The design and implementation of the CAVE. *Computer Graphics (SIGGRAPH '93 Proceedings)*, 27:135–142.

de Boor, C. (1978). *A practical guide to splines*. Springer-Verlag, New York.

Douglas, R. H. and Hawryshyn, C. W. (1990). Behavioral studies of fish vision: an analysis of visual capabilities. In Douglas, R. and Djamgoz, M., editors, *The visual system of fish*, pages 373–418. Chapman & Hall, London.

Dunning, B. B. (1973). *A quantitative and comparative analysis of the tonic electroreceptors of* Gnathonemus, Gymnotus, *and* Kryptopterus. Ph.D., Univ. of Minnesota.

Ekeberg, Ö., Lansner, A., and Grillner, S. (1995). The neural control of fish swimming studied through numerical simulations. *Adaptive behavior*, 3(4):363–384.

Ellis, M. M. (1913). The gymnotid eels of tropical America. *Mem. Carnegie Museum*, 6(3):109–195.

Enger, P. S., Kalmijn, A. J., and Sand, O. (1989). Behavioral investigation on the functions of the lateral line and inner ear in predation. In Coombs, S., Gorner, P., and Münz, H., editors, *The Mechanosensory Lateral Line: Neurobiology and Evolution*. Springer-Verlag.

Essa, I., Sclaroff, S., and Pentland, A. (1993). Physically-based modelling for graphics and vision. In Martin, E., editor, *Directions in geometric computing*. Information Geometers, UK.

Feng, A. S. (1977). The role of the electrosensory system in postural control of the weakly electric fish *Eigenmannia virescens*. *J. Neurobiol.*, 8(5):429–438.

Feng, A. S. and Bullock, T. H. (1977b). Neuronal mechanisms for object discrimination in the weakly electric fish Eigenmannia virescens. *J Exp Biol*, 66:141–158.

Fernald, R. D. (1988). Aquatic adaptations in fish eyes. In Atema, J., Fay, R., Popper, A., and Tarolga, W., editors, *Sensory Biology of Aquatic Animals*, pages 433–466. Springer-Verlag, New York.

Franchina, C. R. and Hopkins, C. D. (1996). The dorsal filament of the weakly electric Apteronotidae (Gymnotiformes: Teleostei) is specialized for electroreception. *Brain Behav. Evol.*, 47:165–178.

Furch, K. (1984a). Seasonal variation of the major cation content of the várzea-lake Lago Camaleão, middle Amazon, Brazil, in 1981 and 1982. *Verh. Int. Verein. Limnol.*, 22:1288–1293.

Furch, K. (1984b). Water chemistry of the Amazon basin: The distribution of chemical elements among freshwaters. In Sioli, H., editor, *The Amazon: Limnology and landscape ecology of a mighty tropical river and its basin*, pages 167–199. Dr. W. Junk, Dordrecht.

Gardner, G. S. (1974). Casting lifelike models from living animals. *Curator*, 17(1):10–15.

Gavrila, D. M. and Davis, L. S. (1996). 3-D model-based tracking of humans in action: a multi-view approach. In *1996 IEEE Computer Society Conference on Computer Vision*

and Pattern Recognition : June 18-20, 1996, San Francisco, California, pages 73–80, Los Alamitos, CA. IEEE Computer Society Press.

Gibson, J. J. (1979). *The ecological approach to visual perception*. Houghton Mifflin, Boston, MA.

Gilbert, C. (1997). Visual control of cursorial prey pursuit by tiger beetles (Cicindelidae). *J. Comp. Physiol. A*, 181(3):217–230.

Hagedorn, M. (1988). Ecology and behavior of a pulse-type electric fish *Hypopomus occidentalis* (Gymnotiformes, Hypopomidae) in a fresh-water stream in Panama. *Copeia*, 1988(2):324–335.

Hagedorn, M. and Keller, C. (1996). Species diversity of gymnotiform fishes in Manu Bioreserve, Pakitza, Perú. In Sandoval, A. and Wilson, D. E., editors, *Manu : the biodiversity of Southeastern Perú*, page 679. Smithsonian Institution,, Washington, D.C.

Hagiwara, S., Szabo, T., and Enger, P. S. (1965). Electroreceptor mechanisms in a high-frequency weakly electric fish, *Sternarchus albifrons*. *J Neurophysiol*, 28:784–799.

Hassan, E.-S., Abdel-Latif, H., and Biebricher, R. (1992). Studies of the effects of Ca^{++} and Co^{++} on the swimming behavior of the blind Mexican cave fish. *J. Comp. Physiol. A*, 171(3):413–419.

Hearn, D. and Baker, M. P. (1997). *Computer Graphics, C version*. Prentice Hall, Upper Saddle River, NJ, 2nd edition.

Heidegger, M. (1977). Phänomenologische interpretation von Kants Kritik der Reinen Vernunft. In Görland, I., editor, *Gesamtausgabe, vol. 25*. Vittorio Klostermann, Frankfurt am Main, Germany.

Heikkilä, J. and Silvén, O. (1996). Calibration procedure for short focal length off-the-shelf CCD cameras. In Kropatsch, W., editor, *Proceedings of the 13th International Conference on Pattern Recognition*, pages 166–170. IEEE Computer Society Press, Los Alamitos, CA USA.

Heikkilä, J. and Silvén, O. (1997). A four-step calibration procedure with implicit image correction. In *Proceedings. 1997 IEEE Computer Society Conference on Computer Vision and Pattern Recognition*, pages 1106–1112. IEEE Computer Society Press, Los Alamitos, CA, USA.

Heiligenberg, W. (1973). Electrolocation of objects in the electric fish *Eigenmannia* (Rhamphichthyidae, Gymnotoidei). *J. Comp. Physiol.*, 87(2):137–164.

Heiligenberg, W. (1975). Theoretical and experimental approaches to spatial aspects of electrolocation. *J. Comp. Physiol.*, 103:247–272.

Heiligenberg, W. and Dye, J. (1982). Labeling of electroreceptive afferents in a gymnotoid fish by intracellular injection of horseradish peroxidase: the mystery of multiple maps. *J Comp Physiol*, 148(3):287–296.

Heiligenberg, W. F. (1991). *Neural nets in electric fish*. MIT Press, Cambridge, MA.

Hinde, R. A. (1970). *Orientation*, chapter 7, pages 146–192. Animal behavior: a synthesis of ethology and comparative psychology. McGraw-Hill, New York, NY, second edition.

Hoekstra, D. and Janssen, J. (1986). Lateral line receptivity in the mottled sculpin (*Cottus bairdi*). *Copeia*, 1:91–96.

Hopkins, C. D. (1972). *Patterns of electrical communication among gymnotid fish*. Ph.D., Rockefeller University.

Hopkins, C. D., Shieh, K. T., McBride, D. W., and Winslow, M. (1997). A quantitative analysis of passive electrolocation behavior in electric fish. *Brain Behav. Evol.*, 50 (suppl. 1):32–59.

Hsu, S. C. (1986). The Kell factor: Past and present. *SMPTE J—Soc Mot Pict & Tel Engin*, 95:206–214.

Hughes, N. F. and Kelly, L. H. (1996). New techniques for 3-D video tracking of fish swimming movements in still or flowing water. *Can J Fish Aquat Sci*, 53(11):2473–2483.

Jack, K. (1993). *Video Demystified. A handbook for the digital engineer*. HighText Publications, Solana Beach, CA.

James, T. (1989). *The prop builder's molding and casting handbook*. Betterway Books, Cincinnati, OH.

Janssen, J. (1997). Comparison of response distance to prey via the lateral line in the ruffe and yellow perch. *J. Fish Biol.*, 51(5):921–930.

Janssen, J., Jones, W. R., Whang, A., and Oshel, P. E. (1995). Use of the lateral line in particulate feeding in the dark by juvenile alewife (*Alosa pseudoharengus*). *Can. J. Fish. Aquat. Sci.*, 52(2):358–363.

Jung, S. Wohn, K. (1997). Tracking and motion estimation of the articulated object: a hierarchical Kalman filter approach. *Real-Time Imaging*, 3(6):415–432.

Kalko, E. K. (1995). Insect pursuit, prey capture and echolocation in pipistrelle bats (Microchiroptera). *Anim. Behav.*, 50:861–880.

Kalmijn, A. J. (1974). The detection of electric fields from inanimate and animate sources other than electric organs. In Fessard, A., editor, *Electroreceptors and other specialized receptors in lower vertebrates (Handbook of sensory physiology, vol III/3)*, pages 147–200. Springer.

Kalmijn, A. J. (1988). Detection of weak electric fields. In Atema, J., Fay, R. R., Popper, A. N., and Tarolga, W. N., editors, *Sensory biology of aquatic animals*, pages 151–186. Springer Verlag, New York, NY.

Karlsen, H. E. and Sand, O. (1987). Selective and reversible blocking of the lateral line in freshwater fish. *J. Exp. Biol.*, 133:249–262.

Kirk, K. L. (1985). Water flows produced by *Daphnia* and *Diaptomus*: Implications for prey selection by mechanosensory predators. *Limnol Oceanogr.*, 30(3):679–686.

Kirschbaum, F. (1979). Reproduction of the weakly electric fish *Eigenmannia virescens* (Rhamphichtyidae, Teleostei) in captivity. 1. Control of gonadal recrudescence and regression by environmental factors. *Behav. Ecol. Sociobiol.*, 4(4):331–355.

Knudsen, E. I. (1974). Behavioral thresholds to electric signals in high frequency electric fish. *J. Comp. Physiol.*, 91(4):333–353.

Knudsen, E. I. (1975). Spatial aspects of the electric fields generated by weakly electric fish. *J. Comp. Physiol.*, 99(2):103–118.

Kramer, B. (1990). *Electrocommunication In Teleost Fishes: Behavior and Experiments*. Springer-Verlag, Berlin.

Kruk, M. R. (1997). Measuring behaviour into the twenty-first century. *Trends Neurosci*, 20(5):187–189.

Kuc, R. (1994). Sensorimotor model of bat echolocation and prey capture. *J. Acoust. Soc. Am.*, 96(4):1965–1978.

Lannoo, M. J. and Lannoo, S. J. (1993). Why do electric fishes swim backwards? An hypothesis based on gymnotiform foraging behavior interpreted through sensory constraints. *Env. Biol. Fishes*, 36(2):157–165.

Leigh, J., Vasilakis, C. A., Defanti, T. A., Grossman, R., Assad, C., Rasnow, B., Protopappas, A., De Schutter, E., and Bower, J. M. (1995). Virtual reality in computational neuroscience. In Jones, H., Vince, J. A., and Earnshaw, R. A., editors, *Virtual Reality Applications*, pages 293–306. Academic Press, London.

Lighthill, J. and Blake, R. (1990). Biofluiddynamics of balistiform and gymnotiform locomotion. 1. Biological background, and analysis by elongated-body theory. *J Fluid Mech*, 212:183–207.

Lissmann, H. W. (1958). On the function and evolution of electric organ in fish. *J. Exp. Biol.*, 35:156–191.

Lissmann, H. W. (1961). Ecological studies on gymnotids. In Chagas, C. and de Carvalho, A. P., editors, *Bioelectrogenesis*, pages 215–223. Elsevier, Amsterdam.

Lissmann, H. W. and Machin, K. E. (1958). The mechanism of object location in *gymnarchus niloticus* and similar fish. *J. Exp. Biol.*, 35:451–486.

Lu, J. and Fishman, H. M. (1995). Ion channels and transporters in the electroreceptive ampullary epithelium from skates. *Biophys. J.*, 69(6):2467–2475.

MacIver, M. A., Horiuchi, T., and Boahen, K. (1999). A biomorphic minor carta. *Published on the web at: http://www.isr.umd.edu/~timmer/minorcarta.html, or http://www.ini.unizh.ch/telluride99/report99/node103.html*.

MacIver, M. A., Lin, J. L., and Nelson, M. E. (1997). Estimation of signal characteristics during electrolocation from video analysis of prey capture behavior in weakly electric fish. In Bower, J., editor, *Computational Neuroscience: Trends in Research, 1997*, pages 729–734. Plenum.

MacIver, M. A. and Nelson, M. E. (1997). Cobalt blocks modulation of ampullary and mechanosensory lateral line units but not tuberous units in the weakly electric fish *Apteronotus leptorhynchus*. *Soc. Neurosci. Abs.*, 23(1):247.

MacIver, M. A. and Nelson, M. E. (1999). Evidence for closed-loop control of prey capture in weakly electric fish. *Abstracts, Eighth Annual Computational Neuroscience Meeting, Pittsburgh, PA July 18-22*.

MacIver, M. A. and Nelson, M. E. (2000). Body modeling and model-based tracking for neuroethology. *J. Neurosci. Meth.*, 95:133–143.

MacIver, M. A. and Nelson, M. E. (2001). A robotic approach to understanding electrosensory signal acquisition in weakly electric fish. *Auton Robots (submitted)*.

MacIver, M. A., Sharabash, N. M., and Nelson, M. E. (2001). Prey-capture behavior in gymnotid electric fish: Motion analysis and effects of water conductivity. *J Exp Biol*, 204(3):543–557.

Marr, D. (1982). *Vision : A computational investigation into the human representation and processing of visual information*. W. H. Freeman & Co, San Francisco, CA.

Marrero, C. (1987). Notas preliminares acerca de la historia natural de los peces del bajo llano. I. Comparación de los hábitos alimentarios de tres especies de peces Gymnotiformes, en el Río Apure (Edo Apure), Venezuela. *Rev. Hydrobiol. Trop.*, 20(1):57–63.

McHenry, M. J., Pell, C. A., and Long-Jr, J. H. (1995). Mechanical control of swimming speed: stiffness and axial wave form in an undulatory fish model. *J Exp Biol*, 198:293–2305.

Mérigoux, S. and Ponton, D. (1998). Body shape, diet and ontogenetic diet shifts in young fish of the Sinnamary River, French Guiana, South America. *J. Fish Biol.*, 52(3):556–569.

Metaxas, D. N. (1996). *Physics-Based Deformable Models*. Kluwer, Boston, MA.

Mochimaru, M. and Yamazaki, N. (1994). Three-dimensional measurement of unconstrained motion using a model-matching method. *Ergonomics*, 37(3):493–510.

Moller, P. (1995). *Electric Fishes: History and Behavior*. Chapman & Hall, London.

Montgomery, J. C. (1989). Lateral line detection of planktonic prey. In Coombs, S., Gorner, P., and Münz, H., editors, *The mechanosensory lateral line: Neurobiology and evolution*, pages 551–574. Springer-Verlag.

Montgomery, J. C. (1991). "Seeing" with nonvisual senses: Mechanosensory and electrosensory systems of fish. *News Physiol. Sci.*, 6(April):73–77.

Montgomery, J. C. and Milton, R. C. (1993). Use of the lateral line for feeding in the torrent fish (*Cheimarrichthys fosteri*). *New Zeal. J. Zool.*, 20:121–125.

Mortenson, M. E. (1985). *Geometric modeling*. Wiley, New York.

Nanjappa, P., Brand, L., and Lannoo, M. J. (2000). Swimming patterns associated with foraging in phylogenetically and ecologically diverse American weakly electric teleosts (Gymnotiformes). *Env. Biol. Fishes*, 58(1):97–104.

Naruse, M. and Kawasaki, M. (1998). Possible involvement of the ampullary electroreceptor system in detection of frequency-modulated electrocommunication signals in *Eigenmannia*. *J. Comp. Physiol. A*, 183(5):543–552.

Nelson, M. E. and MacIver, M. A. (1999). Prey capture in the weakly electric fish *apteronotus albifrons*: Sensory acquisition strategies and electrosensory consequences. *J Exp Biol*, 202(10):1195–1203.

Nelson, M. E., Xu, Z., and Payne, J. R. (1997). Characterization and modeling of P-type electrosensory afferent responses to amplitude modulations in a wave-type electric fish. *J. Comp. Physiol. A*, 181(5):532–544.

Parsons, K. C. (1973). Precision casting: a new method in museum technology. *Amer J Phys Anthro*, 38(3):789–802.

Peters, R. C. and Bretschneider, F. (1972). Electric phenomena in the habitat of the catfish *Ictalurus nebulosus* LeS. *J. Comp. Physiol.*, 81:345–362.

Piegl, L. and Tiller, W. (1995). *The NURBS book*. Springer-Verlag, NY.

Poulson, T. L. (1963). Cave adaptation in amblyopsid fishes. *Am. Midl. Nat.*, 70(2):257–290.

Poynton, C. A. (1996). *A technical introduction to digital video*. J. Wiley, New York.

Rasnow, B. (1994). *The electric field of a weakly electric fish*. PhD dissertation, California Institute of Technology. UMI, Ann Arbor MI.

Rasnow, B. (1996). The effects of simple objects on the electric field of *Apteronotus*. *J. Comp. Physiol. A*, 178(3):397–411.

Rasnow, B., Assad, C., Hartmann, M. J., and Bower, J. M. (1997). Applications of multimedia computers and video mixing to neuroethology. *J Neurosci Meth*, 76(1):83–91.

Rasnow, B. and Bower, J. M. (1996). The electric organ discharges of the gymnotiform fishes: I. *Apteronotus leptorhynchus*. *J. Comp. Physiol. A*, 178(3):383–396.

Ratnam, R. and Nelson, M. E. (2000). Nonrenewal statistics of electrosensory afferent spike trains: implications for the detection of weak sensory signals. *J Neurosci*, 20(17):6672–6683.

Roth, A. (1982). Sensitivity of catfish electroreceptors: Dependence on fresh water ions and skin potential. *J. of Comp. Physiol.*, 147(3):329–338.

Sand, O. (1975). Effects of different ionic environments on the mechano-sensitivity of lateral line organs in the mudpuppy. *J. Comp. Physiol.*, 102:27–42.

Schwan, H. P. (1963). Determination of biological impedances. In Nastuk, W., editor, *Physical techniques in biological research*, volume VI, Pt. B, pages 323–407. Academic Press, New York, NY.

Sfakiotakis, M., Lane, D. M., and Davies, J. B. C. (1999). Review of fish swimming modes for aquatic locomotion. *IEEE J. Oceanic Eng.*, 24(2):237–252.

Shumway, C. A. (1989a). Multiple electrosensory maps in the medulla of weakly electric gymnotiform fish I. Physiological differences. *J. Neurosci*, 9:4388–4399.

Shumway, C. A. (1989b). Multiple electrosensory maps in the medulla of weakly electric gymnotiform fish II. Anatomical differences. *J. Neurosci*, 9:4400–4415.

Simon, H. A. (1969). *The sciences of the artificial*. MIT Press, Cambridge, Massachusetts, first edition.

Spruijt, B. M., Thorwald, H., and Rousseau, J. (1992). Approach, avoidance and contact behavior of individually recognized animals automatically quantified with an imaging technique. *Physiol & Behav*, 51:747–752.

Squire, A. and Moller, P. (1982). Effects of water conductivity on electrocommunication in the weak-electric fish *Brienomyrus niger* (Mormyriformes). *Anim. Behav.*, 30(2):375–382.

Suga, N. (1967). Coding in tuberous and ampullary organs of a gymnotid electric fish gymnotus carapo. *J. Comp. Neurol.*, 131(4):437–451.

Szabo, T. and Yvette, G.-s. (1974). Anatomy of the specialized lateral line organs of electroreception. In Fessard, A., editor, *Electroreceptors and other specialized receptors in lower vertebrates (Handbook of sensory phys iology, vol III/3)*, pages 13–58. Springer.

Terzopoulos, D., Platt, J., Barr, A., and Fleischer, K. (1987). Elastically deformable models. *Comp Graph*, 21(4):205–214.

Terzopoulos, D., Rabie, T., and Grzeszczuk, R. (1997). Perception and learning in artificial animals. In *Artificial life V: proceedings of the Fifth International Workshop on the Synthesis and Simulation of Living Systems*, pages 313–320, Nara, Japan May 1996. MIT Press.

Terzopoulos, D., Tu, X., and Grzeszczuk, R. (1995). Artificial fishes: autonomous locomotion, perception, behavior, and learning in a simulated physical world. *Artificial Life*, 1:327–351.

Tillett, R. D., Onyango, C. M., and Marchant, J. A. (1997). Using model-based image processing to track animal movements. *Computers and Electronics in Agriculture*, 17(2):249–261.

Triantafyllou, M. S. and Triantafyllou, G. S. (1995). An efficient swimming machine. *Sci Amer*, March:40–49.

Tsai, R. Y. (1987). A versatile camera calibration technique for high-accuracy 3D machine vision metrology using off-the-shelf TV cameras and lenses. *IEEE J Robot Automation*, RA-3(4):323–344.

Turner, R. W., Maler, L., and Burrows, M., editors (1999). *Electroreception and electrocommunication*, volume 202(10). J Exp Biol, Cambridge, UK.

Vatine, J. J., Ratner, A., Dvorkin, M., and Seltzer, Z. (1998). A novel computerized system for analyzing motor and social behavior in groups of animals. *J Neurosci Meth*, 85(1):1–11.

von der Emde, G. (1990). Discrimination of objects through electrolocation in the weakly electric fish, Gnathonemus petersii. *J Comp Physiol A*, 167(3):413–422.

von der Emde, G. (1993). The sensing of electrical capacitances by weakly electric Mormyrid fish: effects of water conductivity. *J. Exp. Biol.*, 181(0):157–173.

von der Emde, G. (1994). Active electrolocation helps *Gnathonemus petersii* to find its prey. *Naturwissenschaften*, 81(8):367–369.

von der Emde, G. (1998). Capacitance detection in the wave-type electric fish *Eigenmannia* during active electrolocation. *J. Comp. Physiol. A*, 182(2):217–224.

von der Emde, G. (1999). Active electrolocation of objects in weakly electric fish. *J. Exp. Biol.*, 202(10):1205–1215.

von der Emde, G. and Bleckmann, H. (1998). Finding food: Senses involved in foraging for insect larvae in the electric fish *Gnathonemus petersii*. *J. Exp. Biol.*, 201(7):969–980.

von Holst, E. and Mittelstaedt, H. (1950). Das reafferenzprinzip. *Naturwissenschaften*, 37:464–476.

Waters, P. H. (1983). A review of the moulding and casting materials and techniques in use in the Palaeontology Laboratory British Museum (Natural History). *Conservator*, 7:37–43.

Watt, A. and Watt, M. (1992). *Advanced animation and rendering techniques*. ACM Press, New York.

Webb, B. (2001). Can robots make good models of biological behavior? *Behav Brain Sci*, 24(6):not yet available.

Wickelgren, I. (1996). The strange senses of other species. *IEEE Spectrum*, 33(3):32–37.

Wilkens, L. A., Russell, D. F., Pei, X., and Gurgens, C. (1997). The paddlefish rostrum functions as an electrosensory antenna in plankton feeding. *Proc. R. Soc. Lond. B*, 264(1389):1723–1729.

Winberg, S., Nilsson, G. E., M., S. B., and Höglund, U. (1993). Spontaneous locomotor activity in arctic charr measured by a computerized imaging technique: Role of brain serotonergic activity. *J Exp Biol*, 179:213–232.

Winemiller, K. O. and Adite, A. (1997). Convergent evolution of weakly electric fishes from floodplain habitats in Africa and South America. *Env. Biol. Fishes*, 49(2):175–186.

Wojtenek, W., Pei, X., Wagner, E., and Wilkens, L. A. (1999). Planktonic electric fields and the response of paddlefish primary electroreceptor afferents to live plankton. *Soc. Neurosci. Abs.*, 25:1363.

Wu, C. H. (1984). Electric fish and the discovery of animal electricity. *Am. Scient.*, 72:598–607.

Xu, Z., Payne, J. R., and Nelson, M. E. (1996). Logarithmic time course of sensory adaptation in electrosensory afferent nerve fibers in a weakly electric fish. *J. Neurophysiol.*, 76(3):2020–2032.

Young, L., Poynton, C., Schubin, M., Watkinson, J., and Olson, T., editors (1995). *Pixels, pictures, and perception: The differences and similarities between computer imagery, film, and video*. SMPTE-Society of Motion Picture & Television Engineers, White Plains, N.Y.

Zakon, H. H. (1986). The electroreceptive periphery. In Bullock, T. H. and Heiligenberg, W., editors, *Electroreception*, pages 103–156. Wiley.

CURRICULUM VITAE

Malcolm Angus MacIver, Ph.D.
Beckman Institute for Advanced Science and Technology
405 North Mathews Avenue, Urbana IL 61801
http://soma.npa.uiuc.edu/~mmaciver, mmaciver@spine.npa.edu

Education

June 2001-	Caltech Pasadena, California, USA	Postdoctoral scholar, Dept. of Mechanical Engineering
1994-May 2001	Beckman Institute & University of Illinois,Urbana, Illinois, USA	Ph.D., Neuroscience Program
1992-94	Indiana University Bloomington, Indiana, USA	Two years in Ph.D. program, Cognitive Science
1992	University of Toronto Toronto, Ontario, Canada	M.A., Philosophy
1991	University of Toronto Toronto, Ontario, Canada	B.Sc. Computer Science, High Distinction
1986	Confederation College Thunder Bay, Ontario, Canada	Electronics Engineering Technician Diploma

Scholarships, Internships, and Awards

1999: Selected for attendance at the 1999 Neuromorphic Engineering Workshop, June 27-July 17, Telluride Colorado.

1997: Awarded a 1-year Beckman Institute Research Assistantship. Proposal title*: Active Sensing in an Integrated Neuromechanical Model of the Weakly Electric Fish*.

1995: Scholarship to attend the Princeton Lectures on Biophysics*: Adaptation and learning in the nervous system*. June 25-30, 1995, Princeton New Jersey.

1994: 5-year fellowship for the Ph.D. program in Neuroscience at the University of Illinois, Urbana-Champaign. Majors: Computational Neuroscience, Behavioral Neuroscience. Minor: Cognitive Neuroscience. Advisor: Mark Nelson, Committee: Thomas Anastasio, Albert Feng, Joseph Malpeli, and Neal Cohen.

1994: McDonnell Summer Institute Scholarship to attend the 1994 McDonnell Summer Institute in Cognitive Neuroscience, July 10-23, University of California at Davis.

1993: Cognitive Science Summer Research Fellowship, Indiana University.1993: 4-year Cognitive Science Fellowship for the Ph.D. program in Philosophy and Cognitive Science at Indiana University, Bloomington.

Scholarships, Internships, and Awards (continued)

1992: 2-year Ontario Graduate Scholarship for M.A. in philosophy at the University of Toronto. Areas of specialization: history and philosophy of science, philosophy of mind. Primary research on the history of the medical classification of autism, and how US criminal courts have approached defenses of insanity due to multiple personality disorder (both for Prof. Ian Hacking).

1991: Summer research internship in Artificial Intelligence with the Canadian National Research Council in Ottawa, Ontario, working in the Knowledge Systems Laboratory.

1991: Graduated B.Sc. with High Distinction, University of Toronto.

1989-91: Programmer/System Analyst internship, Toronto Transit Commission, Toronto Ontario.

1986-91: Dean's Honour Award (all years of attendance), University of Toronto.

1986: Confederation College Technology Society Award, highest GPA in 1986 graduation class.

1986: President's Medal for academic excellence, Confederation College, Thunder Bay Ontario.

Research Experience

1994-2001: Animals actively influence the content and quality of sensory information they acquire through the positioning of peripheral sensory surfaces. Investigation of how the body and brain work together for sensory acquisition is hindered by 1) the limited number of techniques for tracking sensory surfaces, few of which provide data on the position of the entire body surface, and by 2) our inability to measure the thousands of sensory afferents stimulated during behavior. In my doctoral research with Dr. Mark Nelson, I conducted research on sensory acquisition in weakly electric fish of the genus *Apteronotus*, where I overcame the first barrier by developing a markerless tracking system and have deployed a computational approach toward overcoming the second barrier. This approach allows estimation of the full sense data stream (≈14,000 afferents) over the course of prey capture trials. Analysis of the tracking data showed how *Apteronotus* modified the position of its electrosensory array during predatory behavior and demonstrated that the fish use a closed-loop adaptive tracking strategy to intercept prey. In addition, nonvisual detection distance was dependent on water conductivity, implying that detection is dominated by the electrosense and providing the first evidence for the involvement of this sense in prey capture behavior of gymnotids. An analysis of the spatiotemporal profile of the estimated sensory signal and its neural correlates showed that the signal was ≈0.1% of the steady-state level at the time of detection, corresponding to a change in the total spikecount across all afferents of ≈0.05%. Due to the regularization of the spikecount over behaviorally relevant time windows, this change may be detectable. Using a simple threshold on the total spikecount, I estimated a neural detection time and found it to be indistinguishable from the behavioral detection time within statistical uncertainty. These results will be useful for understanding the neural and behavioral principles underlying sensory acquisition in vertebrates.

Research experience (continued)

1994: In collaboration with Dr. Joseph Farley at Indiana University, I conducted computer experiments with a Hodgkin-Huxley type quantitative model of the B photoreceptor (a modified neuron) in the marine invertebrate *Hermissenda*. To enable more complex experiments I ported the PC-based model to a high-performance computing platform. The model included six different types of ion channels that are present in this photoreceptor, which has been shown to be the primary locus of change when the animal is classically conditioned to associate light with turbulence.

1994: For Dr. Preston Garraghty at Indiana University, I developed C++ software for computer control of four sound- and light-isolated rat conditioning chambers for Dr. Garraghty's work on the effects of antiepileptics on learning. I implemented a wide variety of appetitive and aversive psychological protocols as state-flow diagrams and a parser that generated the necessary device control structures from the state-flow specification.

1993: Indiana University Cognitive Science Summer Fellowship for research into belief attribution in autism, non-human primates, and young children.

1991: Summer research internship in the Knowledge Systems Laboratory of the National Research Council in Ottawa. During my term, I developed a set of LISP programs for the Research Council's experimental expert system to diagnose jet engine faults on the basis of an array of transduced signals from sensors near the engine. The role of the software was to provide aircraft engine technicians with pseudo-natural language explanations of how the system reaches its diagnoses.

1992: Researcher for the Bertrand Russell Project at the University of Toronto. I developed and tested the feasibility of a computerized system for generating variant lists between multiple versions of Russell's writings for the publication of a critical edition.

Publications: Journals

(PDFs: http://soma.npa.uiuc.edu/~mmaciver)

MacIver, M.A., Nelson, M.E. (2001a) A robotic approach to understanding electrosensory signal acquisition in weakly electric fish. *Autonomous Robots (submitted)*.

MacIver, M.A., Sharabash, N. M., Nelson, M.E. (2001) Prey-capture behavior in gymnotid electric fish: motion analysis and effects of water conductivity. *Journal of Experimental Biology*, 204(3): 543-557.

MacIver, M.A., Nelson, M.E. (2000) Body modeling and model-based tracking for neuroethology. *Journal of Neuroscience Methods*, 95(2):133-143.

Publications: Journals (continued)

Nelson, M.E., MacIver, M.A. (1999a) Prey capture in the weakly electric fish *Apteronotus albifrons*: Sensory acquisition strategies and electrosensory consequences. *Journal of Experimental Biology*, 202(10):1195-1203. Cover.

Publications: Conference Proceeding

MacIver M.A., Lin J.L., Nelson M.E. (1997) Estimation of signal characteristics during electrolocation from video analysis of prey capture behavior in weakly electric fish. In: *Computational Neuroscience: Trends in Research, 1997*. Proceedings of the Fifth Annual Computational Neuroscience Conference held in Boston, MA, USA, July 14-17, 1996. Edited by James M. Bower. Plenum Press, 729-734.

Publications: Conference Abstracts

MacIver, M.A., Nelson, M.E. (2001b). The computational neuroethology of electrolocation in weakly electric fish. *6th International Congress of Neuroethology*, Bonn, Germany, July 27-August 3 2001.

MacIver, M.A., Sharabash, N. M., Nelson, M.E. (2000) Computational neuroethology of electrolocation in weakly electric fish. *Society for Neuroscience 30th Annual Meeting,* New Orleans, LA, November 4-9 2000.

MacIver, M.A., Law, S., Nelson, M.E. (2000) A robotic implementation of electrosensory signal acquisition in electric fish. *NASA/JPL Workshop on biomorphic robotics*, Pasadena, CA, USA, August 14-16 2000.

MacIver M.A., Nelson M.E. (1999b) Evidence for closed-loop control of prey capture in weakly electric fish. *Eighth Annual Computational Neuroscience Meeting,* Pittsburgh, PA July 18-22, 1999.

MacIver M.A., Nelson M.E. (1998) Motor aspects of active sensing in weakly electric fish. *Fifth International Neuroethology Congress Abstracts*, 347.

MacIver M.A., Nelson M.E. (1997) Cobalt blocks modulation of ampullary and mechanosensory lateral line units but not tuberous units in the weakly electric fish *Apteronotus leptorhynchus*. *Society for Neuroscience Abstracts* 23(1), 247.

MacIver M.A., Lin J.L., Nelson M.E. (1996) Estimation of signal characteristics during electrolocation from video analysis of prey capture behavior in weakly electric fish. *Fifth Annual Computational Neuroscience Meeting,* Cambridge, MA, July 14-17, 1996.

Publications: Conference Abstracts (continued)

MacIver M.A., Lin, J.L., Ègo, V.K., Nelson M.E. (1995) Infrared video reconstruction and analysis of prey capture behavior in the weakly electric fish *Apteronotus albifrons*. *Society for Neuroscience Abstracts* 21(1):184.

Publications: Thesis

MacIver M.A. (2001) The computational neuroethology of weakly electric fish: Body modeling, motion analysis, and sensory signal estimation. Ph.D. Dissertation, University of Illinois at Urbana-Champaign. UMI, Ann Arbor, MI, USA.

Selected Talks

The computational neuroethology of weakly electric fish: Body modeling, motion analysis, and sensory estimation. *Neuroscience Program Colloquium, University of Illinois at Urbana-Champaign, Urbana, IL, USA, April 10, 2001.*

The computational neuroethology of weakly electric fish: Understanding active sensing and adaptive signal processing in the brain through sensory reconstruction and robotics. *Caltech, Pasadena, CA, USA, January 10, 2001.*

A robotic implementation of electrosensory signal acquisition in electric fish. *NASA/JPL Workshop on biomorphic robotics, Caltech, Pasadena, CA, USA, August 15, 2000.*

3D digitizing with the MicroScribe and Rhinoceros: How to digitize an electric fish. *Beckman Institute Imaging Technology Group Forum, Beckman Institute of Advanced Science and Technology, Urbana, IL, USA, December 10, 1998.*

Teaching Experience

University of Illinois, “Neurophysiology Laboratory” (PHYSL 416)	1/97-5/97
University of Illinois, “Topics in Neuroethology” (PHYSL 490)	8/96-12/96
University of Illinois, “Introduction to Neurobiology” (BIO 303)	8/94-12/94
Indiana University, “Introduction to Philosophy” (P100)	1/94-5/94
Indiana University, “Introduction to Ethics” (P140)	9/92-12/92
University of Toronto, “How Computers are Used” (CSC104)	1/91-5/91
University of Toronto, “How Computers are Used” (CSC104)	9/91-12/91
University of Toronto, “Computer Programming” (CSC108)	9/90-12/90
University of Toronto, “Science and Pseudo Science” (PHL272)	1/89-7/89
Confederation College, Digital Electronics, Programming	1/86-4/86

Selected Organizational Experience

Designed and constructed exhibits for the 2001 Beckman Open House, including a human field sensing artificial electric fish that I made using a Genisys 3D printer and field sensing circuitry. I also conducted bi-hourly public tours of Mark Nelson's laboratory.

Elected graduate student representative to the UIUC Neuroscience Program Executive for '97-'98.

In the spring of 1995 I obtained the support and interest of graduate students and eight faculty of the University of Illinois Neuroscience Program to establish a new graduate level seminar entitled "Topics in Neuroethology." Dr. Nelson coordinated the course in the fall of 1996 & 2000. I also developed a web site and some of the assignments for the course, which was voted best online resource in Prof. Jack Pettigrew's survey of the scientists on the neuroethology electronic mailing list in April of 2000. Web site at: *http://soma.npa.uiuc.edu/courses/neuroethol*.

For the fall session of 1992 at Indiana University, I developed a graduate-level survey course in Cognitive Science for graduate students who had prior training in the area. The proposed course and detailed syllabus was accepted by the head of the Cognitive Science Program, Richard Shiffrin. I and several other graduate students took the course in 1992.